Chapter 2

Classical Electromagnetism and Optics

The classical electromagnetic phenomena are completely described by Maxwell's Equations. The simplest case we may consider is that of electrodynamics of isotropic media

2.1 Maxwell's Equations of Isotropic Media

Maxwell's Equations are

$$\nabla \times \vec{H} = \frac{\partial \vec{D}}{\partial t} + \vec{J}, \tag{2.1a}$$

$$\nabla \times \vec{E} = -\frac{\partial \vec{B}}{\partial t}, \tag{2.1b}$$

$$\nabla \cdot \vec{D} = \rho, \tag{2.1c}$$

$$\nabla \cdot \vec{B} = 0. \tag{2.1d}$$

The material equations accompanying Maxwell's equations are:

$$\vec{D} = \epsilon_0 \vec{E} + \vec{P}, \tag{2.2a}$$

$$\vec{B} = \mu_0 \vec{H} + \vec{M}. \tag{2.2b}$$

Here, $\vec{E}$ and $\vec{H}$ are the electric and magnetic field, $\vec{D}$ the dielectric flux, $\vec{B}$ the magnetic flux, $\vec{J}$ the current density of free chareges, ρ is the free charge density, $\vec{P}$ is the polarization, and $\vec{M}$ the magnetization.

Note, it is Eqs.(2.2a) and (2.2b) which make electromagnetism an interesting and always a hot topic with never ending possibilities. All advances in engineering of artifical materials or finding of new material properties, such as superconductivity, bring new life, meaning and possibilities into this field.

By taking the curl of Eq. (2.1b) and considering

$$\nabla\times\left(\nabla\times\vec{E}\right)=\nabla\left(\nabla\cdot\vec{E}\right)-\Delta\vec{E},$$

where ∇ is the Nabla operator and Δ the Laplace operator, we obtain

$$\Delta\vec{E}-\mu_0\frac{\partial}{\partial t}\left(\vec{j}+\epsilon_0\frac{\partial\vec{E}}{\partial t}+\frac{\partial\vec{P}}{\partial t}\right)=\frac{\partial}{\partial t}\nabla\times\vec{M}+\nabla\left(\nabla\cdot\vec{E}\right) \tag{2.3}$$

and hence

$$\left(\Delta-\frac{1}{c_0^2}\frac{\partial^2}{\partial t^2}\right)\vec{E}=\mu_0\left(\frac{\partial\vec{j}}{\partial t}+\frac{\partial^2}{\partial t^2}\vec{P}\right)+\frac{\partial}{\partial t}\nabla\times\vec{M}+\nabla\left(\nabla\cdot\vec{E}\right). \tag{2.4}$$

with the vacuum velocity of light

$$c_0=\sqrt{\frac{1}{\mu_0\epsilon_0}}. \tag{2.5}$$

For dielectric non magnetic media, which we often encounter in optics, with no free charges and currents due to free charges, there is $\vec{M}=\vec{0},\quad \vec{J}=\vec{0}$, $\rho=0$, which greatly simplifies the wave equation to

$$\left(\Delta-\frac{1}{c_0^2}\frac{\partial^2}{\partial t^2}\right)\vec{E}=\mu_0\frac{\partial^2}{\partial t^2}\vec{P}+\nabla\left(\nabla\cdot\vec{E}\right). \tag{2.6}$$

2.1.1 Helmholtz Equation

In general, the polarization in dielectric media may have a nonlinear and non local dependence on the field. For linear media the polarizability of the medium is described by a dielectric susceptibility $\chi\left(\vec{r},t\right)$

$$\vec{P}(r,t)=\epsilon_0\int\int d\vec{r}'dt'\;\chi\left(\vec{r}-\vec{r}',t-t'\right)\vec{E}\left(\vec{r}',t'\right). \tag{2.7}$$

The polarization in media with a local dielectric suszeptibility can be described by

$$\vec{P}(r,t) = \epsilon_0 \int dt' \; \chi\left(\vec{r}, t-t'\right) \vec{E}\left(\vec{r}, t'\right). \tag{2.8}$$

This relationship further simplifies for homogeneous media, where the susceptibility does not depend on location

$$\vec{P}(\vec{r},t) = \epsilon_0 \int dt' \; \chi\left(t-t'\right) \vec{E}\left(\vec{r}, t'\right). \tag{2.9}$$

which leads to a dielectric response function or permittivity

$$\epsilon\left(t\right) = \epsilon_0(\delta(t) + \chi\left(t\right)) \tag{2.10}$$

and with it to

$$\vec{D}(r,t) = \int dt' \; \epsilon\left(t-t'\right) \vec{E}\left(\vec{r}, t'\right). \tag{2.11}$$

In such a linear homogeneous medium follows from eq.(2.1c) for the case of no free charges

$$\int dt' \; \epsilon\left(t-t'\right) \left(\nabla \cdot \vec{E}\left(\vec{r}, t'\right)\right) = 0. \tag{2.12}$$

This is certainly fulfilled for $\vec{\nabla} \cdot \vec{E} = 0$, which simplifies the wave equation (2.4) further

$$\left(\Delta - \frac{1}{c_0^2}\frac{\partial^2}{\partial t^2}\right) \vec{E} = \mu_0 \frac{\partial^2}{\partial t^2} \vec{P}. \tag{2.13}$$

This is the wave equation driven by the polarization of the medium. If the medium is linear and has only an induced polarization, completely described in the time domain $\chi\left(t\right)$ or in the frequency domain by its Fourier transform, the complex susceptibility $\tilde{\chi}(\omega) = \tilde{\epsilon}_r(\omega) - 1$ with the relative permittivity $\tilde{\epsilon}_r(\omega) = \tilde{\epsilon}(\omega)/\epsilon_0$, we obtain in the frequency domain with the Fourier transform relationship

$$\widetilde{\vec{E}}(z,\omega) = \int_{-\infty}^{+\infty} \vec{E}(z,t) e^{-j\omega t} dt, \tag{2.14}$$

$$\widetilde{\vec{P}}(\omega) = \epsilon_0 \tilde{\chi}(\omega) \widetilde{\vec{E}}(\omega), \tag{2.15}$$

where, the tildes denote the Fourier transforms in the following. Substituted into (2.13)

$$\left(\Delta + \frac{\omega^2}{c_0^2}\right) \widetilde{\vec{E}}(\omega) = -\omega^2 \mu_0 \epsilon_0 \tilde{\chi}(\omega) \widetilde{\vec{E}}(\omega), \tag{2.16}$$

we obtain

$$\left(\Delta + \frac{\omega^2}{c_0^2}(1 + \tilde{\chi}(\omega)\right) \widetilde{\vec{E}}(\omega) = 0, \tag{2.17}$$

with the refractive index $n(\omega)$ and $1+\tilde{\chi}(\omega) = n(\omega)^2$ results in the Helmholtz equation

$$\left(\Delta + \frac{\omega^2}{c^2}\right) \widetilde{\vec{E}}(\omega) = 0, \tag{2.18}$$

where $c(\omega) = c_0/n(\omega)$ is the velocity of light in the medium. This equation is the starting point for finding monochromatic wave solutions to Maxwell's equations in linear media, as we will study for different cases in the following. Also, so far we have treated the susceptibility $\tilde{\chi}(\omega)$ as a real quantity, which may not always be the case as we will see later in detail.

2.1.2 Plane-Wave Solutions (TEM-Waves) and Complex Notation

The real wave equation (2.13) for a linear medium has real monochromatic plane wave solutions $\vec{E}_{\vec{k}}(\vec{r}, t)$, which can be be written most efficiently in terms of the complex plane-wave solutions $\underline{\vec{E}}_{\vec{k}}(\vec{r}, t)$ according to

$$\vec{E}_{\vec{k}}(\vec{r}, t) = \frac{1}{2}\left[\underline{\vec{E}}_{\vec{k}}(\vec{r}, t) + \underline{\vec{E}}_{\vec{k}}(\vec{r}, t)^*\right] = \Re e\left\{\underline{\vec{E}}_{\vec{k}}(\vec{r}, t)\right\}, \tag{2.19}$$

with

$$\underline{\vec{E}}_{\vec{k}}(\vec{r}, t) = \underline{E}_{\vec{k}}\ e^{\mathrm{j}(\omega t - \vec{k}\cdot\vec{r})}\ \vec{e}(\vec{k}). \tag{2.20}$$

Note, we explicitly underlined the complex wave to indicate that this is a complex quantity. Here, $\vec{e}(\vec{k})$ is a unit vector indicating the direction of the electric field which is also called the polarization of the wave, and $\underline{E}_{\vec{k}}$ is the complex field amplitude of the wave with wave vector $\vec{k}$. Substitution of eq.(2.19) into the wave equation results in the dispersion relation, i.e. a

relationship between wave vector and frequency necessary to satisfy the wave equation

$$|\vec{k}|^2 = \frac{\omega^2}{c(\omega)^2} = k(\omega)^2. \tag{2.21}$$

Thus, the dispersion relation is given by

$$k(\omega) = \pm\frac{\omega}{c_0} n(\omega). \tag{2.22}$$

with the wavenumber

$$k = 2\pi/\lambda, \tag{2.23}$$

where λ is the wavelength of the wave in the medium with refractive index n, ω the angular frequency, $\vec{k}$ the wave vector. Note, the natural frequency $f = \omega/2\pi$. From $\nabla \cdot \vec{E} = 0$, for all time, we see that $\vec{k} \perp \vec{e}$. Substitution of the electric field 2.19 into Maxwell's Eqs. (2.1b) results in the magnetic field

$$\vec{H}_{\vec{k}}(\vec{r}, t) = \frac{1}{2}\left[\underline{\vec{H}}_{\vec{k}}(\vec{r}, t) + \underline{\vec{H}}_{\vec{k}}(\vec{r}, t)^*\right] \tag{2.24}$$

with

$$\underline{\vec{H}}_{\vec{k}}(\vec{r}, t) = \underline{H}_{\vec{k}}\ e^{\mathrm{j}(\omega t - \vec{k}\cdot\vec{r})}\ \vec{h}(\vec{k}). \tag{2.25}$$

This complex component of the magnetic field can be determined from the corresponding complex electric field component using Faraday's law

$$-\mathrm{j}\vec{k} \times \left(\underline{E}_{\vec{k}}\ e^{\mathrm{j}(\omega t - \vec{k}\cdot\vec{r})}\ \vec{e}(\vec{k})\right) = -\mathrm{j}\mu_0\omega\underline{\vec{H}}_{\vec{k}}(\vec{r}, t), \tag{2.26}$$

or

$$\underline{\vec{H}}_{\vec{k}}(\vec{r}, t) = \frac{\underline{E}_{\vec{k}}}{\mu_0\omega} e^{\mathrm{j}(\omega t - \vec{k}\cdot\vec{r})}\vec{k} \times \vec{e} = \underline{H}_{\vec{k}} e^{\mathrm{j}(\omega t - \vec{k}\cdot\vec{r})}\vec{h} \tag{2.27}$$

with

$$\vec{h}(\vec{k}) = \frac{\vec{k}}{|k|} \times \vec{e}(\vec{k}) \tag{2.28}$$

and

$$\underline{H}_{\vec{k}} = \frac{|k|}{\mu_0\omega}\underline{E}_{\vec{k}} = \frac{1}{Z_F}\underline{E}_{\vec{k}}. \tag{2.29}$$

The characteristic impedance of the TEM-wave is the ratio between electric and magnetic field strength

$$Z_F = \mu_0 c = \sqrt{\frac{\mu_0}{\epsilon_0\epsilon_r}} = \frac{1}{n} Z_{F_0} \tag{2.30}$$

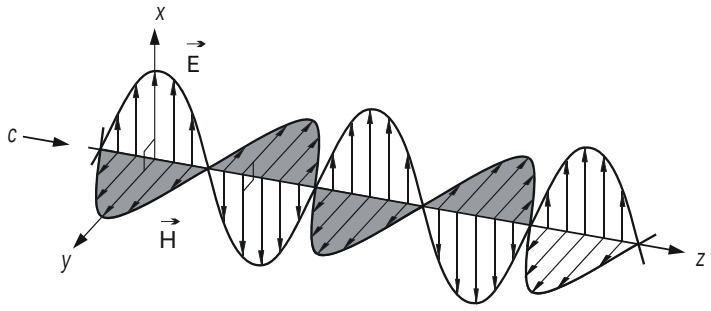

Figure 2.1: Transverse electromagnetic wave (TEM) [6]

with the refractive index $n = \sqrt{\epsilon_r}$ and the free space impedance

$$Z_{F_0} = \sqrt{\frac{\mu_0}{\epsilon_0}} \approx 377\,\Omega. \tag{2.31}$$

Note that the vectors $\vec{e}$, $\vec{h}$ and $\vec{k}$ form an orthogonal trihedral,

$$\vec{e} \perp \vec{h}, \quad \vec{k} \perp \vec{e}, \quad \vec{k} \perp \vec{h}. \tag{2.32}$$

That is why we call these waves transverse electromagnetic (TEM) waves. We consider the electric field of a monochromatic electromagnetic wave with frequency ω and electric field amplitude E_0, which propagates in vacuum along the z-axis, and is polarized along the x-axis, (Fig. 2.1), i.e. $\frac{\vec{k}}{|k|} = \vec{e}_z$, and $\vec{e}(\vec{k}) = \vec{e}_x$. Then we obtain from Eqs.(2.19) and (2.20)

$$\vec{E}(\vec{r}, t) = E_0 \cos(\omega t - kz)\ \vec{e}_x, \tag{2.33}$$

and similiar for the magnetic field

$$\vec{H}(\vec{r}, t) = \frac{E_0}{Z_{F_0}} \cos(\omega t - kz)\ \vec{e}_y, \tag{2.34}$$

see Figure 2.1.Note, that for a backward propagating wave with $\underline{\vec{E}}(\vec{r}, t) = \underline{E}\ e^{\mathrm{j}\omega t + \mathrm{j}\vec{k}\cdot\vec{r}}\ \vec{e}_x$, and $\underline{\vec{H}}(\vec{r}, t) = \underline{H}\ e^{\mathrm{j}(\omega t + \vec{k}\vec{r})}\ \vec{e}_y$, there is a sign change for the magnetic field

$$\underline{H} = -\frac{|k|}{\mu_0 \omega} \underline{E}, \tag{2.35}$$

so that the $(\vec{k}, \vec{E}, \vec{H})$ always form a right handed orthogonal system.

2.1.3 Poynting Vectors, Energy Density and Intensity

The table below summarizes the instantaneous and time averaged energy content and energy transport related to an electromagnetic field

Quantity	Real fields	Complex fields
Electric and magnetic energy density	$w_e = \frac{1}{2}\vec{E}\cdot\vec{D} = \frac{1}{2}\epsilon_0\epsilon_r\vec{E}^2$ $w_m = \frac{1}{2}\vec{H}\cdot\vec{B} = \frac{1}{2}\mu_0\mu_r\vec{H}^2$ $w = w_e + w_m$	$\bar{w}_e = \frac{1}{4}\epsilon_0\epsilon_r\left\lvert\underline{\vec{E}}\right\rvert^2$ $\bar{w}_m = \frac{1}{4}\mu_0\mu_r\left\lvert\underline{\vec{H}}\right\rvert^2$ $\bar{w} = \bar{w}_e + \bar{w}_m$
Poynting vector	$\vec{S} = \vec{E}\times\vec{H}$	$\vec{T} = \frac{1}{2}\underline{\vec{E}}\times\underline{\vec{H}}^*$
Poynting theorem	$\mathrm{div}\vec{S} + \vec{E}\cdot\vec{j} + \frac{\partial w}{\partial t} = 0$	$\mathrm{div}\vec{T} + \frac{1}{2}\underline{\vec{E}}\cdot\underline{\vec{j}}^* +$ $+2j\omega(\bar{w}_m - \bar{w}_e) = 0$
Intensity	$I = \left\lvert\vec{S}\right\rvert = cw$	$I = \mathrm{Re}\{\vec{T}\} = c\bar{w}$

Table 2.1: Poynting vector and energy density in EM-fields

For a plane wave with an electric field $\underline{\vec{E}}(\vec{r},t) = \underline{E}e^{\mathrm{j}(\omega t - kz)}\ \vec{e}_x$ we obtain for the energy density in units of [J/m^3]

$$w = \frac{1}{2}\epsilon_r\epsilon_0|\underline{E}|^2, \tag{2.36}$$

the complex Poynting vector

$$\vec{T} = \frac{1}{2Z_F}|\underline{E}|^2\ \vec{e}_z, \tag{2.37}$$

and the intensity in units of [W/m^2]

$$I = \frac{1}{2Z_F}|\underline{E}|^2 = \frac{1}{2}Z_F|\underline{H}|^2. \tag{2.38}$$

2.1.4 Classical Permittivity

In this section we want to get insight into propagation of an electromagnetic wavepacket in an isotropic and homogeneous medium, such as a glass optical fiber due to the interaction of radiation with the medium. The electromagnetic properties of a dielectric medium is largely determined by the electric polarization induced by an electric field in the medium. The polarization is

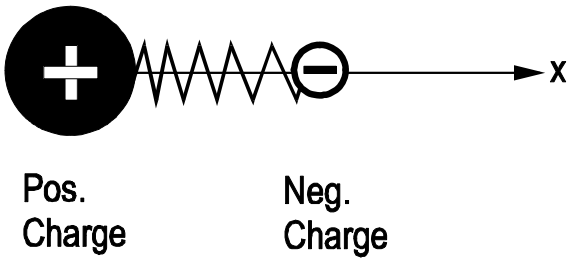

Figure 2.2: Classical harmonic oscillator model for radiation matter interaction

defined as the total induced dipole moment per unit volume. We formulate this directly in the frequency domain

$$\underline{\widetilde{\vec{P}}}(\omega) = \frac{\text{dipole moment}}{\text{volume}} = N \cdot \langle \underline{\widetilde{\vec{p}}}(\omega) \rangle = \epsilon_0 \underline{\widetilde{\chi}}(\omega) \underline{\widetilde{\vec{E}}}(\omega), \tag{2.39}$$

where N is density of elementary units and $\langle \underline{\vec{p}} \rangle$ is the average dipole moment of the unit (atom, molecule, ...). In an isotropic and homogeneous medium the induced polarization is proportional to the electric field and the proportionality constant, $\underline{\widetilde{\chi}}(\omega)$, is called the susceptibility of the medium.

As it turns out (justification later), an electron elastically bound to a positively charged rest atom is not a bad model for understanding the interaction of light with matter at very low electric fields, i.e. the fields do not change the electron distribution in the atom considerably or even ionize the atom, see Figure 2.2. This model is called Lorentz model after the famous physicist A. H. Lorentz (Dutchman) studying electromagnetic phenomena at the turn of the 19th century. He also found the Lorentz Transformation and Invariance of Maxwell's Equations with respect to these transformation, which showed the path to Special Relativity.

The equation of motion for such a unit is the damped harmonic oscillator driven by an electric field in one dimension, x. At optical frequencies, the distance of elongation, x, is much smaller than an optical wavelength (atoms have dimensions on the order of a tenth of a nanometer, whereas optical fields have wavelength on the order of microns) and therefore, we can neglect the spatial variation of the electric field during the motion of the charges within an atom (dipole approximation, i.e. $\vec{E}(\vec{r}, t) = \vec{E}(\vec{r}_A, t) = E(t)\vec{e}_x$).

The equation of motion is

$$m\frac{d^2x}{dt^2} + 2\frac{\Omega_0}{Q}m\frac{dx}{dt} + m\Omega_0^2 x = e_0 E(t), \tag{2.40}$$

where $\underline{E}(t) = \tilde{\underline{E}}e^{\mathrm{j}\omega t}$. Here, m is the mass of the electron assuming the that the rest atom has infinite mass, e_0 the charge of the electron, Ω_0 is the resonance frequency of the undamped oscillator and Q the quality factor of the resonance, which determines the damping of the oscillator. By using the trial solution $x\,(t) = \tilde{x}e^{\mathrm{j}\omega t}$, we obtain for the complex amplitude of the dipole moment $\tilde{p}$ with the time dependent response $p(t) = e_0 x(t) = \underline{\tilde{p}}e^{\mathrm{j}\omega t}$

$$\underline{\tilde{p}} = \frac{\frac{e_0^2}{m}}{(\Omega_0^2 - \omega^2) + 2\mathrm{j}\frac{\Omega_0}{Q}\omega}\underline{\tilde{E}}. \tag{2.41}$$

Note, that we included ad hoc a damping term in the harmonic oscillator equation. At this point it is not clear what the physical origin of this damping term is and we will discuss this at length later in chapter 4. For the moment, we can view this term simply as a consequence of irreversible interactions of the atom with its environment. We then obtain from (2.39) for the susceptibility

$$\underline{\chi}(\omega) = \frac{N\frac{e_0^2}{m}\frac{1}{\epsilon_0}}{(\Omega_0^2 - \omega^2) + 2\mathrm{j}\omega\frac{\Omega_0}{Q}} \tag{2.42}$$

or

$$\underline{\widetilde{\chi}}(\omega) = \frac{\omega_p^2}{(\Omega_0^2 - \omega^2) + 2\mathrm{j}\omega\frac{\Omega_0}{Q}}, \tag{2.43}$$

with ω_p called the plasma frequency, which is defined as $\omega_p^2 = Ne_0^2/m\epsilon_0$. Figure 2.3 shows the normalized real and imaginary part, $\underline{\widetilde{\chi}}(\omega) = \widetilde{\chi}_r(\omega) + \mathrm{j}\widetilde{\chi}_i(\omega)$ of the classical susceptibility (2.43). Note, that there is a small resonance shift (almost invisible) due to the loss. Off resonance, the imaginary part approaches zero very quickly. Not so the real part, which approaches a constant value ω_p^2/Ω_0^2 below resonance for $\omega \to 0$, and approaches zero far above resonance, but much slower than the imaginary part. As we will see later, this is the reason why there are low loss, i.e. transparent, media with refractive index very much different from 1.

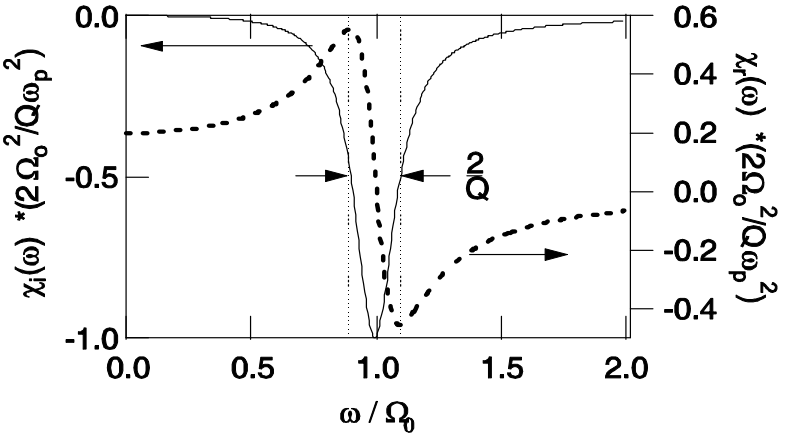

Figure 2.3: Real part (dashed line) and imaginary part (solid line) of the susceptibility of the classical oscillator model for the dielectric polarizability.

2.1.5 Optical Pulses

Optical pulses are wave packets constructed by a continuous superposition of monochromatic plane waves. Consider a TEM-wavepacket, i.e. a superposition of waves with different frequencies, polarized along the x-axis and propagating along the z-axis

$$\underline{\vec{E}}(\vec{r},t) = \int_0^\infty \frac{d\Omega}{2\pi} \underline{\widetilde{E}}(\Omega) e^{\mathrm{j}(\Omega t - K(\Omega)z)} \ \vec{e}_x. \tag{2.44}$$

Correspondingly, the magnetic field is given by

$$\underline{\vec{H}}(\vec{r},t) = \int_0^\infty \frac{d\Omega}{2\pi Z_F(\Omega)} \underline{\widetilde{E}}(\Omega) e^{\mathrm{j}(\Omega t - K(\Omega)z)} \ \vec{e}_y \tag{2.45}$$

Again, the physical electric and magnetic fields are real and related to the complex fields by

$$\vec{E}(\vec{r},t) = \frac{1}{2}\left(\underline{\vec{E}}(\vec{r},t) + \underline{\vec{E}}(\vec{r},t)^*\right) \tag{2.46}$$

$$\vec{H}(\vec{r},t) = \frac{1}{2}\left(\underline{\vec{H}}(\vec{r},t) + \underline{\vec{H}}(\vec{r},t)^*\right). \tag{2.47}$$

Here, $|\underline{\tilde{E}}(\Omega)|e^{\mathrm{j}\varphi(\Omega)}$ is the complex wave amplitude of the electromagnetic wave at frequency Ω and $K(\Omega) = \Omega/c(\Omega) = n(\Omega)\Omega/c_0$ the wavenumber, where,

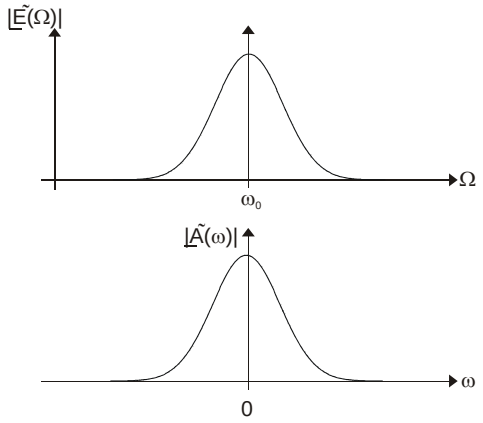

Figure 2.4: Spectrum of an optical wave packet described in absolute and relative frequencies

$n(\Omega)$ is again the refractive index of the medium

$$n^2(\Omega) = 1 + \chi(\Omega), \tag{2.48}$$

c and c_0 are the velocity of light in the medium and in vacuum, respectively. The planes of constant phase propagate with the phase velocity c of the wave.

The wavepacket consists of a superposition of many frequencies with the spectrum shown in Fig. 2.4.

At a given point in space, for simplicity $z = 0$, the complex field of a pulse is given by (Fig. 2.4)

$$\underline{E}(z = 0, t) = \frac{1}{2\pi} \int_0^\infty \underline{\tilde{E}}(\Omega) e^{\mathrm{j}\Omega t} d\Omega. \tag{2.49}$$

Optical pulses often have relatively small spectral width compared to the center frequency of the pulse ω_0, as it is illustrated in the upper part of Figure 2.4. For example typical pulses used in optical communication systems for 10Gb/s transmission speed are on the order of 20ps long and have a center wavelength of $\lambda = 1550$nm. Thus the spectral with is only on the order of 50GHz, whereas the center frequency of the pulse is 200THz, i.e. the bandwidth is 4000 smaller than the center frequency. In such cases it is useful to separate the complex electric field in Eq. (2.49) into a carrier frequency ω_0 and an envelope $\underline{A}(t)$ and represent the absolute frequency as

$\Omega = \omega_0 + \omega$. We can then rewrite Eq.(2.49) as

$$\begin{aligned} \underline{E}(z &= 0, t) = \frac{1}{2\pi}\int_{-\omega_0}^{\infty} \underline{\tilde{E}}(\omega_0+\omega)e^{\mathrm{j}(\omega_0+\omega)t}d\omega \qquad (2.50)\\ &= A(t)e^{\mathrm{j}\omega_0 t}. \end{aligned}$$

The envelope, see Figure 2.8, is given by

$$\begin{aligned} \underline{A}(t) &= \frac{1}{2\pi}\int_{-\omega_0\to-\infty}^{\infty} \underline{\tilde{A}}(\omega)e^{\mathrm{j}\omega t}d\omega \qquad (2.51)\\ &= \frac{1}{2\pi}\int_{-\infty}^{\infty} \underline{\tilde{A}}(\omega)e^{\mathrm{j}\omega t}d\omega, \qquad (2.52) \end{aligned}$$

where $\tilde{A}(\omega)$ is the spectrum of the envelope with, $\tilde{A}(\omega) = 0$ for $\omega \leq -\omega_0$. To be physically meaningful, the spectral amplitude $\tilde{A}(\omega)$ must be zero for negative frequencies less than or equal to the carrier frequency, see Figure 2.8. Note, that waves with zero frequency can not propagate, since the corresponding wave vector is zero. The pulse and its envelope are shown in Figure 2.5.

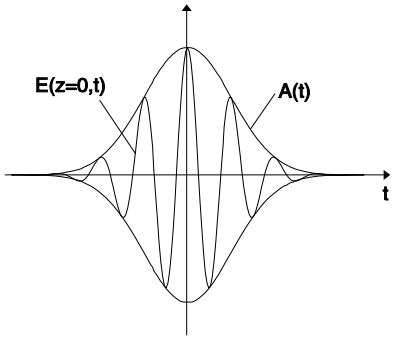

Figure 2.5: Electric field and envelope of an optical pulse.

Table 2.2 shows pulse shape and spectra of some often used pulses as well as the pulse width and time bandwidth products. The pulse width and bandwidth are usually specified as the Full Width at Half Maximum (FWHM) of the intensity in the time domain, $|\underline{A}(t)|^2$, and the spectral density $\left|\underline{\tilde{A}}(\omega)\right|^2$ in the frequency domain, respectively. The pulse shapes and corresponding spectra to the pulses listed in Table 2.2 are shown in Figs 2.6 and 2.7.

Pulse Shape	Fourier Transform	Pulse Width	Time-Bandwidth Product
$\underline{A}(t)$	$\underline{\tilde{A}}(\omega) = \int_{-\infty}^{\infty} a(t) e^{-\mathrm{j}\omega t} dt$	Δt	$\Delta t \cdot \Delta f$
Gaussian: $\mathrm{e}^{-\frac{t^2}{2\tau^2}}$	$\sqrt{2\pi}\tau \mathrm{e}^{-\frac{1}{2}\tau^2\omega^2}$	$2\sqrt{\ln 2}\tau$	0.441
Hyperbolic Secant: $\mathrm{sech}(\frac{t}{\tau})$	$\frac{\tau}{2}\ \mathrm{sech}\big(\frac{\pi}{2}\tau\omega\big)$	1.7627 τ	0.315
Rect-function: $= \begin{cases} 1, & \lvert t\rvert \le \tau/2 \\ 0, & \lvert t\rvert > \tau/2 \end{cases}$	$\tau \frac{\sin(\tau\omega/2)}{\tau\omega/2}$	τ	0.886
Lorentzian: $\frac{1}{1+(t/\tau)^2}$	$2\pi\tau \mathrm{e}^{-\lvert\tau\omega\rvert}$	1.287 τ	0.142
Double-Exp.: $\mathrm{e}^{-\lvert\frac{t}{\tau}\rvert}$	$\frac{\tau}{1+(\omega\tau)^2}$	ln2 τ	0.142

Table 2.2: Pulse shapes, corresponding spectra and time bandwidth products.

Figure 2.6: Fourier transforms to pulse shapes listed in table 2.2 [6].

Figure 2.7: Fourier transforms to pulse shapes listed in table 2.2 continued [6].

2.1.6 Pulse Propagation

Having a basic model for the interaction of light and matter at hand, via section 2.1.4, we can investigate what happens if an electromagnetic wave packet, i.e. an optical pulse propagates through such a medium. We start from Eqs.(2.44) to evaluate the wave packet propagation for an arbitrary

propagation distance z

$$\underline{E}(z,t) = \frac{1}{2\pi}\int_0^\infty \tilde{\underline{E}}(\Omega)e^{\mathrm{j}(\Omega t - K(\Omega)z)}d\Omega. \tag{2.53}$$

Analogous to Eq. (2.50) for a pulse at a given position, we can separate an optical pulse into a carrier wave at frequency ω_0 and a complex envelope $A(z,t)$,

$$\underline{E}(z,t) = \underline{A}(z,t)e^{\mathrm{j}(\omega_0 t - K(\omega_0)z)}. \tag{2.54}$$

By introducing the offset frequency ω, the offset wavenumber $k(\omega)$ and spectrum of the envelope $\tilde{\underline{A}}(\omega)$

$$\begin{aligned} \omega &= \Omega - \omega_0, & (2.55)\\ k(\omega) &= K(\omega_0+\omega) - K(\omega_0), & (2.56)\\ \tilde{\underline{A}}(\omega) &= \tilde{\underline{E}}(\Omega = \omega_0 + \omega). & (2.57) \end{aligned}$$

the envelope at propagation distance z, see Fig.2.8, is expressed as

$$\underline{A}(z,t) = \frac{1}{2\pi}\int_{-\infty}^\infty \tilde{\underline{A}}(\omega)e^{\mathrm{j}(\omega t - k(\omega)z)}d\omega, \tag{2.58}$$

with the same constraints on the spectrum of the envelope as before, i.e. the spectrum of the envelope must be zero for negative frequencies beyond the carrier frequency. Depending on the dispersion relation $k(\omega)$, (see Fig. 2.9),.the pulse will be reshaped during propagation as discussed in the following section.

2.1.7 Dispersion

The dispersion relation indicates how much phase shift each frequency component experiences during propagation. These phase shifts, if not linear with respect to frequency, will lead to distortions of the pulse. If the propagation constant $k(\omega)$ is only slowly varying over the pulse spectrum, it is useful to represent the propagation constant, $k(\omega)$, or dispersion relation $K(\Omega)$ by its Taylor expansion, see Fig. 2.9,

$$k(\omega) = k'\omega + \frac{k''}{2}\omega^2 + \frac{k^{(3)}}{6}\omega^3 + O(\omega^4). \tag{2.59}$$

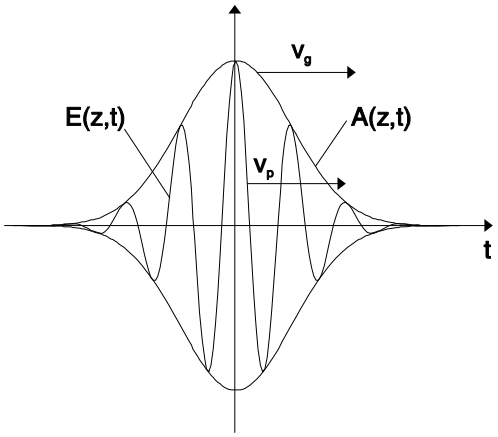

Figure 2.8: Electric field and pulse envelope in time domain.

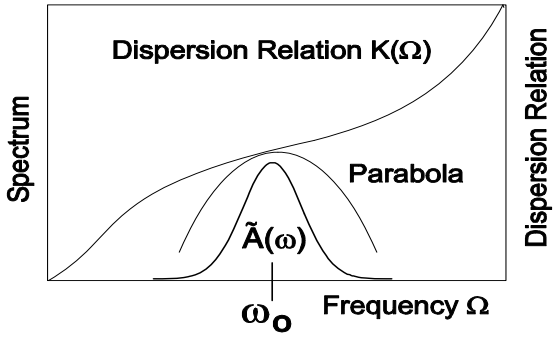

Figure 2.9: Taylor expansion of dispersion relation at the center frequency of the wave packet.

If the refractive index depends on frequency, the dispersion relation is no longer linear with respect to frequency, see Fig. 2.9 and the pulse propagation according to (2.58) can be understood most easily in the frequency domain

$$\frac{\partial \underline{\tilde{A}}(z,\omega)}{\partial z} = -\mathrm{j}k(\omega)\underline{\tilde{A}}(z,\omega). \tag{2.60}$$

Transformation of Eq.() into the time domain gives

$$\frac{\partial \underline{A}(z,t)}{\partial z} = -\mathrm{j}\sum_{n=1}^{\infty} \frac{k^{(n)}}{n!}\left(-\mathrm{j}\frac{\partial}{\partial t}\right)^n \underline{A}(z,t). \tag{2.61}$$

If we keep only the first term, the linear term, in Eq.(2.59), then we obtain for the pulse envelope from (2.58) by definition of the group velocity at frequency ω_0

$$v_{g0} = 1/k' = \left(\left. \frac{dk(\omega)}{d\omega} \right|_{\omega=0} \right)^{-1} \tag{2.62}$$

$$\underline{A}(z,t) = \underline{A}(0, t - z/v_{g0}). \tag{2.63}$$

Thus the derivative of the dispersion relation at the carrier frequency determines the propagation velocity of the envelope of the wave packet or group velocity, whereas the ratio between propagation constant and frequency determines the phase velocity of the carrier

$$v_{p0} = \omega_0/K(\omega_0) = \left(\frac{K(\omega_0)}{\omega_0} \right)^{-1}. \tag{2.64}$$

To get rid of the trivial motion of the pulse envelope with the group velocity, we introduce the retarded time $t' = t - z/v_{g0}$. With respect to this retarded time the pulse shape is invariant during propagation, if we approximate the dispersion relation by the slope at the carrier frequency

$$\underline{A}(z,t) = \underline{A}(0,t'). \tag{2.65}$$

Note, if we approximate the dispersion relation by its slope at the carrier frequency, i.e. we retain only the first term in Eq.(2.61), we obtain

$$\frac{\partial \underline{A}(z,t)}{\partial z} + \frac{1}{v_{g0}} \frac{\partial \underline{A}(z,t)}{\partial t} = 0, \tag{2.66}$$

and (2.63) is its solution. If, we transform this equation to the new coordinate system

$$z' = z, \tag{2.67}$$

$$t' = t - z/v_{g0}, \tag{2.68}$$

with

$$\frac{\partial}{\partial z} = \frac{\partial}{\partial z'} - \frac{1}{v_{g0}} \frac{\partial}{\partial t'}, \tag{2.69}$$

$$\frac{\partial}{\partial t} = \frac{\partial}{\partial t'} \tag{2.70}$$

the transformed equation is

$$\frac{\partial \underline{A}(z',t')}{\partial z'} = 0. \tag{2.71}$$

Since z is equal to z' we keep z in the following.

If the spectrum of the pulse is broad enough, so that the second order term in (2.59) becomes important, the pulse will no longer keep its shape. When keeping in the dispersion relation terms up to second order it follows from (2.58) and (2.69,2.70)

$$\frac{\partial \underline{A}(z,t')}{\partial z} = \mathrm{j}\frac{k''}{2}\frac{\partial^2 \underline{A}(z,t')}{\partial t'^2}. \tag{2.72}$$

This is the first non trivial term in the wave equation for the envelope. Because of the superposition principle, the pulse can be thought of to be decomposed into wavepackets (sub-pulses) with different center frequencies. Now, the group velocity depends on the spectral component of the pulse, see Figure 2.10, which will lead to broadening or dispersion of the pulse.

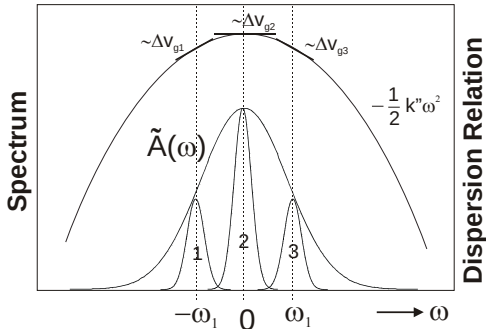

Figure 2.10: Decomposition of a pulse into wave packets with different center frequency. In a medium with dispersion the wavepackets move at different relative group velocity.

Fortunately, for a Gaussian pulse, the pulse propagation equation 2.72 can be solved analytically. The initial pulse is then of the form

$$\underline{E}(z = 0,t) = \underline{A}(z=0,t)e^{\mathrm{j}\omega_0 t} \tag{2.73}$$

$$\underline{A}(z = 0, t = t') = \underline{A}_0 \exp\left[-\frac{1}{2}\frac{t'^2}{\tau^2}\right] \tag{2.74}$$

Eq.(2.72) is most easily solved in the frequency domain since it transforms to

$$\frac{\partial \tilde{\underline{A}}(z,\omega)}{\partial z} = -\mathrm{j}\frac{k''\omega^2}{2}\tilde{\underline{A}}(z,\omega), \tag{2.75}$$

with the solution

$$\tilde{\underline{A}}(z,\omega) = \tilde{\underline{A}}(z=0,\omega)\exp\left[-\mathrm{j}\frac{k''\omega^2}{2}z\right]. \tag{2.76}$$

The pulse spectrum aquires a parabolic phase. Note, that here ω is the Fourier Transform variable conjugate to t' rather than t. The Gaussian pulse has the advantage that its Fourier transform is also a Gaussian

$$\tilde{\underline{A}}(z=0,\omega) = A_0\sqrt{2\pi}\tau\exp\left[-\frac{1}{2}\tau^2\omega^2\right] \tag{2.77}$$

and, therefore, in the spectral domain the solution at an arbitray propagation distance z is

$$\tilde{\underline{A}}(z,\omega) = A_0\sqrt{2\pi}\tau\exp\left[-\frac{1}{2}\left(\tau^2+\mathrm{j}k''z\right)\omega^2\right]. \tag{2.78}$$

The inverse Fourier transform is analogously

$$\underline{A}(z,t') = A_0\left(\frac{\tau^2}{(\tau^2+\mathrm{j}k''z)}\right)^{1/2}\exp\left[-\frac{1}{2}\frac{t'^2}{(\tau^2+\mathrm{j}k''z)}\right] \tag{2.79}$$

The exponent can be written as real and imaginary part and we finally obtain

$$\underline{A}(z,t') = A_0\left(\frac{\tau^2}{(\tau^2+\mathrm{j}k''z)}\right)^{1/2}\exp\left[-\frac{1}{2}\frac{\tau^2t'^2}{\left(\tau^4+\left(k''z\right)^2\right)}+\mathrm{j}\frac{1}{2}k''z\frac{t'^2}{\left(\tau^4+\left(k''z\right)^2\right)}\right] \tag{2.80}$$

As we see from Eq.(2.80) during propagation the FWHM of the Gaussian determined by

$$\exp\left[-\frac{\tau(\tau'_{FWHM}/2)^2}{\left(\tau^4+\left(k''z\right)^2\right)}\right] = 0.5 \tag{2.81}$$

changes from

$$\tau_{FWHM} = 2\sqrt{\ln 2}\,\tau \tag{2.82}$$

at the start to

$$\begin{aligned} \tau'_{FWHM} &= 2\sqrt{\ln 2}\,\tau\sqrt{1+\left(\frac{k''L}{\tau^2}\right)^2} \\ &= \tau_{FWHM}\sqrt{1+\left(\frac{k''L}{\tau^2}\right)^2} \end{aligned} \tag{2.83}$$

at $z = L$. For large stretching this result simplifies to

$$\tau'_{FWHM} = 2\sqrt{\ln 2}\,\left|\frac{k''L}{\tau}\right| \text{ for } \left|\frac{k''L}{\tau^2}\right| \gg 1. \tag{2.84}$$

The strongly dispersed pulse has a width equal to the difference in group delay over the spectral width of the pulse.

Figure 2.11 shows the evolution of the magnitude of the Gaussian wave packet during propagation in a medium which has no higher order dispersion in normalized units. The pulse spreads continuously.

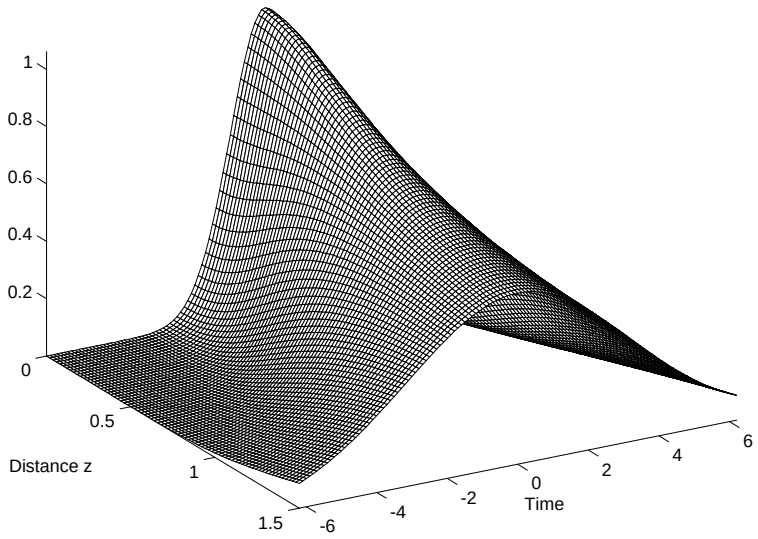

Figure 2.11: Magnitude of the complex envelope of a Gaussian pulse, $|\underline{A}(z,t')|$, in a dispersive medium.

As discussed before, the origin of this spreading is the group velocity dispersion (GVD), $k'' \neq 0$. The group velocity varies over the pulse spectrum significantly leading to a group delay dispersion (GDD) after a propagation distance $z = L$ of $k''L \neq 0$, for the different frequency components. This leads to the build-up of chirp in the pulse during propagation. We can understand this chirp by looking at the parabolic phase that develops over the pulse in time at a fixed propagation distance. The phase is, see Eq.(2.80)

$$\phi(z = L, t') = -\frac{1}{2}\arctan\left[\frac{k''L}{\tau^2}\right] + \frac{1}{2}k''L\frac{t'^2}{\left(\tau^4 + (k''L)^2\right)}. \tag{2.85}$$

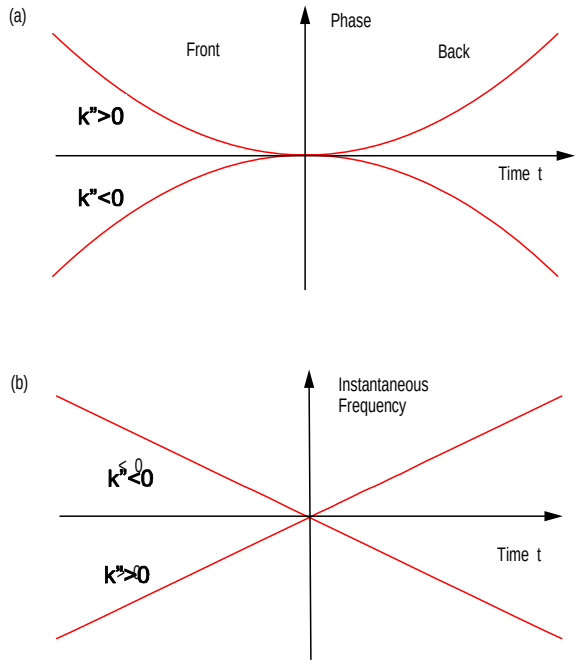

Figure 2.12: (a) Phase and (b) instantaneous frequency of a Gaussian pulse during propagation through a medium with positive or negative dispersion.

This parabolic phase, see Fig. 2.12 (a), can be understood as a localy varying frequency in the pulse, i.e. the derivative of the phase gives the

instantaneous frequency shift in the pulse with respect to the center frequency

$$\omega(z = L, t') = \frac{\partial}{\partial t'}\phi(L, t') = \frac{k''L}{\left(\tau^4 + (k''L)^2\right)}t' \tag{2.86}$$

see Fig.2.12 (b). The instantaneous frequency indicates that for a medium with positive GVD, ie. $k'' > 0$, the low frequencies are in the front of the pulse, whereas the high frequencies are in the back of the pulse, since the sub-pulses with lower frequencies travel faster than sub-pulses with higher frequencies. The opposite is the case for negative dispersive materials.

It is instructive for later purposes, that this behaviour can be completely understood from the center of mass motion of the sub-pulses, see Figure 2.10. Note, we can choose a set of sub-pulses, with such narrow bandwidth, that dispersion does not matter. In the time domain, these pulses are of course very long, because of the time bandwidth relationship. Nevertheless, since they all have different carrier frequencies, they interfere with each other in such a way that the superposition is a very narrow pulse. This interference, becomes destroyed during propagation, since the sub-pulses propagate at different speed, i.e. their center of mass propagates at different speed.

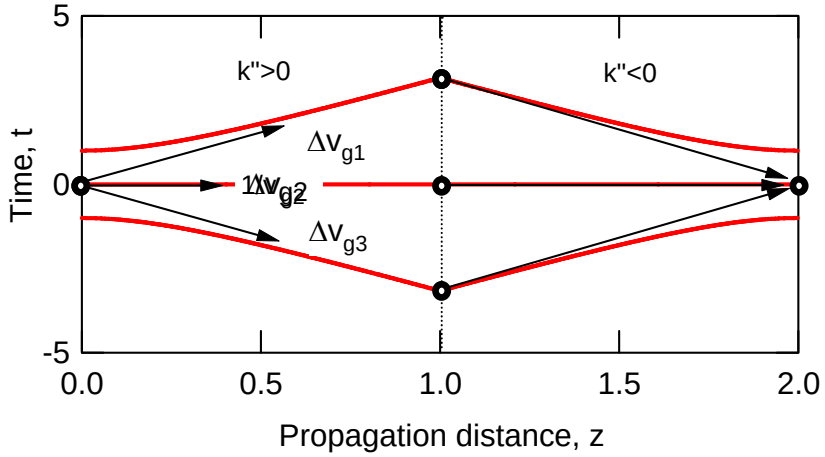

Figure 2.13: Pulse spreading by following the center of mass of sub-pulses according to Fig. 2.10. For $z < 1$, the pulses propagate in a medium with positive dispersion and for $z > 1$ in a medium with negative dispersion.

The differential group delay $\Delta T_g(\omega) = k'' L\omega$ of a sub-pulse with its center frequency ω different from 0, is due to its differential group velocity $\Delta v_g(\omega) = -v_{g0}\Delta T_g(\omega)/T_{g0} = -v_{g0}^2 k''\omega$. Note, that $T_{g0} = L/v_{g0}$. This is illustrated in Figure 2.13 by ploting the trajectory of the relative motion of the center of mass of each sub-pulse as a function of propagation distance, which asymptotically approaches the formula for the pulse width of the highly dispersed pulse Eq.(2.84). If we assume that the pulse propagates through a negative dispersive medium following the positive dispersive medium, the group velocity of each sub-pulse is reversed. The sub-pulses propagate towards each other until they all meet at one point (focus) to produce again a short and unchirped initial pulse, see Figure 2.13. This is a very powerful technique to understand dispersive wave motion and as we will see in the next section is the connection between ray optics and physical optics.

2.1.8 Loss and Gain

If the medium considered has loss, described by the imaginary part of the dielectric susceptibility, see (2.43) and Fig. 2.3, we can incorporate this loss into a complex refractive index

$$\underline{n}(\Omega) = n_r(\Omega) + \mathrm{j}n_i(\Omega) \tag{2.87}$$

via

$$\underline{n}(\Omega) = \sqrt{1 + \underline{\widetilde{\chi}}(\Omega)}. \tag{2.88}$$

For an optically thin medium, i.e. $\underline{\widetilde{\chi}} \ll 1$ the following approximation is very useful

$$\underline{n}(\Omega) \approx 1 + \frac{\underline{\widetilde{\chi}}(\Omega)}{2}. \tag{2.89}$$

As one can show (in Recitations) the complex susceptibility (2.43) can be approximated close to resonance, i.e. $\Omega \approx \Omega_0$, by the complex Lorentzian lineshape

$$\underline{\widetilde{\chi}}(\Omega) = \frac{-\mathrm{j}\chi_0}{1 + \mathrm{j}Q\frac{\Omega-\Omega_0}{\Omega_0}}, \tag{2.90}$$

where $\chi_0 = Q\frac{\omega_p^2}{2\Omega_0^2}$ will turn out to be related to the peak absorption of the line, which is proportional to the density of atoms, Ω_0 is the center frequency

and $\Delta\Omega = \frac{\Omega_0}{Q}$ is the half width half maximum (HWHM) linewidth of the transition. The real and imaginary part of the complex Lorentzian are

$$\widetilde{\chi}_r(\Omega) = \frac{-\chi_0 \frac{(\Omega-\Omega_0)}{\Delta\Omega}}{1+\left(\frac{\Omega-\Omega_0}{\Delta\Omega}\right)^2}, \tag{2.91}$$

$$\widetilde{\chi}_i(\Omega) = \frac{-\chi_0}{1+\left(\frac{\Omega-\Omega_0}{\Delta\Omega}\right)^2},. \tag{2.92}$$

In the derivation of the wave equation for the pulse envelope (2.61) in section 2.1.7, there was no restriction to a real refractive index. Therefore, the wave equation (2.61) also treats the case of a complex refractive index. If we assume a medium with the complex refractive index (2.89), then the wavenumber is given by

$$\underline{K}(\Omega) = \frac{\Omega}{c_0}\left(1+\frac{1}{2}\left(\widetilde{\chi}_r(\Omega)+\mathrm{j}\widetilde{\chi}_i(\Omega)\right)\right). \tag{2.93}$$

Since we introduced a complex wavenumber, we have to redefine the group velocity as the inverse derivative of the real part of the wavenumber with respect to frequency. At line center, we obtain

$$v_g^{-1} = \left.\frac{\partial K_r(\Omega)}{\partial\Omega}\right|_{\Omega_0} = \frac{1}{c_0}\left(1-\frac{\chi_0}{2}\frac{\Omega_0}{\Delta\Omega}\right). \tag{2.94}$$

Thus, for a narrow absorption line, $\chi_0 > 0$ and $\frac{\Omega_0}{\Delta\Omega} \gg 1$, the absolute value of the group velocity can become much larger than the velocity of light in vacuum. The opposite is true for an amplifying medium, $\chi_0 < 0$. There is nothing wrong with this finding, since the group velocity only describes the motion of the peak of a Gaussian wave packet, which is not a causal wave packet. A causal wave packet is identical to zero for some earlier time $t < t_0$, in some region of space. A Gaussian wave packet fills the whole space at any time and can be reconstructed by a Taylor expansion at any time. Therefore, the tachionic motion of the peak of such a signal does not contradict special relativity.

The imaginary part in the wave vector (2.93) leads with $K = \frac{\Omega}{c_0}$ to absorption

$$\alpha(\Omega) = -K\widetilde{\chi}_i(\Omega). \tag{2.95}$$

In the envelope equation (2.60) for a wavepacket with carrier frequency $\omega_0 = \Omega_0$ and $K_0 = \frac{\Omega_0}{c_0}$ the loss leads to a term of the form

$$\left.\frac{\partial \tilde{\underline{A}}(z,\omega)}{\partial z}\right|_{(loss)} = -\alpha(\Omega_0+\omega)\tilde{A}(z,\omega) = \frac{-\chi_0 K_0}{1+\left(\frac{\omega}{\Delta\Omega}\right)^2}\tilde{\underline{A}}(z,\omega). \tag{2.96}$$

In the time domain, we obtain up to second order in the inverse linewidth

$$\left.\frac{\partial \underline{A}(z,t')}{\partial z}\right|_{(loss)} = -\chi_0 K_0\left(1+\frac{1}{\Delta\Omega^2}\frac{\partial^2}{\partial t^2}\right)\underline{A}(z,t'), \tag{2.97}$$

which corresponds to a parabolic approximation of the line shape at line center, (Fig. 2.3). As we will see later, for an amplifying optical transition we obtain a similar equation. We only have to replace the loss by gain

$$\left.\frac{\partial \underline{A}(z,t')}{\partial z}\right|_{(gain)} = g\left(1+\frac{1}{\Omega_g^2}\frac{\partial^2}{\partial t^2}\right)\underline{A}(z,t'), \tag{2.98}$$

where $g = -\chi_0 K_0$ is the peak gain at line center per unit length and Ω_g is the HWHM linewidth of a transition providing gain.

2.1.9 Sellmeier Equation and Kramers-Kroenig Relations

The linear susceptibility is the frequency response or impulse response of a linear system to an applied electric field, see Eq.(2.41). For a real physical system this response is causal, and therefore real and imaginary parts obey Kramers-Kroenig Relations

$$\chi_r(\Omega) = \frac{2}{\pi}\int_0^\infty \frac{\omega\chi_i(\omega)}{\omega^2-\Omega^2}d\omega = n_r^2(\Omega)-1, \tag{2.99}$$

$$\chi_i(\Omega) = -\frac{2}{\pi}\int_0^\infty \frac{\Omega\chi_r(\omega)}{\omega^2-\Omega^2}d\omega. \tag{2.100}$$

For optical media these relations have the consequence that the refractive index and absorption of a medium are not independent, which can often be exploited to compute the index from absorption data or the other way

around. The Kramers-Kroenig Relations also give us a good understanding of the index variations in transparent media, which means the media are used in a frequency range far away from resonances. Then the imaginary part of the susceptibility related to absorption can be approximated by

$$\chi_i(\Omega) = \sum_i A_i \delta(\omega - \omega_i) \tag{2.101}$$

and the Kramers-Kroenig relation results in the Sellmeier Equation for the refractive index

$$n^2(\Omega) = 1 + \sum_i A_i \frac{\omega_i}{\omega_i^2 - \Omega^2} = 1 + \sum_i a_i \frac{\lambda}{\lambda^2 - \lambda_i^2}. \tag{2.102}$$

This formula is very useful in fitting the refractive index of various media over a large frequency range with relatively few coefficients. For example Table 2.3 shows the sellmeier coefficients for fused quartz and sapphire.

	Fused Quartz	Sapphire
a_1	0.6961663	1.023798
a_2	0.4079426	1.058364
a_3	0.8974794	5.280792
λ_1^2	$4.679148 \cdot 10^{-3}$	$3.77588 \cdot 10^{-3}$
λ_2^2	$1.3512063 \cdot 10^{-2}$	$1.22544 \cdot 10^{-2}$
λ_3^2	$0.9793400 \cdot 10^{2}$	$3.213616 \cdot 10^{2}$

Table 2.3: Table with Sellmeier coefficients for fused quartz and sapphire.

In general, each absorption line contributes a corresponding index change to the overall optical characteristics of a material, see Fig. 2.14. A typical situation for a material having resonances in the UV and IR, such as glass, is shown in Fig. 2.15. As Fig. 2.15 shows, due to the Lorentzian line shape, that outside of an absorption line the refractive index is always decreasing as a function of wavelength. This behavior is called normal dispersion and the opposite behavior abnormal dispersion.

$$\frac{dn}{d\lambda} < 0 : \text{normal dispersion (blue refracts more than red)}$$
$$\frac{dn}{d\lambda} > 0 : \text{abnormal dispersion}$$

This behavior is also responsible for the mostly positive group delay dispersion over the transparency range of a material, as the group velocity or group delay dispersion is closely related to $\frac{dn}{d\lambda}$. Fig.2.16 shows the transparency range of some often used media.

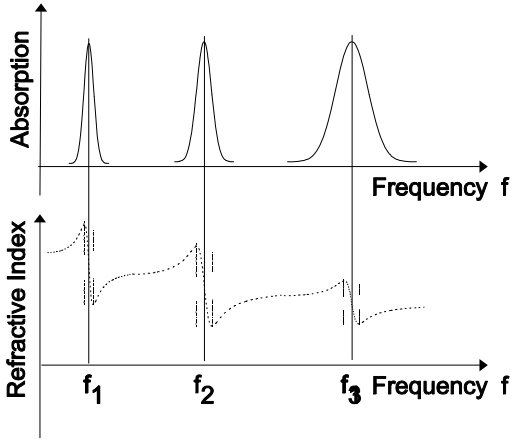

Figure 2.14: Each absorption line must contribute to an index change via the Kramers-Kroenig relations.

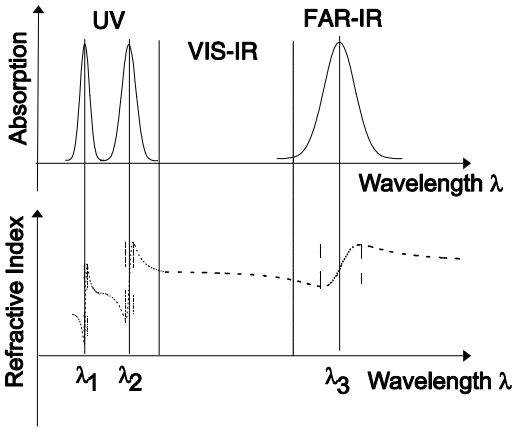

Figure 2.15: Typcial distribution of absorption lines in a medium transparent in the visible.

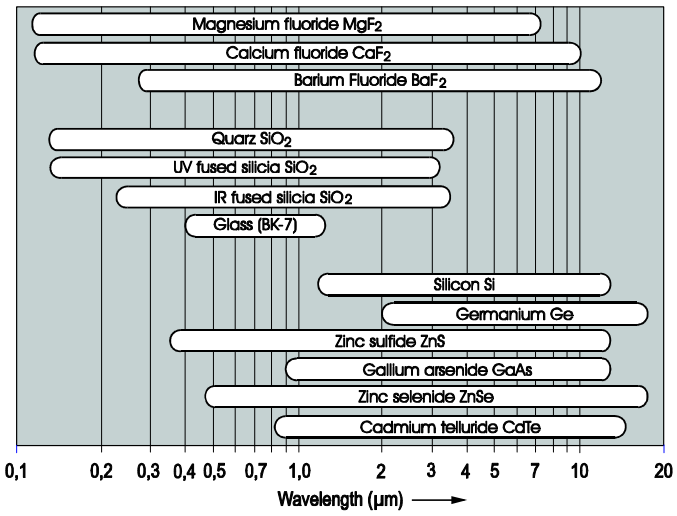

Figure 2.16: Transparency range of some materials according to [6], p. 175.

Often the dispersion GVD and GDD needs to be calculated from the Sellmeier equation, i.e. $n(\lambda)$. The corresponding quantities are listed in Table 2.4. The computations are done by substituting the frequency with the wavelength.

Dispersion Characteristic	Definition	Comp. from $n(\lambda)$
medium wavelength: λ_n	$\frac{\lambda}{n}$	$\frac{\lambda}{n(\lambda)}$
wavenumber: k	$\frac{2\pi}{\lambda_n}$	$\frac{2\pi}{\lambda}n(\lambda)$
phase velocity: v_p	$\frac{\omega}{k}$	$\frac{c_0}{n(\lambda)}$
group velocity: v_g	$\frac{d\omega}{dk}; d\lambda = \frac{-\lambda^2}{2\pi c_0}d\omega$	$\frac{c_0}{n}\left(1-\frac{\lambda}{n}\frac{dn}{d\lambda}\right)^{-1}$
group velocity dispersion: GVD	$\frac{d^2k}{d\omega^2}$	$\frac{\lambda^3}{2\pi c_0^2}\frac{d^2n}{d\lambda^2}$
group delay: $T_g = \frac{L}{v_g} = \frac{d\phi}{d\omega}$	$\frac{d\phi}{d\omega} = \frac{d(kL)}{d\omega}$	$\frac{n}{c_0}\left(1-\frac{\lambda}{n}\frac{dn}{d\lambda}\right)L$
group delay dispersion: GDD	$\frac{dT_g}{d\omega} = \frac{d^2(kL)}{d\omega^2}$	$\frac{\lambda^3}{2\pi c_0^2}\frac{d^2n}{d\lambda^2}L$

Table 2.4: Table with important dispersion characteristics and how to compute them from the wavelength dependent refractive index $n(\lambda)$.

2.2 Electromagnetic Waves and Interfaces

Many microwave and optical devices are based on the characteristics of electromagnetic waves undergoing reflection or transmission at interfaces between media with different electric or magnetic properties characterized by ϵ and μ, see Fig. 2.17. Without restriction we can assume that the interface is the (x-y-plane) and the plane of incidence is the (x-z-plane). An arbitrary incident plane wave can always be decomposed into two components. One component has its electric field parallel to the interface between the media, i.e. it is polarized parallel to the interface and it is called the transverse electric (TE)-wave or also s-polarized wave. The other component is polarized in the plane of incidence and its magnetic field is in the plane of the interface between the media. This wave is called the TM-wave or also p-polarized wave. The most general case of an incident monochromatic TEM-wave is a linear superposition of a TE and a TM-wave.

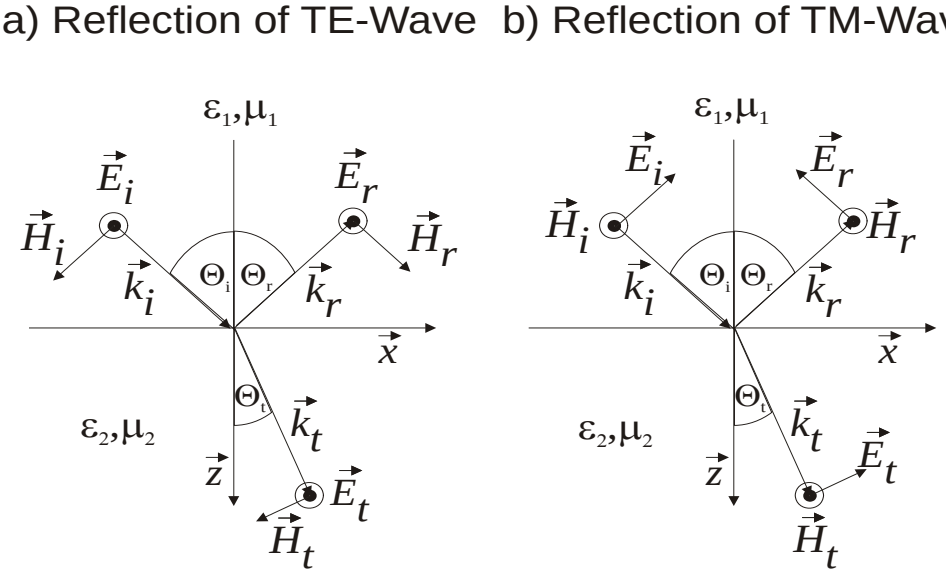

Figure 2.17: a) Reflection of a TE-wave at an interface, b) Reflection of aTM-wave at an interface

The fields for both cases are summarized in table 2.5

TE-wave	TM-wave
$\vec{\underline{E}}_i = \underline{E}_i \; e^{\mathrm{j}(\omega t - \vec{k}_i \cdot \vec{r})} \vec{e}_y$	$\vec{\underline{E}}_i = -\underline{E}_i \; e^{\mathrm{j}(\omega t - \vec{k}_i \cdot \vec{r})} \vec{e}_i$
$\vec{\underline{H}}_i = \underline{H}_i \; e^{\mathrm{j}(\omega t - \vec{k}_i \cdot \vec{r})} \vec{h}_i$	$\vec{\underline{H}}_i = \underline{H}_i \; e^{\mathrm{j}(\omega t - \vec{k}_i \cdot \vec{r})} \vec{e}_y$
$\vec{\underline{E}}_r = \underline{E}_r \; e^{\mathrm{j}(\omega t - \vec{k}_r \cdot \vec{r})} \vec{e}_y$	$\vec{\underline{E}}_r = \underline{E}_r \; e_r^{\mathrm{j}(\omega t - \vec{k}_r \cdot \vec{r})} \vec{e}_r$
$\vec{\underline{H}}_r = \underline{H}_r \; e^{\mathrm{j}(\omega t - \vec{k}_r \cdot \vec{r})} \vec{h}_r$	$\vec{\underline{H}}_r = \underline{E}_r \; e^{\mathrm{j}(\omega t - \vec{k}_r \cdot \vec{r})} \vec{e}_y$
$\vec{\underline{E}}_t = \underline{E}_t \; e^{\mathrm{j}(\omega t - \vec{k}_t \cdot \vec{r})} \vec{e}_y$	$\vec{\underline{E}}_t = \underline{E}_t \; e^{\mathrm{j}(\omega t - \vec{k}_t \cdot \vec{r})} \vec{e}_t$
$\vec{\underline{H}}_t = \underline{H}_t \; e^{\mathrm{j}(\omega t - \vec{k}_t \cdot \vec{r})} \vec{h}_t$	$\vec{\underline{H}}_t = \underline{H}_t \; e^{\mathrm{j}(\omega t - \vec{k}_t \cdot \vec{r})} \vec{e}_y$

Table 2.5: Electric and magnetic fields for TE- and TM-waves.

with wave vectors of the waves given by

$$\begin{aligned} k_i &= k_r = k_0 \sqrt{\epsilon_1 \mu_1}, \\ k_t &= k_0 \sqrt{\epsilon_2 \mu_2}, \\ \vec{k}_{i,t} &= k_{i,t} \left(\sin\theta_{i,t} \; \vec{e}_x + \cos\theta_{i,t} \; \vec{e}_z \right), \\ \vec{k}_r &= k_i \left(\sin\theta_r \; \vec{e}_x - \cos\theta_r \; \vec{e}_z \right), \end{aligned}$$

and unit vectors given by

$$\begin{aligned} \vec{h}_{i,t} &= -\cos\theta_{i,t} \; \vec{e}_x + \sin\theta_{i,t} \; \vec{e}_z, \\ \vec{h}_r &= \cos\theta_r \; \vec{e}_x + \sin\theta_r \; \vec{e}_z, \\ \vec{e}_{i,t} &= -\vec{h}_{i,t} = \cos\theta_{i,t} \; \vec{e}_x - \sin \; \theta_{i,t} \; \vec{e}_z, \\ \vec{e}_r &= -\vec{h}_r = -\cos\theta_r \; \vec{e}_x - \sin\theta_r \; \vec{e}_z. \end{aligned}$$

2.2.1 Boundary Conditions and Snell's law

From 6.013, we know that Stoke's and Gauss' Law for the electric and magnetic fields require constraints on some of the field components at media boundaries. In the absence of surface currents and charges, the tangential electric and magnetic fields as well as the normal dielectric and magnetic fluxes have to be continuous when going from medium 1 into medium 2 for all times at each point along the surface, i.e. $z = 0$

$$E/H_{i,x/y} e^{\mathrm{j}(\omega t - k_{i,x} x)} + E/H_{r,x/y} e^{\mathrm{j}(\omega t - k_{r,x} x)} = E/H_{i,x/y} e^{\mathrm{j}(\omega t - k_{t,x} x)}. \qquad (2.103)$$

This equation can only be fulfilled at all times if and only if the x-component of the k-vectors for the reflected and transmitted wave are equal to (match)

the corresponding component of the incident wave

$$k_{i,x} = k_{r,x} = k_{t,x} \tag{2.104}$$

This phase matching condition is shown in Fig. 2.18 for the case $\sqrt{\epsilon_2\mu_2} > \sqrt{\epsilon_1\mu_1}$ *or* $k_t > k_i$.

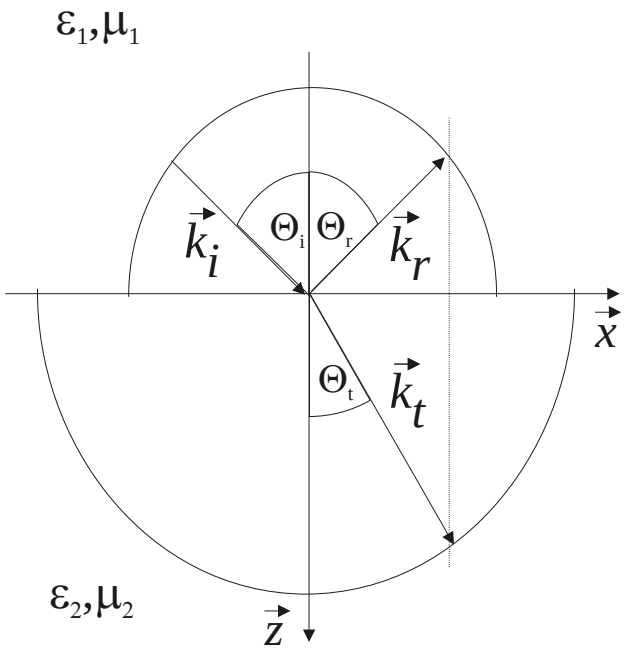

Figure 2.18: Phase matching condition for reflected and transmitted wave

The phase matching condition Eq(2.104) results in $\theta_r = \theta_i = \theta_1$ and Snell's law for the angle $\theta_t = \theta_2$ of the transmitted wave

$$\sin\theta_t = \frac{\sqrt{\epsilon_1\mu_1}}{\sqrt{\epsilon_2\mu_2}} \sin\theta_i \tag{2.105}$$

or for the case of non magnetic media with $\mu_1 = \mu_2 = \mu_0$

$$\sin\theta_t = \frac{n_1}{n_2} \sin\theta_i \tag{2.106}$$

2.2.2 Measuring Refractive Index with Minimum Deviation

Snell's law can be used for measuring the refractive index of materials. Consider a prism prepared from a material with unknown refractive index $n(\lambda)$, see Fig. 2.19 (a).

Figure 2.19: (a) Beam propagating through a prism. (b) For the case of minimum deviation [3] p. 65.

The prism is mounted on a rotation stage as shown in Fig. 2.20. The angle of incidence α is then varied with a fixed incident beam path and the transmitted light is observed on a screen. If one starts of with normal incidence on the first prism surface one notices that after turning the prism one goes through a minium for the deflection angle of the beam. This becomes obvious from Fig. 2.19 (b). There is an angle of incidence α where the beam path through the prism is symmetric. If the input angle is varied around this point, it would be identical to exchange the input and output beams. From that we conclude that the deviation δ must go through an extremum at the symmetry point, see Figure 2.21. It can be shown (Recitations), that the refractive index is then determined by

$$n = \frac{\sin \frac{\alpha(\delta_{\min})+\delta_{\min}}{2}}{\sin \frac{\alpha(\delta_{\min})}{2}}. \tag{2.107}$$

If the measurement is repeated for various wavelength of the incident radiation the complete wavelength dependent refractive index is characterized, see for example, Fig. 2.22.

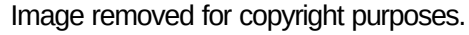

Figure 2.20: Refraction of a Prism with n=1.731 for different angles of incidence alpha. The angle of incidence is stepwise increased by rotating the prism clockwise. The angle of transmission first increases. After the angle for minimum deviation is reached the transmission angle starts to decrease [3] p67.

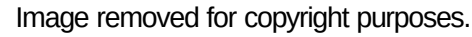

Figure 2.21: Deviation versus incident angel [1]

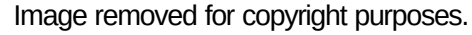

Figure 2.22: Refractive index as a function of wavelength for various media transmissive in the visible [1], p42.

2.2.3 Fresnel Reflection

After understanding the direction of the reflected and transmitted light, formulas for how much light is reflected and transmitted are derived by evaluating the boundary conditions for the TE and TM-wave. According to Eqs.(2.103) and (2.104) we obtain for the continuity of the tangential E and H fields:

TE-wave (s-pol.)	TM-wave (p-pol.)
$\underline{E}_i + \underline{E}_r = \underline{E}_t$	$\underline{E}_i \cos\theta_i - \underline{E}_r \cos\theta_r = \underline{E}_t \cos\theta_t$
$\underline{H}_i \cos\theta_i - \underline{H}_r \cos\theta_r = \underline{H}_t \cos\theta_t$	$\underline{H}_i + \underline{H}_r = \underline{H}_t$

(2.108)

Introducing the characteristic impedances in both half spaces $\underline{Z}_{1/2} = \sqrt{\frac{\mu_0\mu_{1/2}}{\epsilon_0\epsilon_{1/2}}}$, and the impedances that relate the tangential electric and magnetic field components $\underline{Z}_{1/2}^{TE/TM}$ in both half spaces the boundary conditions can be rewritten in terms of the electric or magnetic field components.

TE-wave (s-pol.)	TM-wave (p-pol.)
$\underline{Z}_{1/2}^{TE} = \frac{\underline{E}_{i/t}}{\underline{H}_{i/t} \cos\theta_{i/t}} = \frac{\underline{Z}_{1/2}}{\cos\theta_{1/2}}$	$\underline{Z}_{1/2}^{TM} = \frac{\underline{E}_{i/t} \cos\theta_{i/t}}{\underline{H}_{i/t}} = \underline{Z}_{1/2} \cos\theta_{1/2}$
$\underline{E}_i + \underline{E}_r = \underline{E}_t$	$\underline{H}_i - \underline{H}_r = \frac{\underline{Z}_2^{TM}}{\underline{Z}_1^{TM}} \underline{H}_t$
$\underline{E}_i - \underline{E}_r = \frac{\underline{Z}_1^{TE}}{\underline{Z}_2^{TE}} \underline{E}_t$	$\underline{H}_i + \underline{H}_r = \underline{H}_t$

(2.109)

Amplitude Reflection and Transmission coefficients

From these equations we can easily solve for the reflected and transmitted wave amplitudes in terms of the incident wave amplitudes. By dividing both equations by the incident wave amplitudes we obtain for the amplitude reflection and transmission coeffcients. Note, that reflection and transmission coefficients are defined in terms of the electric fields for the TE-wave and in terms of the magnetic fields for the TM-wave.

TE-wave (s-pol.)	TM-wave (p-pol.)
$\underline{r}^{TE} = \frac{\underline{E}_r}{\underline{E}_i}; \underline{t}^{TE} = \frac{\underline{E}_t}{\underline{E}_i}$	$\underline{r}^{TM} = \frac{\underline{H}_r}{\underline{H}_i}; \underline{t}^{TM} = \frac{\underline{H}_t}{\underline{H}_i}$
$1 + \underline{r}^{TE} = \underline{t}^{TE}$	$1 - \underline{r}^{TM} = \frac{\underline{Z}_2^{TM}}{\underline{Z}_1^{TM}} \underline{t}^{TM}$
$1 - \underline{r}^{TE} = \frac{\underline{Z}_1^{TE}}{\underline{Z}_2^{TE}} \underline{t}^{TE}$	$1 + \underline{r}^{TM} = \underline{t}^{TM}$

(2.110)

or in both cases the amplitude transmission and reflection coefficients are

$$\underline{t}^{TE/TM} = \frac{2}{1+\frac{\underline{Z}_{1/2}^{TE/TM}}{\underline{Z}_{2/1}^{TE/TM}}} = \frac{2\underline{Z}_{2/1}^{TE/TM}}{\underline{Z}_1^{TE/TM}+\underline{Z}_2^{TE/TM}} \tag{2.111}$$

$$\underline{r}^{TE/TM} = \frac{\underline{Z}_{2/1}^{TE/TM}-\underline{Z}_{1/2}^{TE/TM}}{\underline{Z}_1^{TE/TM}+\underline{Z}_2^{TE/TM}} \tag{2.112}$$

Despite the simplicity of these formulas, they describe already an enormous wealth of phenomena. To get some insight, consider the case of purely dielectric and lossless media characterized by its real refractive indices n_1 and n_2. Then Eqs.(2.111) and (2.112) simplify for the TE and TM case to

TE-wave (s-pol.)	TM-wave (p-pol.)
$\underline{Z}_{1/2}^{TE} = \frac{Z_{1/2}}{\cos\theta_{1/2}} = \frac{Z_0}{n_{1/2}\cos\theta_{1/2}}$	$\underline{Z}_{1/2}^{TM} = \underline{Z}_{1/2}\cos\theta_{1/2} = \frac{Z_0}{n_{1/2}}\cos\theta_{1/2}$
$\underline{r}^{TE} = \frac{n_1\cos\theta_1 - n_2\cos\theta_2}{n_1\cos\theta_1 + n_2\cos\theta_2}$	$\underline{r}^{TM} = \frac{\frac{n_2}{\cos\theta_2}-\frac{n_1}{\cos\theta_1}}{\frac{n_2}{\cos\theta_2}+\frac{n_1}{\cos\theta_1}}$
$\underline{t}^{TE} = \frac{2n_1\cos\theta_1}{n_1\cos\theta_1 + n_2\cos\theta_2}$	$\underline{t}^{TM} = \frac{2\frac{n_2}{\cos\theta_2}}{\frac{n_2}{\cos\theta_2}+\frac{n_1}{\cos\theta_1}}$

(2.113)

Figure 2.23 shows the evaluation of Eqs.(2.113) for the case of a reflection at the interface of air and glass with $n_2 > n_1$ and ($n_1 = 1$, $n_2 = 1.5$).

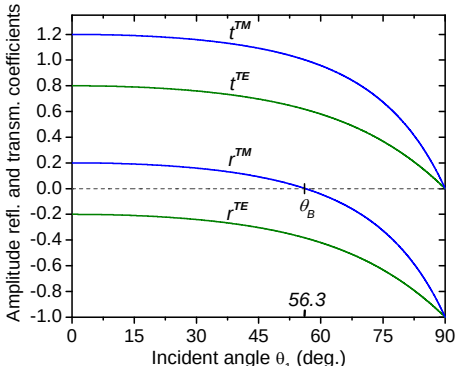

Figure 2.23: The amplitude coefficients of reflection and transmission as a function of incident angle. These correspond to external reflection $n_2 > n_1$ at an air-glas interface ($n_1 = 1$, $n_2 = 1.5$).

For TE-polarized light the reflected light changes sign with respect to the incident light (reflection at the optically more dense medium). This is not so for TM-polarized light under close to normal incidence. It occurs only for angles larger than θ_B, which is called the Brewster angle. So for TM-polarized light the amplitude reflection coefficient is zero at the Brewster angle. This phenomena will be discussed in more detail later.

This behavior changes drastically if we consider the opposite arrangement of media, i.e. we consider the glass-air interface with $n_1 > n_2$, see Figure 2.24. Then the TM-polarized light experiences a π-phase shift upon reflection close to normal incidence. For increasing angle of incidence this reflection coefficient goes through zero at the Brewster angle $\theta_B^{'}$ different from before. However, for large enough angle of incidence the reflection coefficient reaches magnitude 1 and stays there. This phenomenon is called total internal reflection and the angle where this occurs first is the critical angle for total internal reflection, θ_{tot}. Total internal reflection will be discussed in more detail later.

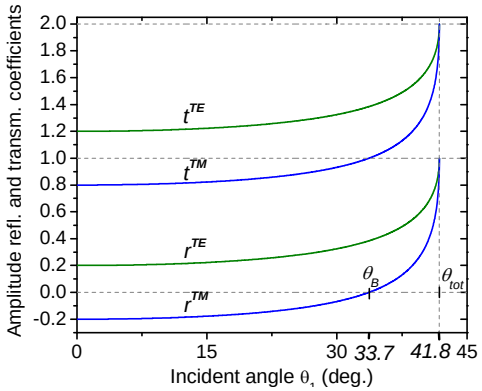

Figure 2.24: The amplitude coefficients of reflection and transmission as a function of incident angle. These correspond to internal reflection $n_1 > n_2$ at a glas-air interface ($n_1 = 1.5$, $n_2 = 1$).

Power reflection and transmission coefficients

Often we are not interested in the amplitude but rather in the optical power reflected or transmitted in a beam of finite size, see Figure 2.25.

Figure 2.25: Reflection and transmission of an incident beam of finite size [1].

Note, that to get the power in a beam of finite size, we need to integrated the corresponding Poynting vector over the beam area, which means multiplication by the beam crosssectional area for a homogenous beam. Since the angle of incidence and reflection are equal, $\theta_i = \theta_r = \theta_1$ this beam crosssectional area drops out in reflection

$$R^{TE/TM} = \frac{I_r^{TE/TM} A \cos\theta_i}{I_i^{TE/TM} A \cos\theta_r} = \left|\underline{r}^{TE/TM}\right|^2 = \left|\frac{\underline{Z}_2^{TE/TM} - \underline{Z}_1^{TE/TM}}{\underline{Z}_1^{TE/TM} + \underline{Z}_2^{TE/TM}}\right|^2 \quad (2.114)$$

However, due to the different angles for the incident and the transmitted beam $\theta_t = \theta_2 \neq \theta_1$, we arrive at

$$\begin{aligned} T^{TE/TM} &= \frac{I_t^{TE/TM} A \cos\theta_t}{I_i^{TE/TM} A \cos\theta_r} \\ &= \frac{\cos\theta_2}{\cos\theta_1} \mathrm{Re}\left\{\frac{1}{\underline{Z}_{2/1}}\right\} \mathrm{Re}\left\{\frac{1}{\underline{Z}_{1/2}}\right\}^{-1} \left|\underline{t}^{TE/TM}\right|^2 . \end{aligned} \quad (2.115)$$

Using in the case of TE-polarization $\frac{\underline{Z}_{1/2}}{\cos\theta_{1/2}} = \underline{Z}_{1/2}^{TE}$ and analogously for TM-polarization $\underline{Z}_{1/2}\cos\theta_{1/2} = \underline{Z}_{1/2}^{TM}$, we obtain

$$T^{TE/TM} = \mathrm{Re}\left\{\frac{1}{\underline{Z}_{1/2}^{TE/TM}}\right\}^{-1} \mathrm{Re}\left\{\frac{4\underline{Z}_{2/1}^{TE/TM}}{\left|\underline{Z}_{1}^{TE/TM} + \underline{Z}_{2}^{TE/TM}\right|^2}\right\} \tag{2.116}$$

Note, for the case where the characteristic impedances are complex this can not be further simplified. If the characteristic impedances are real, i.e. the media are lossless, the transmission coefficient simplifies to

$$T^{TE/TM} = \frac{4Z_{1/2}^{TE/TM} Z_{2/1}^{TE/TM}}{\left(Z_{1}^{TE/TM} + Z_{2}^{TE/TM}\right)^2}. \tag{2.117}$$

To summarize for lossless media the power reflection and transmission coefficients are

TE-wave (s-pol.)	TM-wave (p-pol.)
$Z_{1/2}^{TE} = \frac{Z_{1/2}}{\cos\theta_{1/2}} = \frac{Z_0}{n_{1/2}\cos\theta_{1/2}}$	$Z_{1/2}^{TM} = Z_{1/2}\cos\theta_{1/2} = \frac{Z_0}{n_{1/2}}\cos\theta_{1/2}$
$R^{TE} = \left\lvert\frac{n_2\cos\theta_2 - n_1\cos\theta_1}{n_1\cos\theta_1 + n_2\cos\theta_2}\right\rvert^2$	$R^{TM} = \left\lvert\frac{\frac{n_2}{\cos\theta_2} - \frac{n_1}{\cos\theta_1}}{\frac{n_2}{\cos\theta_2} + \frac{n_1}{\cos\theta_1}}\right\rvert^2$
$T^{TE} = \frac{4n_1\cos\theta_1 n_2\cos\theta_2}{\lvert n_1\cos\theta_1 + n_2\cos\theta_2\rvert^2}$	$T^{TM} = \frac{4\frac{n_2}{\cos\theta_2}\frac{n_1}{\cos\theta_1}}{\lvert\frac{n_2}{\cos\theta_2} + \frac{n_1}{\cos\theta_1}\rvert^2}$
$T^{TE} + R^{TE} = 1$	$T^{TM} + R^{TM} = 1$

(2.118)

A few phenomena that occur upon reflection at surfaces between different media are especially noteworthy and need a more indepth discussion because they enhance or enable the construction of many optical components and devices.

2.2.4 Brewster's Angle

As Figures 2.23 and 2.24 already show, for light polarized parallel to the plane of incidence, p-polarized light, the reflection coefficient vanishes at a given angle θ_B, called the Brewster angle. Using Snell's Law Eq.(2.106),

$$\frac{n_2}{n_1} = \frac{\sin\theta_1}{\sin\theta_2}, \tag{2.119}$$

we can rewrite the reflection and transmission coefficients in Eq.(2.118) only in terms of the angles. For example, we find for the reflection coefficient

$$R^{TM} = \left| \frac{\frac{n_2}{n_1} - \frac{\cos\theta_2}{\cos\theta_1}}{\frac{n_2}{n_1} + \frac{\cos\theta_2}{\cos\theta_1}} \right|^2 = \left| \frac{\frac{\sin\theta_1}{\sin\theta_2} - \frac{\cos\theta_2}{\cos\theta_1}}{\frac{\sin\theta_1}{\sin\theta_2} + \frac{\cos\theta_2}{\cos\theta_1}} \right|^2 \tag{2.120}$$

$$= \left| \frac{\sin 2\theta_1 - \sin 2\theta_2}{\sin 2\theta_1 + \sin 2\theta_2} \right|^2 \tag{2.121}$$

where we used in the last step in addition the relation $\sin 2\alpha = 2\sin\alpha\cos\alpha$. Thus by forcing $R^{TM} = 0$, the Brewster angle is reached for

$$\sin 2\theta_{1,B} - \sin 2\theta_{2,B} = 0 \tag{2.122}$$

or

$$2\theta_{1,B} = \pi - 2\theta_{2,B} \text{ or } \theta_{1,B} + \theta_{2,B} = \frac{\pi}{2} \tag{2.123}$$

This relation is illustrated in Figure 2.26. The reflected and transmitted beams are orthogonal to each other, so that the dipoles induced in the medium by the transmitted beam, shown as arrows in Fig. 2.26, can not radiate into the direction of the reflected beam. This is the physical origin of the zero in the reflection coefficient, only possible for a p-polarized or TM-wave.

The relation (2.123) can be used to express the Brewster angle as a function of the refractive indices, because if we substitute (2.123) into Snell's law we obtain

$$\begin{aligned} \frac{\sin\theta_1}{\sin\theta_2} &= \frac{n_2}{n_1} \\ \frac{\sin\theta_{1,B}}{\sin\left(\frac{\pi}{2} - \theta_{1,B}\right)} &= \frac{\sin\theta_{1,B}}{\cos\theta_{1,B}} = \tan\theta_{1,B}, \end{aligned}$$

or

$$\tan\theta_{1,B} = \frac{n_2}{n_1}. \tag{2.124}$$

Using the Brewster angle condition one can insert an optical component with a refractive index $n \neq 1$ into a TM-polarized beam in air without having reflections, see Figure 2.27. Note, this is not possible for a TE-polarized beam.

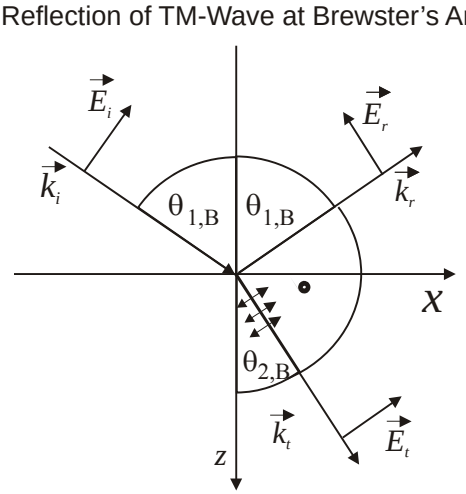

Figure 2.26: Conditions for reflection of a TM-Wave at Brewster's angle. The reflected and transmitted beams are orthogonal to each other, so that the dipoles excited in the medium by the transmitted beam can not radiate into the direction of the reflected beam.

Image removed for copyright purposes.

Figure 2.27: A plate under Brewster's angle does not reflect TM-light. The plate can be used as a window to introduce gas filled tubes into a laser beam without insertion loss (ideally), [6] p. 209.

2.2.5 Total Internal Reflection

Another striking phenomenon, see Figure 2.24, occurs for the case where the beam hits the surface from the side of the optically denser medium, i.e. $n_1 > n_2$. There is obviously a critical angle of incidence, beyond which all light is reflected. How can that occur? This is easy to understand from the phase matching diagram at the surface, see Figure 2.18, which is redrawn for this case in Figure 2.28.

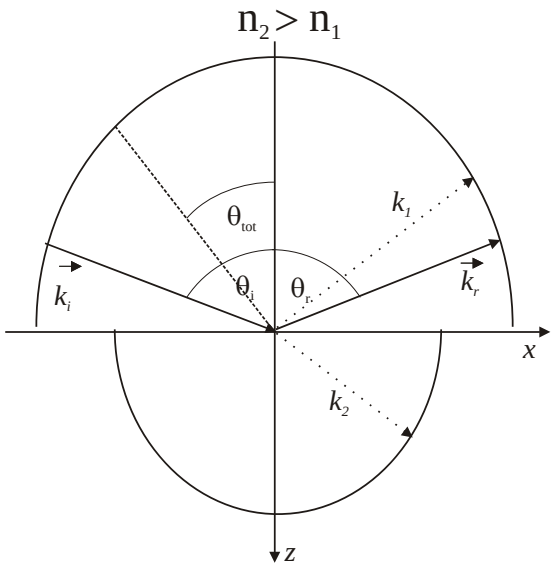

Figure 2.28: Phase matching diagram for total internal reflection.

There is no real wavenumber in medium 2 possible as soon as the angle of incidence becomes larger than the critical angle for total internal reflection

$$\theta_i > \theta_{tot} \tag{2.125}$$

with

$$\sin\theta_{tot} = \frac{n_2}{n_1}. \tag{2.126}$$

Figure 2.29 shows the angle of refraction and incidence for the two cases of external and internal reflection, when the angle of incidence approaches the critical angle.

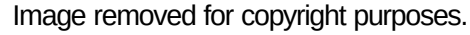

Figure 2.29: Relation between angle of refraction and incidence for external refraction and internal refraction ([6], p. 11).

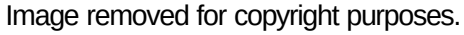

Figure 2.30: Relation between angle of refraction and incidence for external refraction and internal refraction ([1], p. 81).

Total internal reflection enables broadband reflectors. Figure 2.30 shows

again what happens when the critical angle of reflection is surpassed. Figure 2.31 shows how total internal reflection can be used to guide light via reflection at a prism or by multiple reflections in a waveguide.

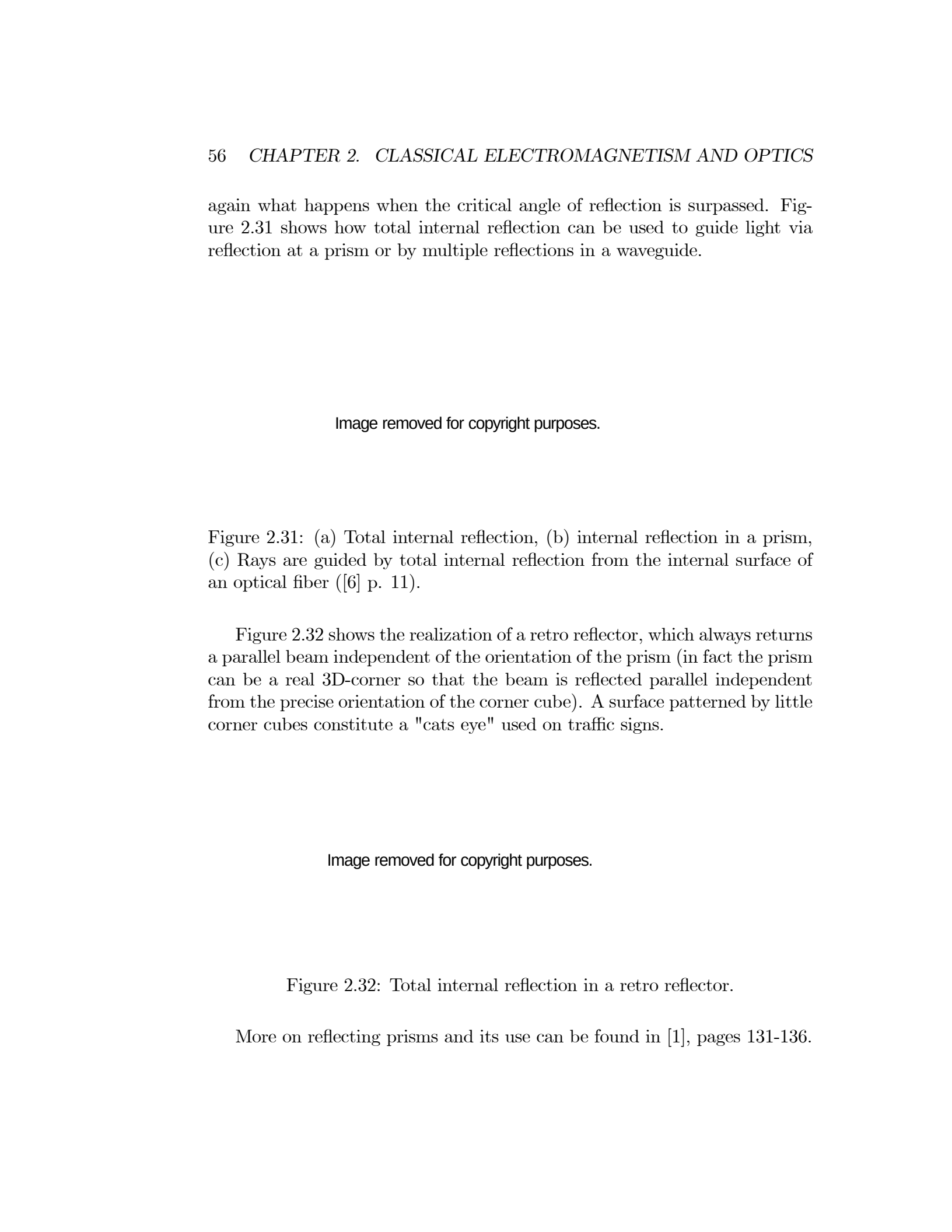

Figure 2.31: (a) Total internal reflection, (b) internal reflection in a prism, (c) Rays are guided by total internal reflection from the internal surface of an optical fiber ([6] p. 11).

Figure 2.32 shows the realization of a retro reflector, which always returns a parallel beam independent of the orientation of the prism (in fact the prism can be a real 3D-corner so that the beam is reflected parallel independent from the precise orientation of the corner cube). A surface patterned by little corner cubes constitute a "cats eye" used on traffic signs.

Figure 2.32: Total internal reflection in a retro reflector.

More on reflecting prisms and its use can be found in [1], pages 131-136.

Evanescent Waves

What is the field in medium 2 when total internal reflection occurs? Is it identical to zero? It turns out phase matching can still occur if the propagation constant in z-direction becomes imaginary, $k_{2z} = -\mathrm{j}\kappa_{2z}$, because then we can fulfill the wave equation in medium 2. This is equivalent to the dispersion relation

$$k_{2x}^2 + k_{2z}^2 = k_2^2,$$

or with $k_{2x} = k_{1x} = k_1 \sin\theta_1$, we obtain for the imaginary wavenumber

$$\begin{aligned} \kappa_{2z} &= \sqrt{k_1^2 \sin^2\theta_1 - k_2^2}, && (2.127) \\ &= k_1 \sqrt{\sin^2\theta_1 - \sin^2\theta_{tot}}. && (2.128) \end{aligned}$$

The electric field in medium 2 is then, for the example for a TE-wave, given by

$$\begin{aligned} \underline{\vec{E}}_t &= \underline{E}_t \, \vec{e}_y \, e^{\mathrm{j}(\omega t - \vec{k}_t \cdot \vec{r})}, && (2.129) \\ & \quad \underline{E}_t \, \vec{e}_y \, e^{\mathrm{j}(\omega t - k_{2,x} x)} e^{-\kappa_{2z} z}. && (2.130) \end{aligned}$$

Thus the wave penetrates into medium 2 exponentially with a 1/e-depth δ, given by

$$\delta = \frac{1}{\kappa_{2z}} = \frac{1}{k_1 \sqrt{\sin^2\theta_1 - \sin^2\theta_{tot}}} \qquad (2.131)$$

Figure 2.33 shows the penetration depth as a function of angle of incidence for a silica/air interface and a silicon/air interface. The figure demonstrates that light from inside a semiconductor material with a relatively high index around n=3.5 is mostly captured in the semiconductor material (Problem of light extraction from light emitting diodes (LEDs)), see problem set 2.

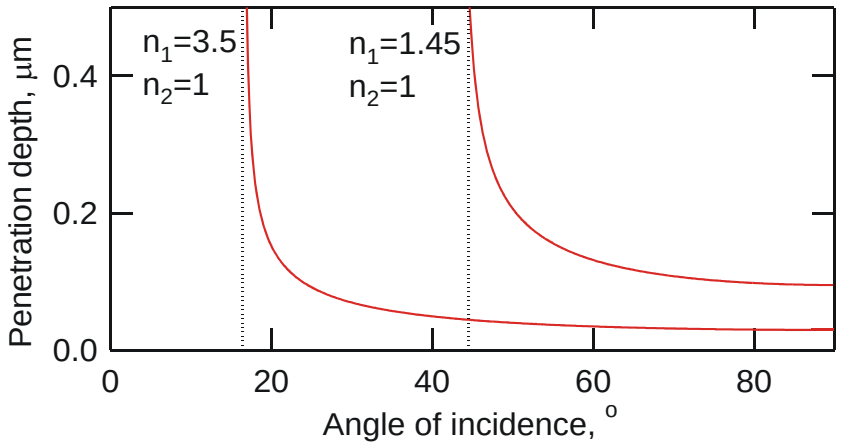

Figure 2.33: Penetration depth for total internal reflection at a silica/air and a silicon/air interface for $\lambda = 0.633$nm.

As the magnitude of the reflection coefficient is 1 for total internal reflection, the power flowing into medium 2 must vanish, i.e. the transmission is zero. Note, that the transmission and reflection coefficients in Eq.(2.113) can be used beyond the critical angle for total internal reflection. We only have to be aware that the electric field in medium 2 has an imaginary dependence in the exponent for the z-direction, i.e. $k_{2z} = k_2 \cos\theta_2 = -j\kappa_{2z}$. Thus $\cos\theta_2$ in all formulas for the reflection and transmission coefficients has to be replaced by the imaginary number

$$\begin{aligned} \cos\theta_2 &= \frac{k_{2z}}{k_2} = -\mathrm{j}\frac{k_1}{k_2}\sqrt{\sin^2\theta_1 - \sin^2\theta_{tot}} \\ &= -\mathrm{j}\frac{n_1}{n_2}\sqrt{\sin^2\theta_1 - \sin^2\theta_{tot}} \\ &= -\mathrm{j}\sqrt{\left(\frac{\sin\theta_1}{\sin\theta_{tot}}\right)^2 - 1}. \end{aligned} \tag{2.132}$$

Then the reflection coefficients in Eq.(2.113) change to all-pass functions

TE-wave (s-pol.)	TM-wave (p-pol.)
$\underline{r}^{TE} = \frac{n_1\cos\theta_1 - n_2\cos\theta_2}{n_1\cos\theta_1 + n_2\cos\theta_2}$	$\underline{r}^{TM} = \frac{\frac{n_2}{\cos\theta_2} - \frac{n_1}{\cos\theta_1}}{\frac{n_2}{\cos\theta_2} + \frac{n_1}{\cos\theta_1}}$
$\underline{r}^{TE} = \frac{\cos\theta_1 + \mathrm{j}\frac{n_2}{n_1}\sqrt{\left(\frac{\sin\theta_1}{\sin\theta_{tot}}\right)^2 - 1}}{\cos\theta_1 - \mathrm{j}\frac{n_2}{n_1}\sqrt{\left(\frac{\sin\theta_1}{\sin\theta_{tot}}\right)^2 - 1}}$	$\underline{r}^{TM} = \frac{\cos\theta_1 + \mathrm{j}\frac{n_1}{n_2}\sqrt{\left(\frac{\sin\theta_1}{\sin\theta_{tot}}\right)^2 - 1}}{\cos\theta_1 - \mathrm{j}\frac{n_1}{n_2}\sqrt{\left(\frac{\sin\theta_1}{\sin\theta_{tot}}\right)^2 - 1}}$
$\tan\frac{\phi^{TE}}{2} = \frac{1}{\cos\theta_1}\frac{n_2}{n_1}\sqrt{\left(\frac{\sin\theta_1}{\sin\theta_{tot}}\right)^2 - 1}$	$\tan\frac{\phi^{TM}}{2} = \frac{1}{\cos\theta_1}\frac{n_1}{n_2}\sqrt{\left(\frac{\sin\theta_1}{\sin\theta_{tot}}\right)^2 - 1}$

(2.133)

Thus the magnitude of the reflection coefficient is 1. However, there is a non-vanishing phase shift for the light field upon total internal reflection, denoted as ϕ^{TE} and ϕ^{TM} in the table above. Figure 2.34 shows these phase shifts for the glass/air interface and for both polarizations.

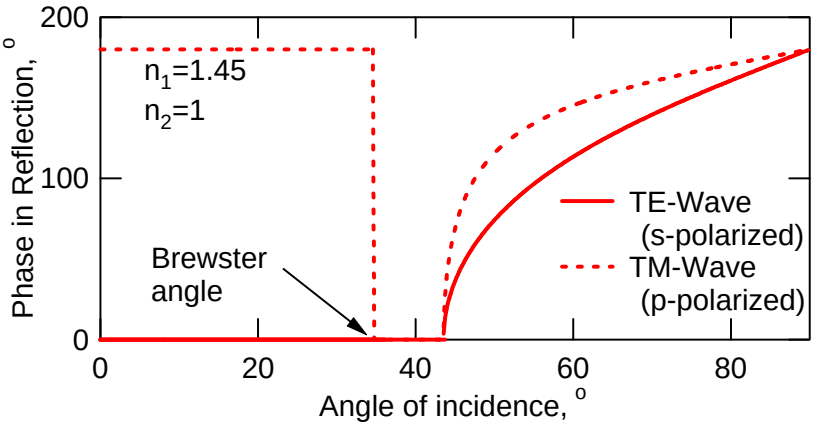

Figure 2.34: Phase shifts for TE- and TM- wave upon reflection from a silica/air interface, with $n_1 = 1.45$ and $n_2 = 1$.

Goos-Haenchen-Shift

So far, we looked only at plane waves undergoing reflection at surface due to total internal reflection. If a beam of finite transverse size is reflected from

such a surface it turns out that it gets displaced by a distance Δz, see Figure 2.35 (a), called Goos-Haenchen-Shift.

Figure 2.35: (a) Goos-Haenchen Shift and related beam displacement upon reflection of a beam with finite size; (b) Accumulation of phase shifts in a waveguide.

Detailed calculations show (problem set 2), that the displacement is given by

$$\Delta z = 2\delta^{TE/TM} \tan\theta_1, \tag{2.134}$$

as if the beam was reflected at a virtual layer with depth $\delta^{TE/TM}$ into medium 2. It turns out, that for TE-waves

$$\delta^{TE} = \delta, \tag{2.135}$$

where δ is the penetration depth according to Eq.(2.131) for evanescent waves. But for TM-waves

$$\delta^{TM} = \frac{\delta}{\left[1 + \left(\frac{n_1}{n_2}\right)^2\right] \sin^2\theta_1 - 1} \tag{2.136}$$

These shifts accumulate when the beam is propagating in a waveguide, see Figure 2.35 (b) and is important to understand the dispersion relations of waveguide modes. The Goos-Haenchen shift can be observed by reflection at a prism partially coated with a silver film, see Figure 2.36. The part reflected from the silver film is shifted with respect to the beam reflected due to total internal reflection, as shown in the figure.

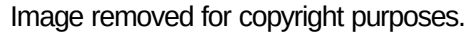

Figure 2.36: Experimental proof of the Goos-Haenchen shift by total internal reflection at a prism, that is partially coated with silver, where the penetration of light can be neglected. [3] p. 486.

Frustrated total internal reflection

Another proof for the penetration of light into medium 2 in the case of total internal reflection can be achieved by putting two prisms, where total internal reflection occurs back to back, see Figure 2.37. Then part of the light, depending on the distance between the two interfaces, is converted back into a propagating wave that can leave the second prism. This effect is called frustrated internal reflection and it can be used as a beam splitter as shown in Figure 2.37.

Figure 2.37: Frustrated total internal reflection. Part of the light is picked up by the second surface and converted into a propagating wave.

2.3 Mirrors, Interferometers and Thin-Film Structures

One of the most striking wave phenomena is interference. Many optical devices are based on the concept of interfering waves, such as low loss dielectric mirrors and interferometers and other thin-film optical coatings. After having a quick look into the phenomenon of interference, we will develope a powerful matrix formalism that enables us to evaluate efficiently many optical (also microwave) systems based on interference.

2.3.1 Interference and Coherence

Interference

Interference of waves is a consequence of the linearity of the wave equation (2.13). If we have two individual solutions of the wave equation

$$\vec{E}_1(\vec{r},t) = E_1 \cos(\omega_1 t - \vec{k}_1 \cdot \vec{r} + \varphi_1)\ \vec{e}_1, \tag{2.137}$$

$$\vec{E}_2(\vec{r},t) = E_2 \cos(\omega_2 t - \vec{k}_1 \cdot \vec{r} + \varphi_2)\ \vec{e}_2, \tag{2.138}$$

with arbitrary amplitudes, wave vectors and polarizations, the sum of the two fields (superposition) is again a solution of the wave equation

$$\vec{E}(\vec{r},t) = \vec{E}_1(\vec{r},t) + \vec{E}_2(\vec{r},t). \tag{2.139}$$

If we look at the intensity, wich is proportional to the amplitude square of the total field

$$\vec{E}(\vec{r},t)^2 = \left(\vec{E}_1(\vec{r},t) + \vec{E}_2(\vec{r},t)\right)^2, \tag{2.140}$$

we find

$$\vec{E}(\vec{r},t)^2 = \vec{E}_1(\vec{r},t)^2 + \vec{E}_2(\vec{r},t)^2 + 2\vec{E}_1(\vec{r},t)\cdot\vec{E}_2(\vec{r},t) \tag{2.141}$$

with

$$\vec{E}_1(\vec{r},t)^2 = \frac{E_1^2}{2}\left(1+\cos 2(\omega_1 t - \vec{k}_1\cdot\vec{r}+\varphi_1)\right), \tag{2.142}$$

$$\vec{E}_2(\vec{r},t)^2 = \frac{E_2^2}{2}\left(1+\cos 2(\omega_2 t - \vec{k}_2\cdot\vec{r}+\varphi_2)\right), \tag{2.143}$$

$$\begin{aligned}\vec{E}_1(\vec{r},t)\cdot\vec{E}_2(\vec{r},t) &= (\vec{e}_1\cdot\vec{e}_2)\,E_1E_2\cos(\omega_1 t - \vec{k}_1\cdot\vec{r}+\varphi_1)\cdot \\ &\quad\cdot\cos(\omega_2 t - \vec{k}_2\cdot\vec{r}+\varphi_2)\end{aligned} \tag{2.144}$$

$$\vec{E}_1(\vec{r},t)\cdot\vec{E}_2(\vec{r},t) = \frac{1}{2}(\vec{e}_1\cdot\vec{e}_2)\,E_1E_2\cdot \tag{2.145}$$

$$\cdot\left[\begin{array}{l}\cos\left((\omega_1-\omega_2)\,t-\left(\vec{k}_1-\vec{k}_2\right)\cdot\vec{r}+(\varphi_1-\varphi_2)\right) \\ +\cos\left((\omega_1+\omega_2)\,t-\left(\vec{k}_1+\vec{k}_2\right)\cdot\vec{r}+(\varphi_1+\varphi_2)\right)\end{array}\right] \tag{2.146}$$

Since at optical frequencies neither our eyes nor photo detectors, can ever follow the optical frequency itself and certainly not twice as large frequencies, we drop the rapidly oscillating terms. Or in other words we look only on the cycle-averaged intensity, which we denote by a bar

$$\begin{aligned}\overline{\vec{E}(\vec{r},t)^2} &= \frac{E_1^2}{2}+\frac{E_2^2}{2}+(\vec{e}_1\cdot\vec{e}_2)\,E_1E_2\cdot \\ &\quad\cdot\cos\left((\omega_1-\omega_2)\,t-\left(\vec{k}_1-\vec{k}_2\right)\cdot\vec{r}+(\varphi_1-\varphi_2)\right)\end{aligned} \tag{2.147}$$

Depending on the frequencies ω_1 and ω_2 and the deterministic and stochastic properties of the phases φ_1 and φ_2, we can detect this periodically varying intensity pattern called interference pattern. Interference of waves can be best visuallized with water waves, see Figure 2.38. Note, however, that water waves are a scalar field, whereas the EM-waves are vector waves. Therefore, the interference phenomena of EM-waves are much richer in nature than

for water waves. Notice, from Eq.(2.147), it follows immedicatly that the interference vanishes in the case of orthogonally polarized EM-waves, because of the scalar product involved. Also, if the frequencies of the waves are not identical, the interference pattern will not be stationary in time.

Figure 2.38: Interference of water waves from two point sources in a ripple tank [1] p. 276.

If the frequencies are identical, the interference pattern depends on the wave vectors, see Figure 2.39. The interference pattern which has itself a wavevector given by

$$\vec{k}_1 - \vec{k}_2 \tag{2.148}$$

shows a period of

$$\Lambda = \frac{2\pi}{\left|\vec{k}_1 - \vec{k}_2\right|}. \tag{2.149}$$

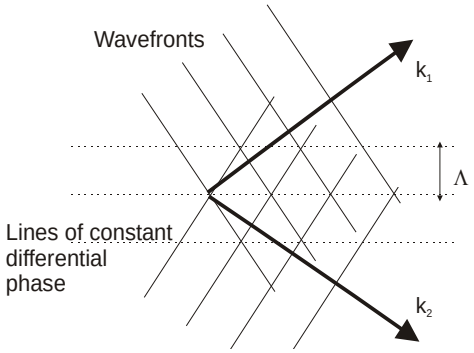

Figure 2.39: Interference pattern generated by two monochromatic plane waves.

Coherence

The ability of waves to generate an interference pattern is called coherence. Coherence can be quantified both temporally or spatially. For example, if we are at a certain position $\vec{r}$ in the interference pattern described by Eq.(2.147), we will only have stationary conditions over a time interval

$$T_{coh} << \frac{2\pi}{\omega_1 - \omega_2}.$$

Thus the spectral width of the waves determines the temporal coherence. However, it depends very often on the expermental arrangement whether a given situation can still lead to interference or not. Even so the interfering light may be perfectly temporally coherent, i.e. perfectly monochromatic, $\omega_1 = \omega_2$,yet the wave vectors may not be stable over time and the spatial inteference pattern may wash out, i.e. there is insufficient spatial coherence. So for stable and maximum interference three conditions must be fulfilled:

- stable and identical polarization
- small change in the relative phase between the beams involved over the observation time, temporal coherence, often achieved by using narrrow linewidth light
- stable beam propagation or guiding of light to achieve spatial coherence.

It is by no means trivial to arrive at a light source and an experimental setup that enables good coherence and strong interference of the beams involved.

Interference of beams can be used to measure relative phase shifts between them which may be proportional to a physical quantity that needs to be measured. Such phase shifts between two beams can also be used to modulate the light output at a given position in space via interference. In 6.013, we have already encountered interference effects between forward and backward traveling waves on transmission lines. This is very closely related to what we use in optics, therefore, we quickly relate the TEM-wave progagation to the transmission line formalism developed in Chapter 5 of 6.013.

2.3.2 TEM-Waves and TEM-Transmission Lines

The motion of voltage V and current I along a TEM transmission line with an inductance L' and a capacitance $C\prime$ per unit length is satisfies

$$\frac{\partial V(t,z)}{\partial z} = -L'\frac{\partial I(t,z)}{\partial t} \tag{2.150}$$

$$\frac{\partial I(t,z)}{\partial z} = -C'\frac{\partial V(t,z)}{\partial t} \tag{2.151}$$

Substitution of these equations into each other results in wave equations for either the voltage or the current

$$\frac{\partial^2 V(t,z)}{\partial z^2} - \frac{1}{c^2}\frac{\partial^2 V(t,z)}{\partial t^2} = 0, \tag{2.152}$$

$$\frac{\partial^2 I(t,z)}{\partial z^2} - \frac{1}{c^2}\frac{\partial^2 I(t,z)}{\partial t^2} = 0, \tag{2.153}$$

where $c = 1/\sqrt{L'C'}$ is the speed of wave propagation on the transmission line. The ratio between voltage and current for monochomatic waves is the characteristic impedance $Z = \sqrt{L'/C'}$.

The equations of motion for the electric and magnetic field of a x-polarized TEM wave according to Figure 2.1, with $E-$field along the x-axis and H-fields along the y- axis follow directly from Faraday's and Ampere's law

$$\frac{\partial E(t,z)}{\partial z} = -\mu\frac{\partial H(t,z)}{\partial t}, \tag{2.154}$$

$$\frac{\partial H(t,z)}{\partial z} = -\varepsilon\frac{\partial E(t,z)}{\partial t}, \tag{2.155}$$

which are identical to the transmission line equations (2.150) and (2.151). Substitution of these equations into each other results again in wave equations for electric and magnetic fields propagating at the speed of light $c = 1/\sqrt{\mu\varepsilon}$ and with characteristic impedance $Z_F = \sqrt{\mu/\varepsilon}$.

The solutions of the wave equation are forward and backward traveling waves, which can be decoupled by transforming the fields to the forward and backward traveling waves

$$a(t,z) = \sqrt{\frac{A_{eff}}{2Z_F}}\left(E(t,z) + Z_{Fo}H(t,z)\right), \tag{2.156}$$

$$b(t,z) = \sqrt{\frac{A_{eff}}{2Z_F}}\left(E(t,z) - Z_{Fo}H(t,z)\right), \tag{2.157}$$

which fulfill the equations

$$\left(\frac{\partial}{\partial z} + \frac{1}{c}\frac{\partial}{\partial t}\right)a(t,z) = 0, \tag{2.158}$$

$$\left(\frac{\partial}{\partial z} - \frac{1}{c}\frac{\partial}{\partial t}\right)b(t,z) = 0. \tag{2.159}$$

Note, we introduced that cross section A_{eff} such that $|a|^2$ is proportional to the total power carried by the wave. Clearly, the solutions are

$$a(t,z) = f(t - z/c_0), \tag{2.160}$$

$$b(t,z) = g(t + z/c_0), \tag{2.161}$$

which resembles the D'Alembert solutions of the wave equations for the electric and magnetic field

$$E(t,z) = \sqrt{\frac{Z_{Fo}}{2A_{eff}}}\left(a(t,z) + b(t,z)\right), \tag{2.162}$$

$$H(t,z) = \sqrt{\frac{1}{2Z_{Fo}A_{eff}}}\left(a(t,z) - b(t,z)\right). \tag{2.163}$$

Here, the forward and backward propagating fields are already normalized such that the Poynting vector multiplied with the effective area gives already the total power transported by the fields in the effective cross section A_{eff}

$$P = \vec{S}\cdot\left(A_{eff}\ \vec{e}_z\right) = A_{eff}E(t,z)H(t,z) = |a(t,z)|^2 - |b(t,z)|^2. \tag{2.164}$$

In 6.013, it was shown that the relation between sinusoidal current and voltage waves

$$V(t,z) = \mathrm{Re}\left\{\underline{V}(z)e^{j\omega t}\right\} \text{ and } I(t,z) = \mathrm{Re}\left\{\underline{I}(z)e^{j\omega t}\right\} \tag{2.165}$$

along the transmission line or corresponding electric and magnetic fields in one dimensional wave propagation is described by a generalized complex impedance $\underline{Z}(z)$ that obey's certain transformation rules, see Figure 2.40 (a).

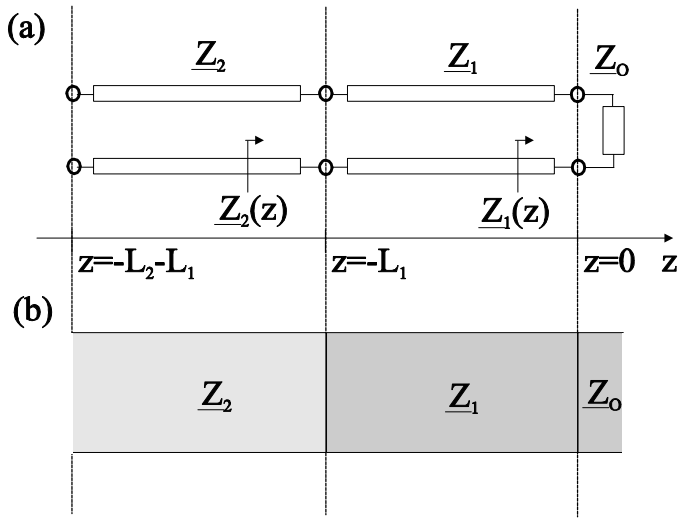

Figure 2.40: (a) Transformation of generalized impedance along transmission lines, (b) Transformation of generalized impedance accross free space sections with different characterisitc wave impedances in each section.

Along the first transmission line, which is terminated by a load impedance, the generalized impedance transforms according to

$$\underline{Z}_1(z) = \underline{Z}_1 \cdot \frac{\underline{Z}_0 - j\underline{Z}_1 \tan(k_1 z)}{\underline{Z}_1 - j\underline{Z}_0 \tan(k_1 z)} \tag{2.166}$$

with $k_1 = k_0\underline{n}_1$ and along the second transmission line the same rule applies as an example

$$\underline{Z}_2(z) = \underline{Z}_2 \cdot \frac{\underline{Z}_1(-L_1) - j\underline{Z}_2 \tan(k_2 z)}{\underline{Z}_2 - j\underline{Z}_1(-L_1) \tan(k_2 z)} \tag{2.167}$$

with $k_2 = k_0 n_2$. Note, that the media can also be lossy, then the characteristic impedances of the transmission lines and the propagation constants are already themselves complex numbers. The same formalism can be used to solve corresponding one dimensional EM-wave propagation problems.

Antireflection Coating

The task of an antireflection (AR-)coating, analogous to load matching in transmission line theory, is to avoid reflections between the interface of two media with different optical properties. One method of course could be to place the interface at Brewster's angle. However, this is not always possible. Let's assume we want to put a medium with index n into a beam under normal incidence, without having reflections on the air/medium interface. The medium can be for example a lens. This is exactly the situation shown in Figure 2.40 (b). $\underline{Z}_2$ describes the refractive index of the lense material, e.g. $n_2 = 3.5$ for a silicon lense, we can deposit on the lens a thin layer of material with index n_1 corresponding to $\underline{Z}_1$ and this layer should match to the free space index $n_0 = 1$ or impedance $\underline{Z}_0 = 377\Omega$. Using (2.166) we obtain

$$\underline{Z}_2 = \underline{Z}_1(-L_1) = \underline{Z}_1 \frac{\underline{Z}_0 - j\underline{Z}_1 \tan(-k_1 L_1)}{\underline{Z}_1 - j\underline{Z}_0 \tan(-k_1 L_1)} \tag{2.168}$$

If we choose a quarter wave thick matching layer $k_1 L_1 = \pi/2$, this simplifies to the famous result

$$\underline{Z}_2 = \frac{\underline{Z}_1^2}{\underline{Z}_0}, \tag{2.169}$$

$$\text{or } n_1 = \sqrt{n_2 n_0} \text{ and } L_1 = \frac{\lambda}{4 n_1}. \tag{2.170}$$

Thus a quarter wave AR-coating needs a material which has an index corresponding to the geometric mean of the two media to be matched. In the current example this would be $n_2 = \sqrt{3.5} \approx 1.87$

2.3.3 Scattering and Transfer Matrix

Another formalism to analyze optical systems (or microwave circuits) can be formulated using the forward and backward propagating waves, which transform much simpler along a homogenous transmission line than the total fields, i.e. the sum of forward adn backward waves. However, at interfaces

scattering of these waves occurs whereas the total fields are continuous. For monochromatic forward and backward propagating waves

$$\underline{a}(t,z) = \underline{a}(z)e^{j\omega t} \text{ and } \underline{b}(t,z) = \underline{b}(z)e^{j\omega t} \tag{2.171}$$

propagating in z-direction over a distance z with a propagation constant k, we find from Eqs.(2.158) and (2.159)

$$\begin{pmatrix} \underline{a}(z) \\ \underline{b}(z) \end{pmatrix} = \begin{pmatrix} e^{-jkz} & 0 \\ 0 & e^{jkz} \end{pmatrix} \begin{pmatrix} \underline{a}(0) \\ \underline{b}(0) \end{pmatrix}. \tag{2.172}$$

A piece of transmission line is a two port. The matrix transforming the amplitudes of the waves at the input port (1) to those of the output port (2) is called the transfer matrix, see Figure 2.41

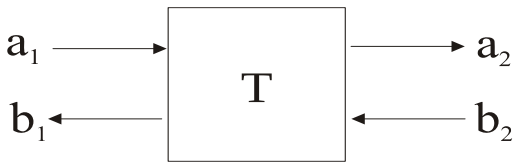

Figure 2.41: Definition of the wave amplitudes for the transfer matrix T.

For example, from Eq.(2.172) follows that the transfer matrix for free space propagation is

$$\mathbf{T} = \begin{pmatrix} e^{-jkz} & 0 \\ 0 & e^{jkz} \end{pmatrix}. \tag{2.173}$$

This formalism can be expanded to arbitrary multiports. Because of its mathematical properties the scattering matrix that describes the transformation between the incoming and outgoing wave amplitudes of a multiport is often used, see Figure 2.42.

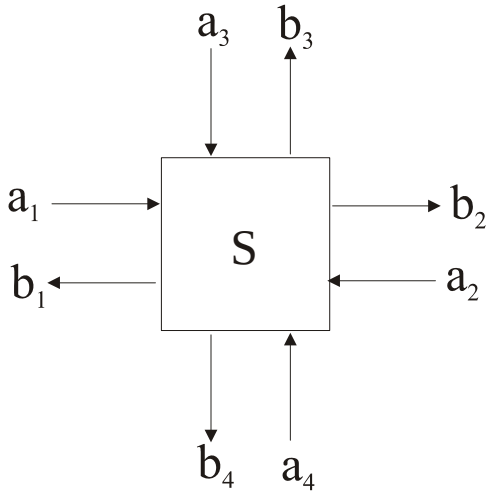

Figure 2.42: Scattering matrix and its port definition.

The scattering matrix defines a linear transformation from the incoming to the outgoing waves

$$\vec{\underline{b}} = \underline{\mathbf{S}}\vec{\underline{a}}, \text{ with } \underline{a} = (a_1, a_2, ...)^T \,, \; \underline{b} = (b_1, b_2, ...)^T \,. \tag{2.174}$$

Note, that the meaning between forward and backward waves no longer coincides with $\underline{a}$ and $\underline{b}$, a connection, which is difficult to maintain if several ports come in from many different directions.

The transfer matrix T has advantages, if many two ports are connected in series with each other. Then the total transfer matrix is the product of the individual transfer matrices.

2.3.4 Properties of the Scattering Matrix

Physial properties of the system reflect itself in the mathematical properties of the scattering matrix.

Reciprocity

A system with constant scalar dielectric and magnetic properties must have a symmetric scattering matrix (without proof)

$$\underline{\mathbf{S}} = \underline{\mathbf{S}}^T. \tag{2.175}$$

Losslessness

In a lossless system the total power flowing into the system must be equal to the power flowing out of the system in steady state

$$|\vec{\underline{a}}|^2 = \left|\vec{\underline{b}}\right|^2, \tag{2.176}$$

i.e.

$$\underline{\mathbf{S}}^+\underline{\mathbf{S}} = 1 \text{ or } \underline{\mathbf{S}}^{-1}=\underline{\mathbf{S}}^+. \tag{2.177}$$

The scattering matrix of a lossless system must be unitary.

Time Reversal

To find the scattering matrix of the time reversed system, we realize that incoming waves become outgoing waves under time reversal and the other way around, i.e. the meaning of $\underline{a}$ and $\underline{b}$ is exchanged and on top of it the waves become negative frequency waves.

$$\underline{a}e^{j(\omega t-kz)} \overset{\text{time reversal}}{\rightarrow} \underline{a}e^{j(-\omega t-kz)}. \tag{2.178}$$

To obtain the complex amplitude of the corresponding positive frequency wave, we need to take the complex conjugate value. So to obtain the equations for the time reversed system we have to perform the following substitutions

$$\begin{array}{cc} \text{Original system} & \text{Time reversed system} \\ \vec{\underline{b}} = \underline{\mathbf{S}}\vec{\underline{a}} & \vec{\underline{a}}^* = \underline{\mathbf{S}}\vec{\underline{b}}^* \rightarrow \vec{\underline{b}} = \left(\underline{\mathbf{S}}^{-1}\right)^* \vec{\underline{a}} \end{array}. \tag{2.179}$$

2.3.5 Beamsplitter

As an example, we look at the scattering matrix for a partially transmitting mirror, which could be simply formed by the interface between two media with different refractive index, which we analyzed in the previous section, see Figure 2.43. (Note, for brevity we neglect the reflections at the normal surface input to the media, or we put an AR-coating on them.) In principle, this device has four ports and should be described by a 4x4 matrix. However, most often only one of the waves is used at each port, as shown in Figure 2.43.

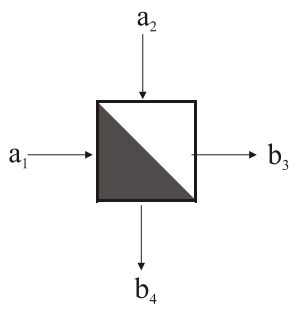

Figure 2.43: Port definitions for the beam splitter

The scattering matrix is determined by

$$\vec{\underline{b}} = \underline{\mathbf{S}}\vec{\underline{a}}, \text{ with } \underline{a} = (a_{1,}a_2)^T \ , \ \underline{b} = (b_3, b_4)^T \tag{2.180}$$

and

$$\mathbf{S}= \begin{pmatrix} r & jt \\ jt & r \end{pmatrix}, \text{ with } r^2 + t^2 = 1. \tag{2.181}$$

The matrix $\mathbf{S}$ was obtained using using the S-matrix properties described above. From Eqs.(2.113) we could immediately identify r as a function of the refractive indices, angle of incidence and the polarization used. Note, that the off-diagonal elements of $\mathbf{S}$ are identical, which is a consequence of reciprocity. That the main diagonal elements are identical is a consequence of unitarity for a lossless beamsplitter and furthermore $t = \sqrt{1 - r^2}$. For a given frequency r and t can always be made real by choosing proper reference planes at the input and the output of the beam splitter. Beamsplitters can be made in many ways, see for example Figure 2.37.

2.3.6 Interferometers

Having a valid description of a beamsplitter at hand, we can build and analyze various types of interferometers, see Figure 2.44.

Figure 2.44: Different types of interferometers: (a) Mach-Zehnder Interferometer; (b) Michelson Interferometer; (c) Sagnac Interferometer [6] p. 66.

Each of these structures has advantages and disadvantages depending on the technology they are realized. The interferometer in Figure 2.44 (a) is called Mach-Zehnder interferometer, the one in Figure 2.44 (b) is called Michelson Interferometer. In the Sagnac interferometer , Figure 2.44 (c) both beams see identical beam path and therefore errors in the beam path can be balance out and only differential changes due to external influences lead to an output signal, for example rotation, see problem set 3.

To understand the light transmission through an interferometer we analyze as an example the Mach-Zehnder interferometer shown in Figure 2.45. If we excite input port 1 with a wave with complex amplitude $\underline{a}_0$ and no input at port 2 and assume 50/50 beamsplitters, the first beam splitter will

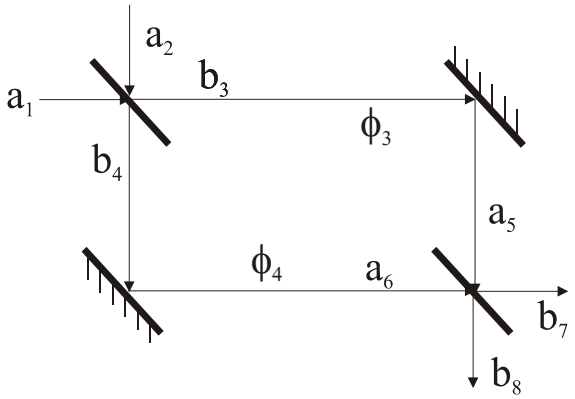

Figure 2.45: Mach-Zehnder Interferometer

produce two waves with complex amplitudes

$$\begin{aligned} \underline{b}_3 &= \tfrac{1}{\sqrt{2}}\underline{a}_0 \\ \underline{b}_4 &= j\tfrac{1}{\sqrt{2}}\underline{a}_0 \end{aligned} \tag{2.182}$$

During propagation through the interferometer arms, both waves pick up a phase delay $\phi_3 = kL_3$ and $\phi_4 = kL_4$, respectively

$$\begin{aligned} a_5 &= \tfrac{1}{\sqrt{2}}\underline{a}_0 e^{-j\phi_3}, \\ a_6 &= j\tfrac{1}{\sqrt{2}}\underline{a}_0 e^{-j\phi_4}. \end{aligned} \tag{2.183}$$

After the second beam splitter with the same scattering matrix as the first one, we obtain

$$\begin{aligned} b_7 &= \tfrac{1}{2}\underline{a}_0 \left(e^{-j\phi_3} - e^{-j\phi_4}\right), \\ b_8 &= j\tfrac{1}{2}\underline{a}_0 \left(e^{-j\phi_3} + e^{-j\phi_4}\right). \end{aligned} \tag{2.184}$$

The transmitted power to the output ports is

$$\begin{aligned} |b_7|^2 &= \tfrac{|\underline{a}_0|^2}{4}\left|1 - e^{-j(\phi_3-\phi_4)}\right|^2 = \tfrac{|\underline{a}_0|^2}{2}\left[1 - \cos\left(\phi_3 - \phi_4\right)\right], \\ |b_8|^2 &= \tfrac{|\underline{a}_0|^2}{4}\left|1 + e^{-j(\phi_3-\phi_4)}\right|^2 = \tfrac{|\underline{a}_0|^2}{2}\left[1 + \cos\left(\phi_3 - \phi_4\right)\right]. \end{aligned} \tag{2.185}$$

The total output power is equal to the input power, as it must be for a lossless system. However, depending on the phase difference $\Delta\phi = \phi_3 - \phi_4$ between both arms, the power is split differently between the two output ports, see Figure 2.46.With proper biasing, i.e. $\phi_3 - \phi_4 = \pi/2 + \Delta\phi$, the difference in

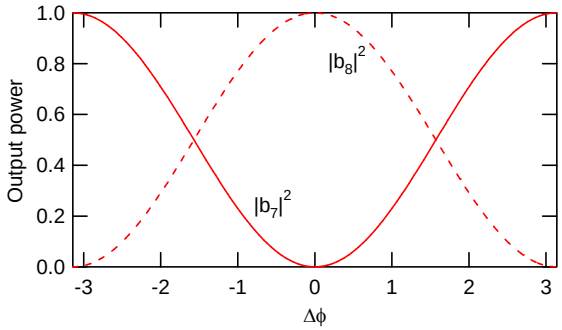

Figure 2.46: Output power from the two arms of an interfereometer as a function of phase difference.

output power between the two arms can be made directly proportional to the phase difference $\Delta\phi$.

Opening up the beam size in the interferometer and placing optics into the beam enables to visualize beam distortions due to imperfect optical components, see Figures 2.47 and 2.48.

Image removed for copyright purposes.

Figure 2.47: Twyman-Green Interferometer to test optics quality [1] p. 324.

Figure 2.48: Interference pattern with a hot iron placed in one arm of the interferometer ([1], p. 395).

2.3.7 Fabry-Perot Resonator

Interferometers can act as filters. The phase difference between the interferometer arms depends on frequency, therefore, the transmission from input to output depends on frequency, see Figure 2.46. However, the filter function is not very sharp. The reason for this is that only a two beam interference is used. Much more narrowband filters can be constructed by multipass interferences such as in a Fabry-Perot Resonator, see Figure 2.49. The simplest Fabry Perot is described by a sequence of three layers where at least the middle layer has an index different from the other two layers, such that reflections occur on these interfaces.

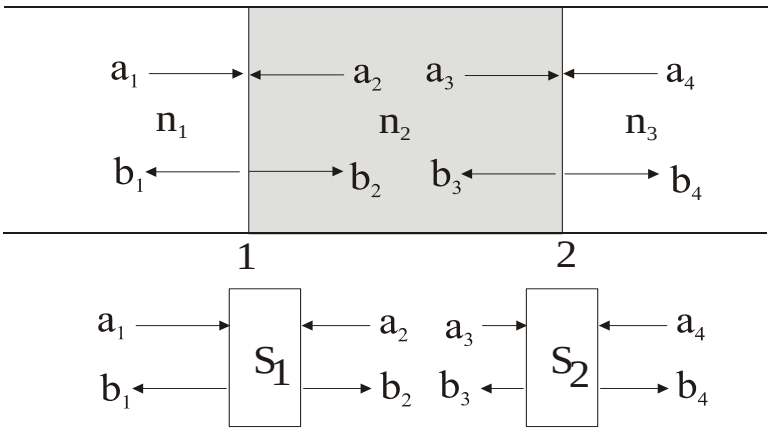

Figure 2.49: Multiple intereferences in a Fabry Perot resonator. In the simplest implementation a Fabry Perot only consists of a sequence of three layers with different refractive index so that two reflections occur with multiple interferences. Each of this discontinuites can be described by a scattering matrix.

Any kind of device that has reflections at two parallel interfaces may act as a Fabry Perot such as two semitransparent mirrors. A thin layer of material against air can act as a Fabry-Perot and is often called etalon. Given the reflection and transmission coefficients at the interfaces 1 and 2, we can write down the scattering matrices for both interfaces according to Eqs.(2.180) and (2.181).

$$\begin{pmatrix} \tilde{\underline{b}}_1 \\ \tilde{\underline{b}}_2 \end{pmatrix} = \begin{pmatrix} r_1 & jt_1 \\ jt_1 & r_1 \end{pmatrix} \begin{pmatrix} \tilde{\underline{a}}_1 \\ \tilde{\underline{a}}_2 \end{pmatrix} \text{ and } \begin{pmatrix} \tilde{\underline{b}}_3 \\ \tilde{\underline{b}}_4 \end{pmatrix} = \begin{pmatrix} r_2 & jt_2 \\ jt_2 & r_2 \end{pmatrix} \begin{pmatrix} \tilde{\underline{a}}_3 \\ \tilde{\underline{a}}_4 \end{pmatrix}. \tag{2.186}$$

If we excite the Fabry-Perot with a wave from the right with amplitude. $\tilde{\underline{a}}_1 \neq 0$, then a fraction of that wave will be transmitted to the interface into the Fabry-Perot as wave $\tilde{\underline{b}}_2$ and part will be already reflected into $\tilde{\underline{b}}_1$,

$$\tilde{\underline{b}}_1^{(0)} = r_1 \tilde{\underline{a}}_1. \tag{2.187}$$

The transmitted wave will then propagate and pick up a phase factor $e^{-j\phi/2}$, with $\phi = 2k_2 L$ and $k_2 = \frac{2\pi}{\lambda} n_2$,

$$\tilde{\underline{a}}_3 = \mathrm{j}t\tilde{\underline{a}}_1 e^{-j\phi/2}. \tag{2.188}$$

After propagation it will be reflected off from the second interface which has a reflection coefficient

$$\Gamma_2 = \left.\frac{\tilde{\underline{b}}_3}{\tilde{\underline{a}}_3}\right|_{\underline{a}_4=0} = r_2. \tag{2.189}$$

Then the reflected wave $\tilde{\underline{b}}_3$ propagates back to interface 1, picking up another phase factor $e^{-j\phi/2}$ resulting in an incoming wave after one roundtrip of $\tilde{\underline{a}}_2^{(1)} = jt_1r_2e^{-j\phi}\tilde{\underline{a}}_1$. Upon reflection on interface 1, part of this wave is transmitted leading to an output

$$\tilde{\underline{b}}_1^{(1)} = jt_1jt_1r_2e^{-j\phi}\tilde{\underline{a}}_1. \tag{2.190}$$

The partial wave $\underline{a}_2^{(1)}$ is reflected again and after another roundtrip it arrives at interface 1 as $\tilde{\underline{a}}_2^{(2)} = (r_1r_2)\,e^{-j\phi}\cdot jt_1r_2e^{-j\phi}\tilde{\underline{a}}_1$. Part of this wave is transmitted and part of it is reflected back to go through another cycle. Thus in total if we sum up all partial waves that contribute to the output at port 1 of the Fabry-Perot filter, we obtain

$$\begin{aligned}
\tilde{\underline{b}}_1 &= \sum_{n=0}^{\infty}\tilde{\underline{b}}_1^{(n)} \\
&= \left(r_1 - t_1^2r_2e^{-j\phi}\sum_{n=0}^{\infty}r_1r_2e^{-j\phi}\right)\tilde{\underline{a}}_1 \\
&= \left(r_1 - t_1^2r_2\frac{e^{-j\phi}}{1-r_1r_2e^{-j\phi}}\right)\tilde{\underline{a}}_1 \\
&= \frac{r_1 - r_2e^{-j\phi}}{1-r_1r_2e^{-j\phi}}\tilde{\underline{a}}_1
\end{aligned} \tag{2.191}$$

Note, that the coefficient in front of Eq.(2.191) is the coefficient S_{11} of the scattering matrix of the Fabry-Perot. In a similar manner, we obtain

$$\begin{pmatrix} \tilde{\underline{b}}_3 \\ \tilde{\underline{b}}_4 \end{pmatrix} = \underline{\mathbf{S}}\begin{pmatrix} \tilde{\underline{a}}_1 \\ \tilde{\underline{a}}_2 \end{pmatrix} \tag{2.192}$$

and

$$\underline{\mathbf{S}} = \frac{1}{1-r_1r_2e^{-j\phi}}\begin{pmatrix} r_1 - r_2e^{-j\phi} & -t_1t_2e^{-j\phi/2} \\ -t_1t_2e^{-j\phi/2} & r_2 - r_1e^{-j\phi} \end{pmatrix} \tag{2.193}$$

In the following, we want to analyze the properties of the Fabry-Perot for the case of symmetric reflectors, i.e. $r_1 = r_2$ and $t_1 = t_2$. Then we obtain for

the power transmission coefficient of the Fabry-Perot, $|S_{21}|^2$ in terms of the power reflectivity of the interfaces $R = r^2$

$$|S_{21}|^2 = \left| \frac{1-R}{1-Re^{-j\phi}} \right|^2 = \frac{(1-R)^2}{(1-R)^2 + 4R\sin^2(\phi/2)} \tag{2.194}$$

Figure 2.50 shows the transmission $|S_{21}|^2$ of the Fabry-Perot interferometer for equal reflectivities $|r_1|^2 = |r_2|^2 = R$.

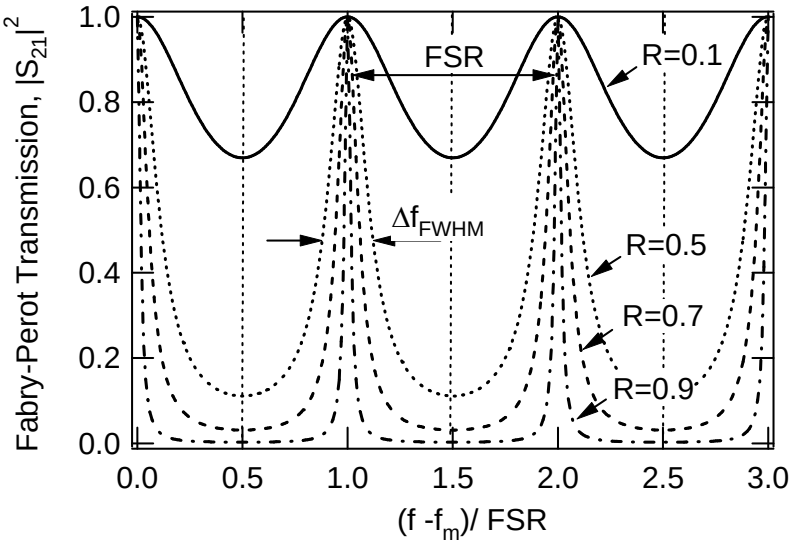

Figure 2.50: Transmission of a lossless Fabry-Perot interferometer with $|r_1|^2 = |r_2|^2 = R$

At very low reflectivity R of the mirror the transmission is almost everywhere 1, there is only a slight sinusoidal modulation due to the first order interferences which are periodically in phase and out of phase, leading to 100% transmission or small reflection. For large reflectivity R, due to the then multiple interference operation of the Fabry-Perot Interferometer, very narrow transmission resonances emerge at frequencies, where the roundtrip phase in the resonator is equal to a multiple of 2π

$$\phi = \frac{2\pi f}{c_0} n_2 2L = 2\pi m, \tag{2.195}$$

which occurs at a comb of frequencies, see Figure 2.51

$$f_m = m\frac{c_0}{2n_2L}. \tag{2.196}$$

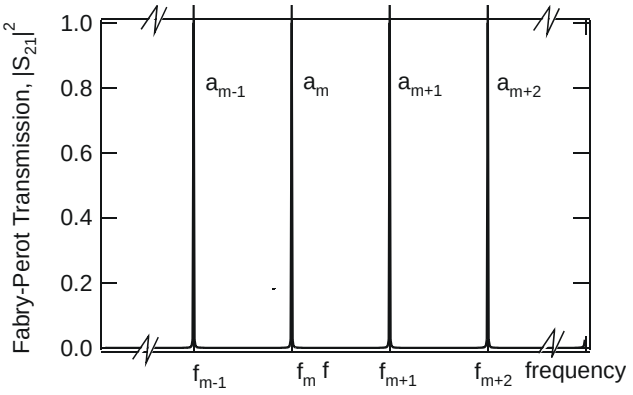

Figure 2.51: Developement of a set of discrete resonances in a one-dimensionsal resonator.

On a large frequency scale, a set of discrete frequencies, resonances or modes arise. The frequency range between resonances is called free spectral range (FSR) of the Fabry-Perot Interferometer

$$FSR = \frac{c_0}{2n_2L} = \frac{1}{T_R}, \tag{2.197}$$

which is the inverse roundtrip time T_R of the light in the one-dimensonal cavity or resonator formed by the mirrors. The filter characteristic of each resonance can be approximately described by a Lorentzian line derived from Eq.(2.194) by substituting $f = f_m + \Delta f$ with $\Delta f \ll FSR$,

$$\begin{aligned} |S_{21}|^2 &= \frac{(1-R)^2}{(1-R)^2 + 4R\sin^2\left(\left[m2\pi + 2\pi\frac{\Delta f}{FSR}\right]/2\right)} \\ &\approx \frac{1}{1+\left(\frac{2\pi\sqrt{R}}{1-R}\frac{\Delta f}{FSR}\right)^2}, \qquad (2.198) \\ &\approx \frac{1}{1+\left(\frac{\Delta f}{\Delta f_{FWHM/2}}\right)^2}, \qquad (2.199) \end{aligned}$$

where we introduced the FWHM of the transmission filter

$$\Delta f_{FWHM} = \frac{FSR}{F}, \tag{2.200}$$

with the finesse of the interferometer defined as

$$F = \frac{\pi\sqrt{R}}{1-R} \approx \frac{\pi}{T}. \tag{2.201}$$

The last simplification is valid for a highly reflecting mirror $R \approx 1$ and T is the mirror transmission. From this relation it is immediately clear that the finesse has the additional physical meaning of the optical power enhancement inside the Fabry-Perot at resonance besides the factor of π, since the power inside the cavity must be larger by $1/T$, if the transmission through the Fabry-Perot is unity.

2.3.8 Quality Factor of Fabry-Perot Resonances

Another quantity often used to characterize a resonator or a resonance is its quality factor Q, which is defined as the ratio between the resonance frequency and the decay rate for the energy stored in the resonator, which is also often called inverse photon lifetime, τ_{ph}^{-1}

$$Q = \tau_{ph} f_m. \tag{2.202}$$

Lets assume, energy is stored in one of the resonator modes which occupies a range of frequencies $[f_m - FSR/2, f_m + FSR/2]$ as indicated in Figure 2.52. Then the fourier integral

$$\underline{a}_m(t) = \int_{-FSR/2}^{+FSR/2} \underline{\tilde{b}}_2(f) e^{j2\pi(f-f_m)t}\, df, \tag{2.203}$$

where $\left|\underline{\tilde{b}}_2(f)\right|^2$ is normalized such that it describes the power spectral density of the forward traveling wave in the resonator gives the mode amplitude of the m-th mode and its magnitude square is the energy stored in the mode. Note, that we could have taken any of the internal waves $\underline{\tilde{a}}_2, \underline{\tilde{b}}_2, \underline{\tilde{a}}_3$, and $\underline{\tilde{b}}_3$. The time dependent field we create corresponds to the field of the forward or backward traveling wave at the corresponding reference plane in the resonator.

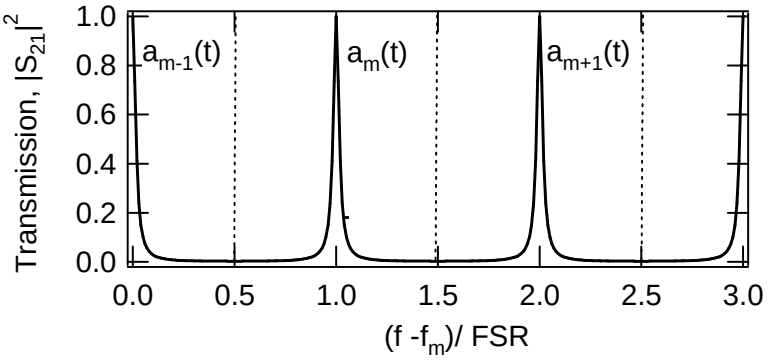

Figure 2.52: Integration over all frequency components within the frequency range $[f_m - FSR/2, f_m + FSR/2]$ defines a mode amplitude $a(t)$ with a slow time dependence

We now make a "Gedanken-Experiment". We switch on the incoming waves $\tilde{\underline{a}}_1(\omega)$ and $\tilde{\underline{a}}_4(\omega)$ to load the cavity with energy and evaluate the internal wave $\tilde{\underline{b}}_2(\omega)$. Instead of summing up all the multiple reflections like we did in constructing the scattering matrix (2.192), we exploit our skills in analyzing feedback systems, which the Fabry-Perot filter is. The scattering equations set force by the two scattering matrices characterizing the resonator mirrors in the Fabry-Perot can be visuallized by the signal flow diagram in Figure 2.53

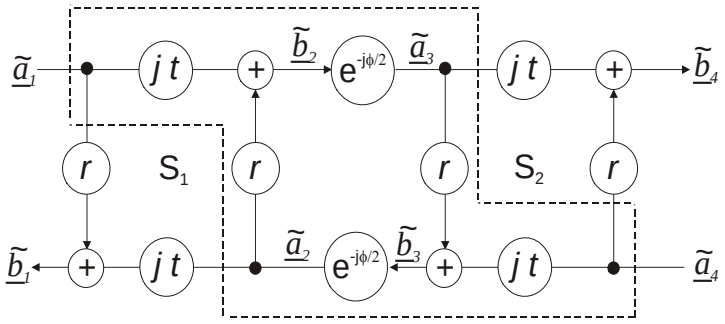

Figure 2.53: Representation of Fabry-Perot resonator by a signal flow diagram

For the task to find the relationship between the internal waves feed by the incoming wave only the dashed part of the signal flow is important. The internal feedback loop can be clearly recognized with a closed loop transfer function

$$r^2 e^{-j\phi},$$

which leads to the resonance denominator

$$1 - r^2 e^{-j\phi}$$

in every element of the Fabry-Perot scattering matrix (2.192). Using Blacks formula from 6.003 and the superposition principle we immediately find for the internal wave

$$\underline{\tilde{b}}_2 = \frac{jt}{1 - r^2 e^{-j\phi}} \left(\underline{\tilde{a}}_1 + r e^{-j\phi/2} \underline{\tilde{a}}_4 \right). \tag{2.204}$$

Close to one of the resonance frequencies, $\Omega = 2\pi f_m + \omega$, using $t = 1 - r^2$, (2.204) can be approximated by

$$\begin{aligned} \underline{\tilde{b}}_2(\omega) &\approx \frac{j}{1 + j\frac{R}{1-R}\omega T_R} \left(\underline{\tilde{a}}_1(\omega) + r(-1)^m e^{-j\omega T_R/2} \underline{\tilde{a}}_4(\omega) \right), & (2.205) \\ &\approx \frac{j}{1 + j\omega T_R/T} \left(\underline{\tilde{a}}_1(\omega) + r(-1)^m e^{-j\omega T_R/2} \underline{\tilde{a}}_4(\omega) \right) & (2.206) \end{aligned}$$

for high reflectivity R. Multiplication of this equation with the resonant denominator

$$(1 + j\omega T_R/T)\, \underline{\tilde{b}}_2(\omega) \approx j \left(\underline{\tilde{a}}_1(\omega) + r(-1)^m e^{-j\omega T_R/2} \underline{\tilde{a}}_4(\omega) \right) \tag{2.207}$$

and inverse Fourier-Transform in the time domain, while recognizing that the internal fields vanish far off resonance, i.e.

$$\underline{a}_m(t) = \int_{-\pi \cdot FSR}^{+\pi \cdot FSR} \underline{\tilde{b}}_2(\omega) e^{j\omega t}\, d\omega = \int_{-\infty}^{+\infty} \underline{\tilde{b}}_2(\omega) e^{j\omega t}\, d\omega, \tag{2.208}$$

we obtain the following differential equation for the mode amplitude slowly varying in time

$$T_R \frac{d}{dt} \underline{a}_m(t) = -T \left(\underline{a}_m(t) + j\underline{a}_1(t) + j(-1)^m \underline{a}_4(t - T_R/2) \right) \tag{2.209}$$

with the input fields

$$\underline{a}_{1/4}(t) = \int_{-\pi \cdot FSR}^{+\pi \cdot FSR} \tilde{\underline{a}}_{1/4}(\omega) e^{j\omega t}\, d\omega. \tag{2.210}$$

Despite the pain to derive this equation the physical interpretation is remarkably simple and far reaching as we will see when we apply this equation later on to many different situations. Lets assume, we switch off the loading of the cavity at some point, i.e. $\underline{a}_{1/4}(t) = 0$, then Eq.(2.209) results in

$$\underline{a}_m(t) = \underline{a}_m(0) e^{-t/(T_R/T)} \tag{2.211}$$

And the power decays accordingly

$$|\underline{a}_m(t)|^2 = |\underline{a}_m(0)|^2 e^{-t/(T_R/2T)} \tag{2.212}$$

twice as fast as the amplitude. The energy decay time of the cavity is often called the cavity energy decay time, or photon lifetime, τ_{ph}, which is here

$$\tau_{ph} = \frac{T_R}{2T}.$$

Note, the factor of two comes from the fact that each mirror of the Fabry-Perot has a transmission T per roundtrip time. For exampl a $L = 1.5m$ long cavity with mirrors of 0.5% transmission, i.e. $T_R = 10$ns and $2T = 0.01$ has a photon lifetime of 1μs. It needs hundred bounces on the mirror for a photon to be essentially lost from the cavity.

Highest quality dielectric mirrors may have a reflection loss of only $10^{-5\ldots-6}$, this is not really transmission but rather scattering loss in the mirror. Such high reflectivity mirrors may lead to the construction of cavities with photon lifetimes on the order of milliseconds.

Now, that we have an expression for the energy decay time in the cavity, we can evaluate the quality factor of the resonator

$$Q = f_m \cdot \tau_{ph} = \frac{m}{2T}. \tag{2.213}$$

Again for a resonator with the same parameters as before and at optical frequencies of 300THz corresponding to 1μm wavelength, we obtain $Q = 2 \cdot 10^8$.

2.3.9 Thin-Film Filters

Transfer matrix formlism is an efficient method to analyze the reflection and transmission properties of layered dielectric media, such as the one shown in Figure 2.54. Using the transfer matrix method, it is an easy task to compute the transmission and reflection coefficients of a structure composed of layers with arbitrary indices and thicknesses. A prominent example of a thin-film filter are Bragg mirrors. These are made of a periodic arrangement of two layers with low and high index n_1 and n_2, respectively. For maximum reflection bandwidth, the layer thicknesses are chosen to be quarter wave for the wavelength maximum reflection occures, $n_1 d_1 = \lambda_0/4$ and $n_2 d_2 = \lambda_0/4$

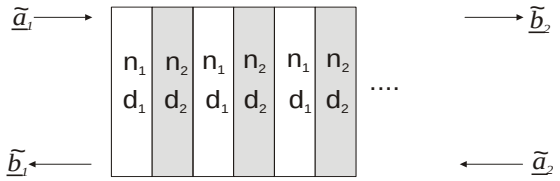

Figure 2.54: Thin-Film dielectric mirror composed of alternating high and low index layers.

As an example Figure 2.55 shows the reflection from a Bragg mirror with $n_1 = 1.45, n_2 = 2.4$ for a center wavelength of $\lambda_0 = 800$nm. The layer thicknesses are then $d_1 = 134$nm and $d_2 = 83$nm.

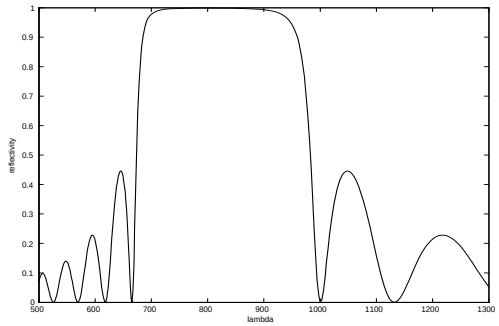

Figure 2.55: Reflectivity of an 8 pair quarter wave Bragg mirror with $n_1 = 1.45$ and $n_2 = 2.4$ designed for a center wavelength of 800nm. The mirror is embedded in the same low index material.

2.4 Paraxial Wave Equation and Gaussian Beams

So far, we have only treated optical systems operating with plane waves, which is an idealization. In reality plane waves are impossible to generate because of there infinite amount of energy required to do so. The simplest (approximate) solution of Maxwell's equations describing a beam of finite size is the Gaussian beam. In fact many optical systems are based on Gaussian beams. Most lasers are designed to generate a Gaussian beam as output. Gaussian beams stay Gaussian beams when propagating in free space. However, due to its finite size, diffraction changes the size of the beam and lenses are imployed to reimage and change the cross section of the beam. In this section, we want to study the properties of Gaussian beams and its propagation and modification in optical systems.

2.4.1 Paraxial Wave Equation

We start from the Helmholtz Equation (2.18)

$$\left(\Delta + k_0^2\right) \widetilde{\vec{E}}(x,y,z,\omega) = 0, \tag{2.214}$$

with the free space wavenumber $k_0 = \omega/c_0$. This equation can easily be solved in the Fourier domain, and one set of solutions are of course the plane waves with wave vector $|\vec{k}|^2 = k_0^2$. We look for solutions which are polarized in x-direction

$$\widetilde{\vec{E}}(x,y,z,\omega) = \widetilde{E}(x,y,z)\ \vec{e}_x. \tag{2.215}$$

We want to construct a beam with finite transverse extent into the x-y-plane and which is mainly propagating into the positive z-direction. As such we may try a superposition of plane waves with a dominant z-component of the k-vector, see Figure 2.56. The k-vectors can be written as

$$\begin{aligned} k_z &= \sqrt{k_0^2 - k_x^2 - k_y^2}, \\ &\approx k_0 \left(1 - \frac{k_x^2 - k_y^2}{2k_0^2}\right). \end{aligned} \tag{2.216}$$

with $k_x, k_y << k_0$.

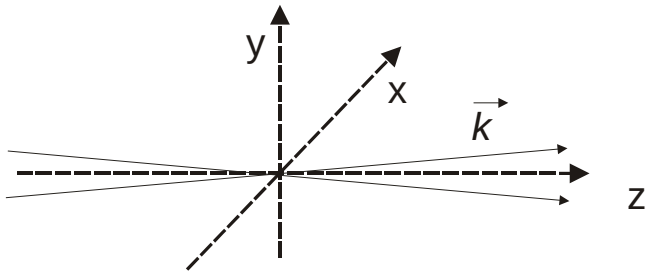

Figure 2.56: Construction of a paraxial beam by superimposing many plane waves with a dominante k-component in z-direction.

Then we obtain for the propagating field

$$\begin{aligned}\widetilde{E}(x,y,z) &= \int_{-\infty}^{+\infty}\int_{-\infty}^{+\infty}\widetilde{E}_0(k_x,k_y)\cdot \\ &\quad \exp\left[-jk_0\left(1-\frac{k_x^2+k_y^2}{2k_0^2}\right)z-jk_xx-jk_yy\right]dk_xdk_y, \\ &= \int_{-\infty}^{+\infty}\int_{-\infty}^{+\infty}\widetilde{E}_0(k_x,k_y)\cdot \\ &\quad \exp\left[j\left(\frac{k_x^2+k_y^2}{2k_0}\right)z-jk_xx-jk_yy\right]dk_xdk_ye^{-jk_0z}, \quad (2.217)\end{aligned}$$

where $\widetilde{E}_0(k_x,k_y)$ is the amplitude for the waves with the corresponding transverse k-component. This function should only be nonzero within a small range $k_x, k_y \ll k_0$. The function

$$\widetilde{E}_0(x,y,z)=\int_{-\infty}^{+\infty}\int_{-\infty}^{+\infty}\widetilde{E}_0(k_x,k_y)\exp\left[j\left(\frac{k_x^2+k_y^2}{2k_0}\right)z-jk_xx-jk_yy\right]dk_xdk_y \quad (2.218)$$

is a slowly varying function in the transverse directions x and y, and it can be easily verified that it fulfills the paraxial wave equation

$$\frac{\partial}{\partial z}\widetilde{E}_0(x,y,z)=\frac{-j}{2k_0}\left(\frac{\partial^2}{\partial x^2}+\frac{\partial^2}{\partial x^2}\right)\widetilde{E}_0(x,y,z). \quad (2.219)$$

Note, that this equation is in its structure identical to the dispersive spreading of an optical pulse. The difference is that this spreading occurs now in the two transverse dimensions and is called diffraction.

2.4.2 Gaussian Beams

Since the kernel in Eq.(2.218) is quadratic in the transverse k-components using a two-dimensional Gaussian for the amplitude distribution leads to a beam in real space which is also Gaussian in the radial direction because of the resulting Gaussian integral. By choosing for the transverse amplitude distribution

$$\widetilde{E}_0(k_x, k_y) = \exp\left[-\frac{k_x^2 + k_y^2}{2k_T^2}\right], \tag{2.220}$$

Eq.(2.218) can be rewritten as

$$\widetilde{E}_0(x, y, z) = \int_{-\infty}^{+\infty}\int_{-\infty}^{+\infty} \exp\left[j\left(\frac{k_x^2 + k_y^2}{2k_0}\right)(z + jz_R) - jk_x x - jk_y y\right] dk_x dk_y, \tag{2.221}$$

with the parameter $z_R = k_0/k_T^2$, which we will later identify as the Rayleigh range. Thus, Gaussian beam solutions with different finite transverse width in k-space and real space behave as if they propagate along the z-axis with different imaginary z-component z_R. Carrying out the Fourier transformation results in the Gaussian Beam in real space

$$\widetilde{E}_0(x, y, z) = \frac{j}{z + jz_R} \exp\left[-jk_0\left(\frac{x^2 + y^2}{2(z + jz_R)}\right)\right]. \tag{2.222}$$

The Gaussian beam is often formulated in terms of the complex beam parameter or q-parameter.

The propagation of the beam in free space and later even through optical imaging systems can be efficiently described by a proper transformation of the q-parameter

$$\widetilde{E}_0(r, z) = \frac{1}{q(z)} \exp\left[-jk_0\left(\frac{r^2}{2q(z)}\right)\right]. \tag{2.223}$$

Free space propagation is then described by

$$q(z) = z + jz_R \tag{2.224}$$

Using the inverse q-parameter, decomposed in real and imagniary parts,

$$\frac{1}{q(z)} = \frac{1}{R(z)} - j\frac{\lambda}{\pi w^2(z)}. \tag{2.225}$$

leads to

$$\widetilde{E}_0(r,z) = \frac{\sqrt{2P}}{\sqrt{\pi}w(z)} \exp\left[-\frac{r^2}{w^2(z)} - jk_0\frac{r^2}{2R(z)} + j\zeta(z)\right]. \tag{2.226}$$

Thus $w(z)$ is the waist of the beam and $R(z)$ is the radius of the phase fronts. We normalized the beam such that the Gaussian beam intensity $I(z,r) = \left|\widetilde{E}_0(r,z)\right|^2$ expressed in terms of the power P carried by the beam is given by

$$I(r,z) = \frac{2P}{\pi w^2(z)} \exp\left[-\frac{2r^2}{w^2(z)}\right], \tag{2.227}$$

$$\text{i.e.} \quad P = \int_0^{\infty}\int_0^{2\pi} I(r,z)\ r dr\ d\varphi. \tag{2.228}$$

The use of the q-parameter simplifies the description of Gaussian beam propagation. In free space propagation from z_1 to z_2, the variation of the beam parameter q is simply governed by

$$q_2 = q_1 + z_2 - z_1. \tag{2.229}$$

where q_2 and q_1 are the beam parameters at z_1 and z_2.

If the beam waist, at which the beam has a minimum spot size w_0 and a planar wavefront ($R = \infty$), is located at $z = 0$, the variations of the beam spot size and the radius of curvature of the phase fronts are explicitly expressed as

$$w(z) = w_o\left[1 + \left(\frac{z}{z_R}\right)^2\right]^{1/2}, \tag{2.230}$$

and

$$R(z) = z\left[1 + \left(\frac{z_R}{z}\right)^2\right], \tag{2.231}$$

where z_R is called the Rayleigh range. The Rayleigh range is the distance over which the cross section of the beam doubles. The Rayleigh range is related to the initial beam waist and the wavelength of light according to

$$z_R = \frac{\pi w_o^2}{\lambda}. \tag{2.232}$$

Intensity

Figure 2.57 shows the intensity of the Gaussian beam according to Eq.(2.227) for different propagation distances.

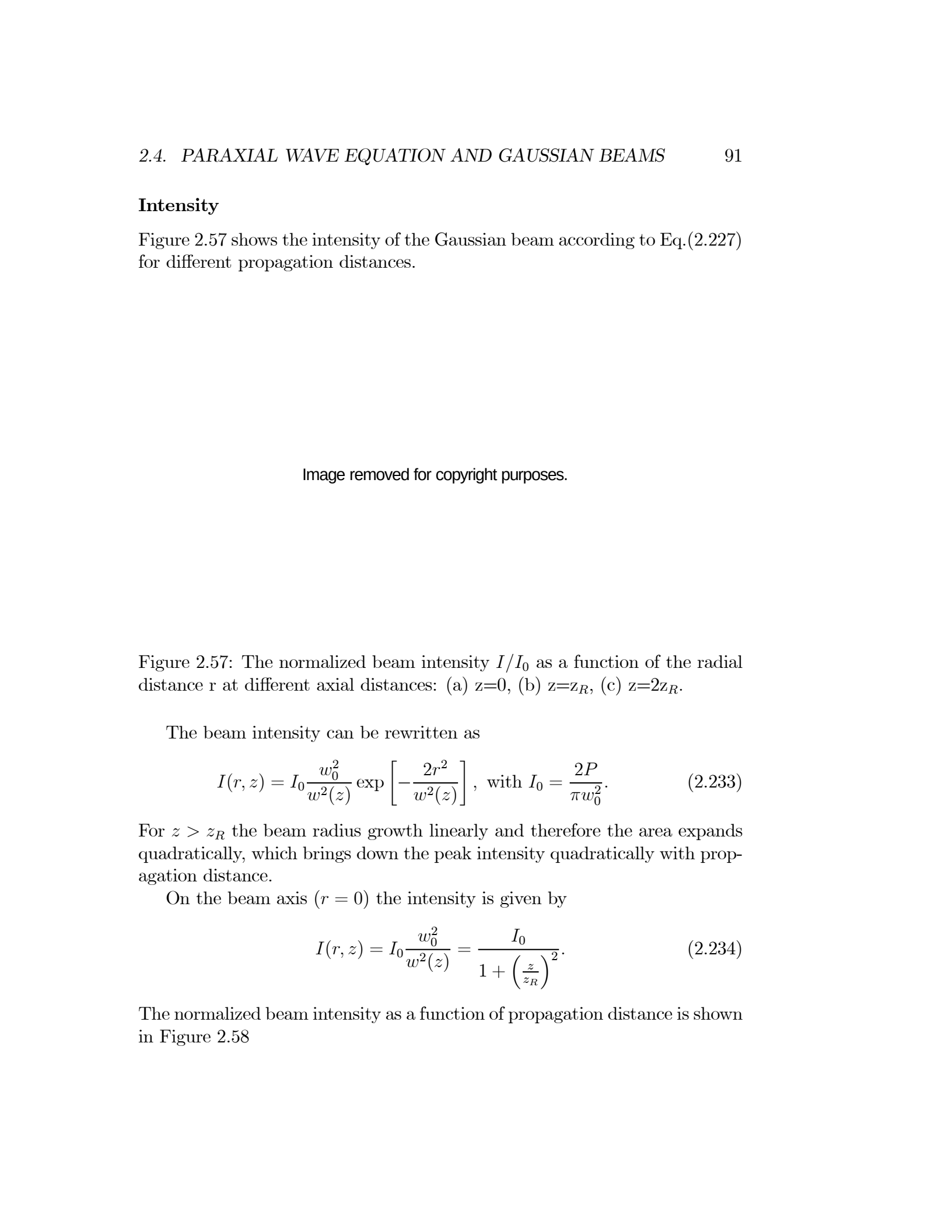

Figure 2.57: The normalized beam intensity I/I_0 as a function of the radial distance r at different axial distances: (a) z=0, (b) z=z_R, (c) z=2z_R.

The beam intensity can be rewritten as

$$I(r,z) = I_0 \frac{w_0^2}{w^2(z)} \exp\left[-\frac{2r^2}{w^2(z)}\right], \text{ with } I_0 = \frac{2P}{\pi w_0^2}. \tag{2.233}$$

For $z > z_R$ the beam radius growth linearly and therefore the area expands quadratically, which brings down the peak intensity quadratically with propagation distance.

On the beam axis ($r = 0$) the intensity is given by

$$I(r,z) = I_0 \frac{w_0^2}{w^2(z)} = \frac{I_0}{1 + \left(\frac{z}{z_R}\right)^2}. \tag{2.234}$$

The normalized beam intensity as a function of propagation distance is shown in Figure 2.58

Figure 2.58: The normalized Beam intensity $I(r=0)/I_0$ on the beam axis as a function of propagation distance z [6], p. 84.

Power

The fraction of the total power contained in the beam up to a certain radius is

$$\begin{aligned} \frac{P(r<r_0)}{P} &= \frac{2\pi}{P}\int_0^{r_0} I(r,z)rdr \\ &= \frac{4}{w^2(z)}\int_0^{r_0} \exp\left[-\frac{2r^2}{w^2(z)}\right] rdr \\ &= 1-\exp\left[-\frac{2r_0^2}{w^2(z)}\right]. \end{aligned} \tag{2.235}$$

Thus, there is a certain fraction of power within a certain radius of the beam

$$\frac{P(r<w(z))}{P} = 0.86, \tag{2.236}$$

$$\frac{P(r<1.5w(z))}{P} = 0.99. \tag{2.237}$$

Beam radius

Due to diffraction, the smaller the spot size at the beam waist, the faster the beam diverges according to 2.230 as illustrated in Figure **??**.

Figure 2.59: Gaussian beam and its characteristics.

Beam divergence

The angular divergence of the beam is inversely proportional to the beam waist. In the far field, the half angle divergence is given by

$$\theta = \frac{\lambda}{\pi w_o}, \tag{2.238}$$

see Figure 2.59.

Confocal parameter and depth of focus

In linear microscopy, only a layer which has the thickness over which the beam is focused, called depth of focus, will contribute to a sharp image. In nonlinear microscopy (see problem set) only a volume on the order of beam cross section times depth of focus contributes to the signal. Therefore, the depth of focus or confocal parameter of the Gaussian beam, is the distance over which the beam stays focused and is defined as twice the Rayleigh range

$$b = 2z_R = \frac{2\pi w_o^2}{\lambda}. \tag{2.239}$$

The confocal parameter depends linear on the spot size (area) of the beam and is inverse to the wavelength of light. At a wavelength of $1\mu m$ a beam with a radius of $w_o = 1cm$,.the beam will stay focussed ove distances as long

600m. However, if the beam is stronlgy focussed down to $w_o = 10\mu m$ the field of depth is only 600μm.

Phase

The phase delay of the Gaussian beam is

$$\Phi(r,z) = k_0 z - \zeta(z) + k_0 \frac{r^2}{2R(z)} \tag{2.240}$$

$$\zeta(z) = \arctan\left(\frac{z}{z_R}\right). \tag{2.241}$$

On beam axis, there is the additional phase $\zeta(z)$ when the beam undergoes focussing as shown in Figure 2.60. This is in addition to the phase shift that a uniform plane wave already aquires.

Figure 2.60: Phase delay of a Gaussian beam relative to a uniform plane wave on the beam axis [6], p. 87. This phase shift is known as Guoy-Phase-Shift.

This effect is known as Guoy-Phase-Shift. The third term in the phase shift is parabolic in the radius and describes the wavefront (planes of constant phase) bending due to the focusing, i.e. distortion from the uniform plane wave.

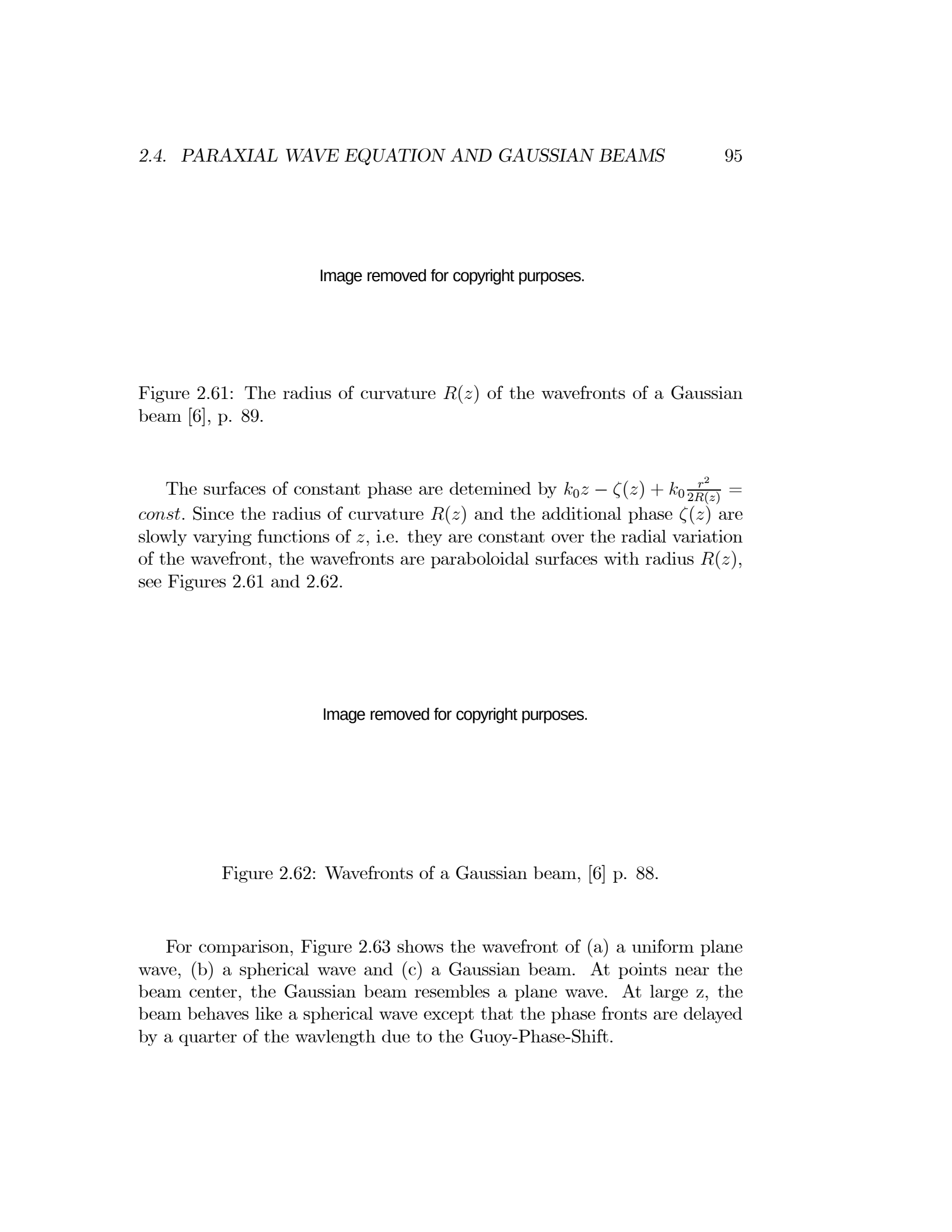

Figure 2.61: The radius of curvature $R(z)$ of the wavefronts of a Gaussian beam [6], p. 89.

The surfaces of constant phase are detemined by $k_0 z - \zeta(z) + k_0 \frac{r^2}{2R(z)} = const.$ Since the radius of curvature $R(z)$ and the additional phase $\zeta(z)$ are slowly varying functions of z, i.e. they are constant over the radial variation of the wavefront, the wavefronts are paraboloidal surfaces with radius $R(z)$, see Figures 2.61 and 2.62.

Figure 2.62: Wavefronts of a Gaussian beam, [6] p. 88.

For comparison, Figure 2.63 shows the wavefront of (a) a uniform plane wave, (b) a spherical wave and (c) a Gaussian beam. At points near the beam center, the Gaussian beam resembles a plane wave. At large z, the beam behaves like a spherical wave except that the phase fronts are delayed by a quarter of the wavlength due to the Guoy-Phase-Shift.

Figure 2.63: Wavefronts of (a) a uniform plane wave;(b) a spherical wave; (c) a Gaussian beam [5], p. 89.

2.5 Rays and Optical Systems

Now, that we understand how a beam of finite size as a solution of Maxwell's Equations can be constructed, we are interested how such a beam can be imaged by an optical system. Propagation of a Gaussian beam in free space leads to spreading of the beam because of the diffraction. We need means to focus the beam again. The output beam from a laser may have a certain size but we may need a different size for a given experiment. We can change the size or focus the beam by an optical imaging system. Optical systems are studied and analyzed using ray optics. What is a ray? We have already discussed that diffraction of a beam is similar to dispersion of an optical pulse. Dispersion of a pulse we understood because of the different group velocity of different frequency components or sub-pulses. It turns out that

these sub-pulses are the temporal analog to the rays. In the same way we can construct a short pulse by a superposition of sub-pulses with different center frequencies, we can construct a Gaussian beam by sub-beams with different center transverse k-vectors and a very narrow spread in transverse k-vectors. These are Gaussian beams with a large beam diameter such that diffraction is not any longer important. These beams are called rays. The ray only experiences a phase shift during propagation depending on the local refractive index $n(r)$. Therefore, we can completely understand the imaging of Gaussian beams in paraxial optical systems by the imaging properties of rays.

2.5.1 Ray Propagation

A ray propagating in an optical system, see Figure 2.64, can be described by its position r with respect to the optical axis and its inclination with respect to the optical axis r'. It is advantageous to use not (r, r') as the ray coordinates but the combination $(r, n\ r')$, where n is the local refractive index at the position of the ray. Due to propagation, the ray coordinates may change, which can be desribed by a marix, that maps initial position and inclination into the corresponding quantitaties after the propagation

$$\begin{pmatrix} r_2 \\ n_2 r_2' \end{pmatrix} = \begin{pmatrix} A & B \\ C & D \end{pmatrix} \begin{pmatrix} r_1 \\ n_1 r_1' \end{pmatrix}. \tag{2.242}$$

This imaging matrix is called an ABCD-matrix.

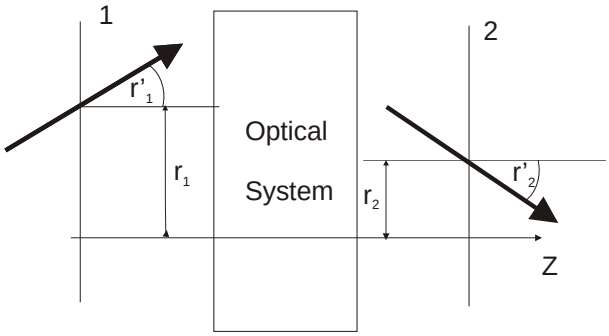

Figure 2.64: Description of optical ray propagation by its distance and inclination from the optical axis

The advantage in using $(r, n\ r')$ as the ray coordinates is that it preserves the phase space volume, i.e. for lossless optical systems the determinant of the ABCD-matrix must be 1. Also Snell's law for paraxial rays has then a simple form, see Figure 2.65. For paraxial rays the angles to the interface normal, θ_1 and θ_2, are much smaller than 1, and we can write

$$r'_1 = \tan\theta_1 \approx \sin\theta_1 \approx \theta_1, \text{ and } r'_2 = \tan\theta_2 \approx \sin\theta_2 \approx \theta_2.$$

Then Snell's law is

$$n_1\ r'_1 = n_2\ r'_2. \tag{2.243}$$

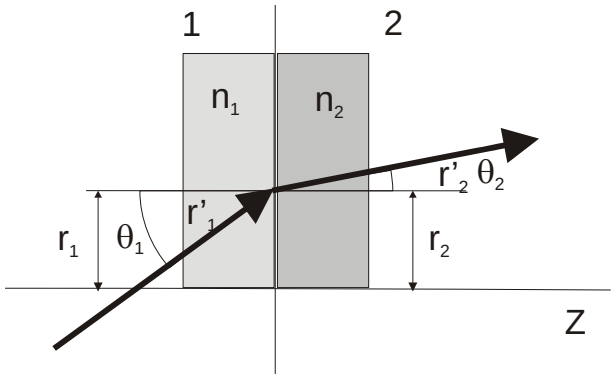

Figure 2.65: Snell's law for paraxial rays

The ABCD-matrix describing a ray going from a medium with index n_1 to a medium with index n_2 is the unity matrix

$$r_2 = r_1 \tag{2.244}$$
$$n_2\ r'_2 = n_1\ r'_1. \tag{2.245}$$

Free space propagation

For propagation in free space, see Figure 2.66, the relationship between input and output ray parameters is

$$r_2 = r_1 + r'_1 \cdot L$$
$$r'_2 = r'_1$$

or the propagation matrix is

$$\mathbf{M} = \begin{pmatrix} 1 & L \\ 0 & 1 \end{pmatrix}. \tag{2.246}$$

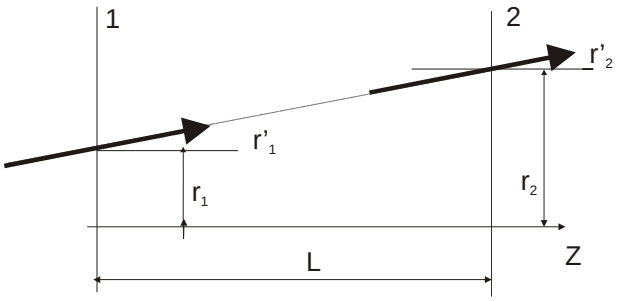

Figure 2.66: Free space propagation

Propagation in medium with length L and index n

Free propagation through a medium with index n does result in a reduced position shift with respect to the optical axis in comparison to free space, because the beam is first bent to the optical axis according to Snell's law, see Figure 2.67. Therefore the corresponding ABCD-matrix is

$$\mathbf{M} = \begin{pmatrix} 1 & L/n \\ 0 & 1 \end{pmatrix}. \tag{2.247}$$

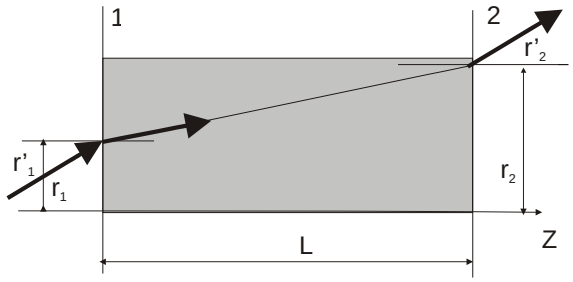

Figure 2.67: Ray propagation through a medium with refractive index n, shortens the path length of the beam by a factor of n.

Parbolic surface or thin lens

Plano-Convex Lens When a ray penetrates a parabolic surface between two media with refractive indices n_1 and n_2, it changes its inclination. A parabolic surface can be closely approximated by the surface of a sphere, see Figure 2.68. Snells law in paraxial approximation is

$$n_1 \ (r_1' + \alpha) = n_2 \ (r_2' + \alpha) \, . \tag{2.248}$$

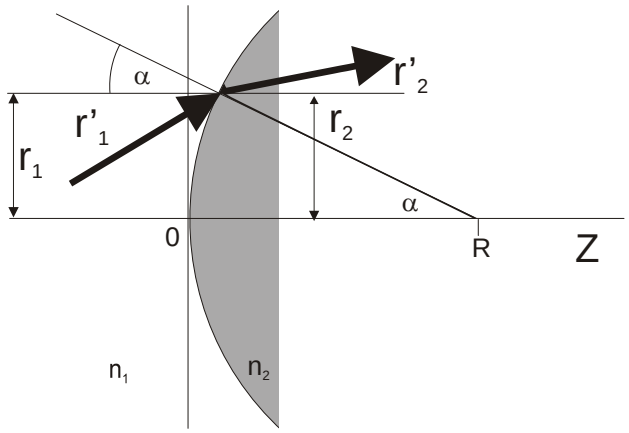

Figure 2.68: Derivation of ABCD-matrix of a thin plano-convex lens.

The small angle α can be approximated by $\alpha \approx r_1/R$. In total we then obtain the mapping

$$r_2 = r_1 \tag{2.249}$$

$$n_2 \, r_2' = n_1 \, r_1' + \frac{n_1 - n_2}{R} r_1 \tag{2.250}$$

or

$$\mathbf{M} = \begin{pmatrix} 1 & 0 \\ \frac{n_1 - n_2}{R} & 1 \end{pmatrix} . \tag{2.251}$$

Note, the second normal interface does not change the ray propagation matrix and therefore Eq.(2.251) describes correctly the ray propagation through a thin plano-convex lens.

Biconvex Lens If the lens would have a second convex surface, this would refract the ray twice as strongly and we would obtain

$$\mathbf{M} = \begin{pmatrix} 1 & 0 \\ 2\frac{n_1-n_2}{R} & 1 \end{pmatrix}. \tag{2.252}$$

The quantity $2\frac{n_2-n_1}{R}$ is called the refractive strength of the biconvex lense or inverse focal length $1/f$.Because the system of a thin lens plus free space propagation results in the matrix (calculated in the reverse order)

$$\mathbf{M}_{tot} = \begin{pmatrix} 1 & f \\ 0 & 1 \end{pmatrix} \begin{pmatrix} 1 & 0 \\ -\frac{1}{f} & 1 \end{pmatrix} = \begin{pmatrix} 0 & f \\ -\frac{1}{f} & 1 \end{pmatrix}, \tag{2.253}$$

which ensures that each ray parallel to the optical axis goes through the on axis focal point at the end of the free space section, see Figure 2.69.

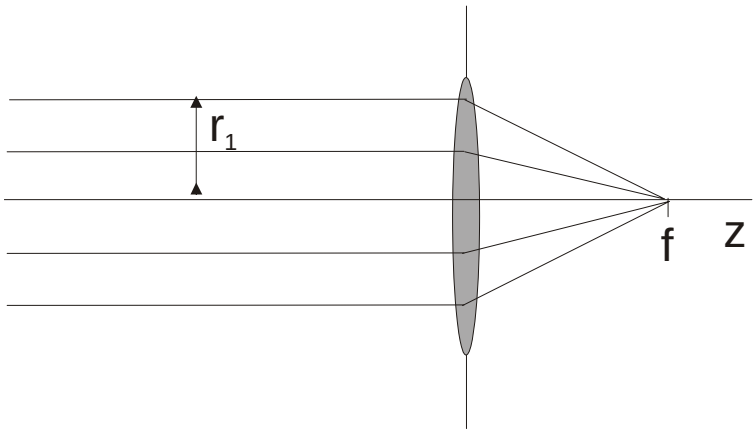

Figure 2.69: Imaging of parallel rays through a lens with focal length f.

Curved Mirrors

Other often used optical components in imaging systems are curved mirrors with radius of curvature $ROC = R$, see Figure 2.70. The advantage of reflective optics is that the rays don't have to pass through dispersive material like through a lense, which is very disturbing for ultrashort pulses.

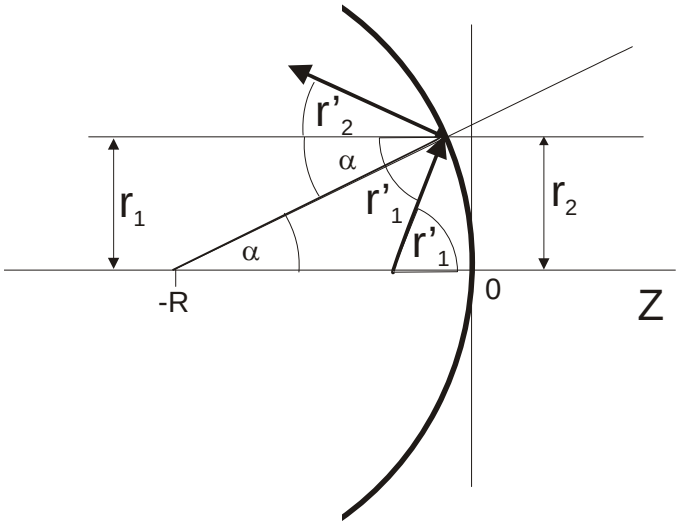

Figure 2.70: Derivation of ray matrix for concave mirror with Radius R.

As in the case of the thin lens,e the imaging does not change the distance of the ray from the optical axis, however, the slope of the rays obey

$$r_1' - \alpha = r_2' + \alpha. \tag{2.254}$$

with $\alpha \approx r_1/R$ in paraxial approximation. Therefore the ABCD matrix describing the reflection of rays at a curved mirror with $ROC = R$ is

$$\mathbf{M} = \begin{pmatrix} 1 & 0 \\ -\frac{1}{f} & 1 \end{pmatrix}, \text{ with } f = \frac{R}{2}. \tag{2.255}$$

2.5.2 Gauss' Lens Formula

As a simple application of the ray matrices for optical system design, we derive Gauss' lens formula, which says that all rays emitted from an orignial placed a distance d_1 from a lens with focal length f form an image at a distance d_2, which is related to d_1 by

$$\frac{1}{d_1} + \frac{1}{d_2} = \frac{1}{f}, \tag{2.256}$$

see Figure 2.71.

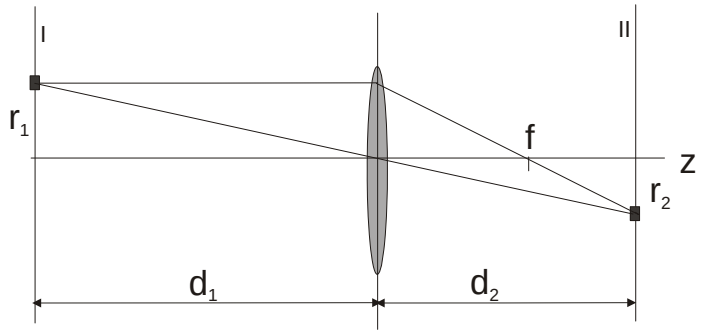

Figure 2.71: Gauss' lens formula.

The magnification of the lens system is $M_r = \frac{r_2}{r_1} = \frac{d_2}{d_1} = \left|\frac{f}{d_1 - f}\right|$. The ray matrix that describes the imagaing from the orignal plane I to the image plane II is described by the product

$$\begin{aligned}\begin{pmatrix} A & B \\ C & D \end{pmatrix} &= \begin{pmatrix} 1 & d_2 \\ 0 & 1 \end{pmatrix} \begin{pmatrix} 1 & 0 \\ -\frac{1}{f} & 1 \end{pmatrix} \begin{pmatrix} 1 & d_1 \\ 0 & 1 \end{pmatrix} \\ &= \begin{pmatrix} 1 - \frac{d_2}{f} & \left(1 - \frac{d_2}{f}\right) d_1 + d_2 \\ -\frac{1}{f} & 1 - \frac{d_1}{f} \end{pmatrix}. \end{aligned} \tag{2.257}$$

In order that the distance r_2 only depends on r_1, but not on r_1', B must be 0, which is Eq. (2.256). Thus in total we have

Magnification	$M_r =$	$\left\|\frac{f}{d_1 - f}\right\|$	
Distance to focus	$d_2 - f = M_r^2 (d_1 - f)$		

(2.258)

More complicated imaging systems, such as thick lenses, can be described by ray matrices and arbitrary paraxial optical systems can be analyzed with them, which shall not be pursued further here. Rather, we want to study how Gaussian beams are imaged by paraxial optical systems

2.6 Gaussian Beams and Resonators

2.6.1 Gaussian Beam Propagation

The propagation of Gaussian beams through paraxial optical systems can be efficiently evaluated using the ABCD-law [4], which states that the q-

parameter of a Gaussian beam passing a optical system described by an ABCD-marix is given by

$$q_2 = \frac{Aq_1 + B}{Cq_1 + D}, \tag{2.259}$$

where q_1 and q_2 are the beam parameters at the input and the output planes of the optical system or component, see Figure 2.72

Figure 2.72: Gaussian beam transformation by ABCD law, [6], p. 99.

To proove this law, we realize that it is true for the case of free space propagation, i.e. pure diffraction, comparing (2.259) with (2.229) and (2.246). If we can proove that it is additionally true for a thin lens, then we are finished, because every ABCD matrix (2x2 matrix) can be written as a product of a lower and upper triangular matrix (LR-decomposition) like the one for free space propagation and the thin lens. Note, the action of the lens is identical to the action of free space propagation, but in the Fourier-domain. In the Fourier domain the Gaussian beam parameter is replaced by its inverse (2.222)

$$\widetilde{E}_0(x, y, z) = \frac{j}{q(z)} \exp\left[-jk_0\left(\frac{x^2 + y^2}{2q(z)}\right)\right]. \tag{2.260}$$

$$\widetilde{E}_0(k_z, k_y, z) = 2\pi j \exp\left[-jq(z)\left(\frac{k_z^2 + k_y^2}{2k_0}\right)\right] \tag{2.261}$$

But the inverse q-parameter transforms according to (2.259)

$$\frac{1}{q_2} = \frac{D\frac{1}{q_1} + C}{B\frac{1}{q_1} + A}, \tag{2.262}$$

which leads for a thin lens to

$$\frac{1}{q_2} = \frac{1}{q_1} - \frac{1}{f}. \tag{2.263}$$

This is exactly what a thin lens does, see Eq.(2.225), it changes the radius of curvature of the phase front but not the waist of the beam according to

$$\frac{1}{R_2} = \frac{1}{R_1} - \frac{1}{f}. \tag{2.264}$$

With that finding, we have proven the ABCD law for Gaussian beam propagation through paraxial optical systems.

The ABCD-matrices of the optical elements discussed so far including nonnomal incidence are summarized in Table 2.6. As an application of the

Optical Element	ABCD-Matrix
Propagation in Medium with index n and length L	$\begin{pmatrix} 1 & L/n \\ 0 & 1 \end{pmatrix}$
Thin Lens with focal length f	$\begin{pmatrix} 1 & 0 \\ -1/f & 1 \end{pmatrix}$
Mirror under Angle θ to Axis and Radius R Sagittal Plane	$\begin{pmatrix} 1 & 0 \\ \frac{-2\cos\theta}{R} & 1 \end{pmatrix}$
Mirror under Angle θ to Axis and Radius R Tangential Plane	$\begin{pmatrix} 1 & 0 \\ \frac{-2}{R\cos\theta} & 1 \end{pmatrix}$
Brewster Plate under Angle θ to Axis and Thickness d, Sagittal Plane	$\begin{pmatrix} 1 & \frac{d}{n} \\ 0 & 1 \end{pmatrix}$
Brewster Plate under Angle θ to Axis and Thickness d, Tangential Plane	$\begin{pmatrix} 1 & \frac{d}{n^3} \\ 0 & 1 \end{pmatrix}$

Table 2.6: ABCD matrices for commonly used optical elements.

Gaussian beam propagation, lets consider the imaging of a Gaussian beam with a waist w_{01} by a thin lens at a distance d_1 away from the waist to a beam with a different size w_{02}, see Figure 2.73.

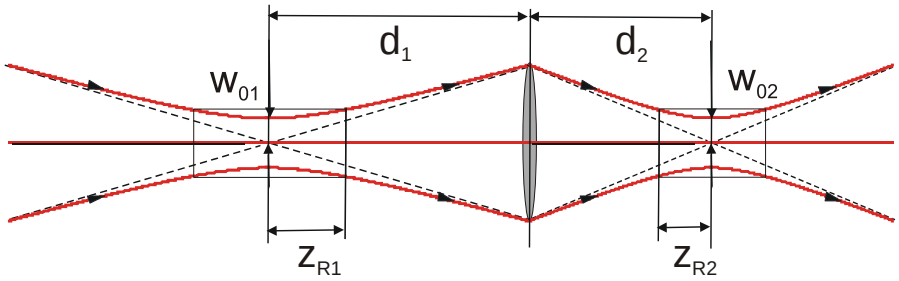

Figure 2.73: Focusing of a Gaussian beam by a lens.

There will be a new focus at a distance d_2.The corresponding ABCD matrix is of course the one from Eq.(2.257), which is repeated here

$$\begin{pmatrix} A & B \\ C & D \end{pmatrix} = \begin{pmatrix} 1-\frac{d_2}{f} & \left(1-\frac{d_2}{f}\right) d_1 + d_2 \\ -\frac{1}{f} & 1-\frac{d_1}{f} \end{pmatrix}. \tag{2.265}$$

The q-parameter of the Gaussian beam at the position of minimum waist is purely imaginary $q_1 = jz_{R1} = j\frac{\pi w_{01}^2}{\lambda}$ and $q_2 = jz_{R2} = j\frac{\pi w_{02}^2}{\lambda}$, where

$$q_2 = \frac{A\ q_1 + B}{C\ q_1 + D} = \frac{jz_{R1}A + B}{jz_{R1}C + D} = \frac{jz_{R1}A + B}{jz_{R1}C + D} = jz_{R2}. \tag{2.266}$$

In the limit of ray optics, where the beam waists can be considered to by zero, i.e. $z_{R1} = z_{R2} = 0$ we obtain $B = 0$, i.e. the imaging rule of classical ray optics Eq.(2.256). It should not come at a surprise that for the Gaussian beam propagation this law does not determine the exact distance d_2 of the position of the new waist. Because, in the ray analysis we neglected diffraction. Therefore, the Gaussian beam analysis, although it uses the same description of the optical components, gives a slightly different and improved answer for the position of the focal point. To find the position d_2, we request that the real part of the right hand side of (2.266) is zero,

$$BD - z_{R1}^2 AC = 0 \tag{2.267}$$

which can be rewritten as

$$\frac{1}{d_2} = \frac{1}{f} - \frac{1}{d_1 + \frac{z_{R1}^2}{d_1 - f}}. \tag{2.268}$$

Again for $z_{R1} \to 0$, we obtain the ray optics result. And the imaginary part of Eq.(2.266) leads to

$$\frac{1}{z_{R2}} = \frac{1}{z_{R1}} \left(D^2 + z_{R1}^2 C^2 \right), \tag{2.269}$$

or

$$\frac{1}{w_{02}^2} = \frac{1}{w_{01}^2} \left(1 - \frac{d_1}{f} \right)^2 \left[1 + \left(\frac{z_{R1}}{d_1 - f} \right)^2 \right]. \tag{2.270}$$

With the magnification M for the spot size, with is closely related to the Magnification M_r of ray optics, we can rewrite the results as

Magnification	$M = M_r/\sqrt{1+\xi^2}$, with $\xi = \frac{z_{R1}}{d_1 - f}$ and $M_r = \left\lvert \frac{f}{d_1 - f} \right\rvert$
Beam waist	$w_{02} = M \cdot w_{01}$
Confocal parameter	$2z_{R2} = M^2\ 2z_{R2}$
Distance to focus	$d_2 - f = M^2 (d_1 - f)$
Divergence	$\theta_{02} = \theta_{01}/M$

(2.271)

2.6.2 Resonators

With the Gaussian beam solutions, we can finally construct optical resonators with finite transverse extent, i.e. real Fabry-Perots, by inserting into the Gaussian beam, see Figure 2.74, curved mirrors with the proper radius of curvature, such that the beam is imaged upon itself.

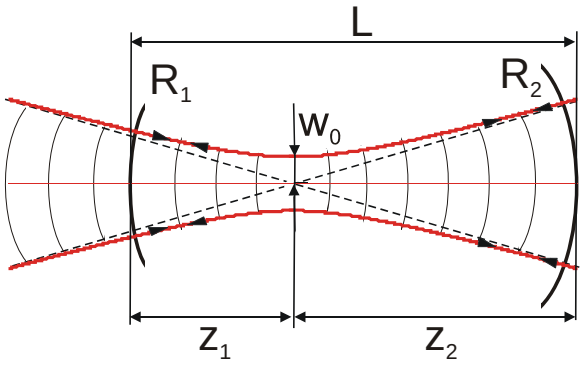

Figure 2.74: Fabry-Perot resonator with finite beam cross section by inserting curved mirrors into the beam to back reflect the beam onto itself.

Any resonator can be unfolded into a sequence of lenses and free space propagation. Here, we replace the curved mirrors by equivalent lenses with $f_1 = R_1/2$, and $f_2 = R_2/2$, see Figure 2.75.

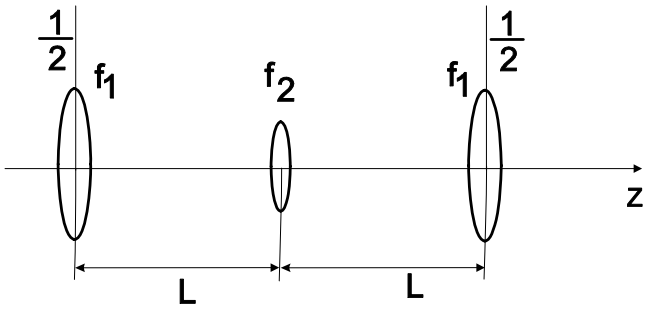

Figure 2.75: Two-mirror resonator unfolded. Note, only one half of the focusing strength of mirror 1 belongs to a fundamental period describing one resonator roundtrip.

The product of ABCD matrices describing one roundtrip of the beam in the resonator according to Figure 2.75 is

$$M = \begin{pmatrix} 1 & 0 \\ \frac{-1}{2f_1} & 1 \end{pmatrix} \begin{pmatrix} 1 & L \\ 0 & 1 \end{pmatrix} \begin{pmatrix} 1 & 0 \\ \frac{-1}{f_2} & 1 \end{pmatrix} \begin{pmatrix} 1 & L \\ 0 & 1 \end{pmatrix} \begin{pmatrix} 1 & 0 \\ \frac{-1}{2f_1} & 1 \end{pmatrix}. \quad (2.272)$$

To carry out this product and to formulate the cavity stability criteria, it is convenient to use the cavity parameters $g_i = 1 - L/R_i, i = 1, 2$. The resulting cavity roundtrip ABCD-matrix can be written in the form

$$M = \begin{pmatrix} (2g_1g_2 - 1) & 2g_2L \\ 2g_1\left(g_1g_2 - 1\right)/L & (2g_1g_2 - 1) \end{pmatrix} = \begin{pmatrix} A & B \\ C & D \end{pmatrix}. \quad (2.273)$$

Resonator Stability

The ABCD matrices describe the dynamics of rays propagating inside the resonator. The resonator is stable if no ray escapes after many round-trips, which is the case when the magnitude of the eigenvalues of the matrix M are less than one. Since we have a lossless resonator, i.e. $\det|M| = 1$, the product of the eigenvalues has to be 1 and, therefore, the stable resonator

corresponds to the case of a complex conjugate pair of eigenvalues with a magnitude of 1. The eigenvalue equation to M is given by

$$\det|M-\lambda\cdot 1| = \det\left|\begin{pmatrix} (2g_1g_2-1)-\lambda & 2g_2L \\ 2g_1(g_1g_2-1)/L & (2g_1g_2-1)-\lambda \end{pmatrix}\right| = 0, \quad (2.274)$$

$$\lambda^2 - 2(2g_1g_2-1)\lambda + 1 = 0. \quad (2.275)$$

The eigenvalues are

$$\lambda_{1/2} = (2g_1g_2-1) \pm \sqrt{(2g_1g_2-1)^2-1}, \quad (2.276)$$

$$= \begin{cases} \exp(\pm\theta), \cosh\theta = 2g_1g_2-1, \text{ for } |2g_1g_2-1|>1 \\ \exp(\pm j\psi), \cos\psi = 2g_1g_2-1, \text{ for } |2g_1g_2-1|\le 1 \end{cases} \quad (2.277)$$

The case of a complex conjugate pair corresponds to a stable resontor. Therefore, the stability criterion for a stable two mirror resonator is

$$|2g_1g_2-1| \le 1. \quad (2.278)$$

The stable and unstable parameter ranges are given by

$$\text{stable} : 0 \le g_1\cdot g_2 = S \le 1 \quad (2.279)$$

$$\text{unstable} : g_1g_2 \le 0; \text{ or } g_1g_2 \ge 1. \quad (2.280)$$

where $S = g_1\cdot g_2$, is the stability parameter of the cavity. The stability criterion can be easily interpreted geometrically. Of importance are the distances between the mirror mid-points M_i and the cavity end points, i.e. $g_i = (R_i - L)/R_i = -S_i/R_i$, as shown in Figure 2.76.

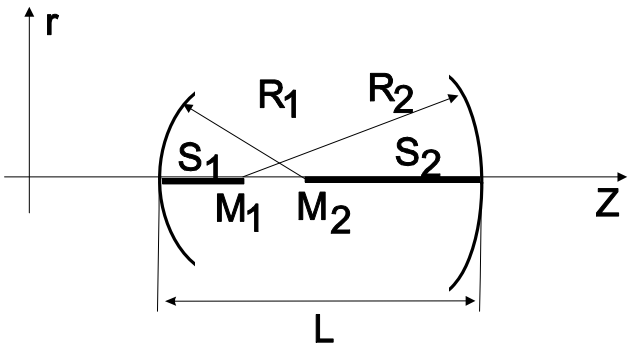

Figure 2.76: The stability criterion involves distances between the mirror mid-points M_i and the cavity end points. i.e. $g_i = (R_i - L)/R_i = -S_i/R_i$.

The following rules for a stable resonator can be derived from Figure 2.76 using the stability criterion expressed in terms of the distances S_i. Note, that the distances and radii can be positive and negative

$$\text{stable} : 0 \leq \frac{S_1 S_2}{R_1 R_2} \leq 1. \tag{2.281}$$

The rules are:

- A resonator is stable if the mirror radii, laid out along the optical axis, overlap.
- A resonator is unstable if the radii do not overlap or one lies within the other.

Figure 2.77 shows stable and unstable resonator configurations.

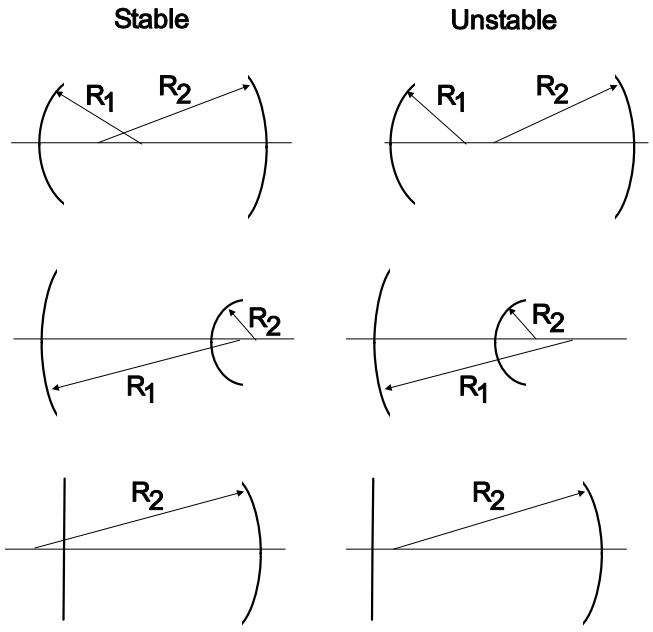

Figure 2.77: Illustration of stable and unstable resonator configurations.

For a two-mirror resonator with concave mirrors and $R_1 \leq R_2$, we obtain the general stability diagram as shown in Figure 2.78.

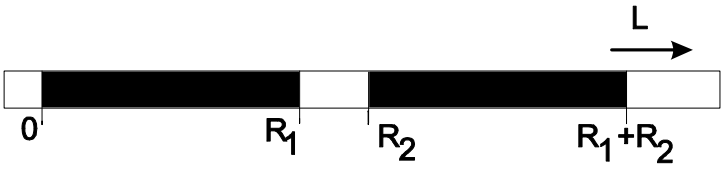

Figure 2.78: Stabile regions (black) for the two-mirror resonator.

There are two ranges for the mirror distance L, within which the cavity is stable, $0 \leq L \leq R_1$ and $R_2 \leq L \leq R_1 + R_2$. It is interesting to investigate the spot size at the mirrors and the minimum spot size in the cavity as a function of the mirror distance L.

Resonator Mode Characteristics

The stable modes of the resonator reproduce themselves after one round-trip, i.e.

$$q_1 = \frac{Aq_1 + B}{Cq_1 + D} \tag{2.282}$$

The inverse q-parameter, which is directly related to the phase front curvature and the spot size of the beam, is determined by

$$\left(\frac{1}{q}\right)^2 + \frac{A-D}{B}\left(\frac{1}{q}\right) + \frac{1-AD}{B^2} = 0. \tag{2.283}$$

The solution is

$$\left(\frac{1}{q}\right)_{1/2} = -\frac{A-D}{2B} \pm \frac{j}{2\,|B|}\sqrt{(A+D)^2 - 1} \tag{2.284}$$

If we apply this formula to (2.273), we find the spot size on mirror 1

$$\left(\frac{1}{q}\right)_{1/2} = -\frac{j}{2\,|B|}\sqrt{(A+D)^2 - 1} = -j\frac{\lambda}{\pi w_1^2}. \tag{2.285}$$

or

$$w_1^4 = \left(\frac{2\lambda L}{\pi}\right)^2 \frac{g_2}{g_1}\frac{1}{1-g_1g_2} \tag{2.286}$$

$$= \left(\frac{\lambda R_1}{\pi}\right)^2 \frac{R_2 - L}{R_1 - L}\left(\frac{L}{R_1 + R_2 - L}\right). \tag{2.287}$$

By symmetry, we find the spot size on mirror 3 by switching index 1 and 2:

$$w_2^4 = \left(\frac{2\lambda L}{\pi}\right)^2 \frac{g_1}{g_2}\frac{1}{1-g_1g_2} \tag{2.288}$$

$$= \left(\frac{\lambda R_2}{\pi}\right)^2 \frac{R_1-L}{R_2-L}\left(\frac{L}{R_1+R_2-L}\right). \tag{2.289}$$

The intracavity focus can be found by transforming the focused Gaussian beam with the propagation matrix

$$M = \begin{pmatrix} 1 & z_1 \\ 0 & 1 \end{pmatrix}\begin{pmatrix} 1 & 0 \\ \frac{-1}{2f_1} & 1 \end{pmatrix}$$

$$= \begin{pmatrix} 1-\frac{z_1}{2f_1} & z_1 \\ \frac{-1}{2f_1} & 1 \end{pmatrix}, \tag{2.290}$$

to its new focus by properly choosing z_1, see Figure 2.74. A short calculation results in

$$z_1 = L\frac{g_2\,(g_1-1)}{2g_1g_2-g_1-g_2} \tag{2.291}$$

$$= \frac{L(L-R_2)}{2L-R_1-R_2}, \tag{2.292}$$

and, again, by symmetry

$$z_2 = L\frac{g_1\,(g_2-1)}{2g_1g_2-g_1-g_2} \tag{2.293}$$

$$= \frac{L(L-R_1)}{2L-R_1-R_2} = L-z_1. \tag{2.294}$$

The spot size in the intracavity focus is

$$w_o^4 = \left(\frac{\lambda L}{\pi}\right)^2 \frac{g_1g_2\,(1-g_1g_2)}{(2g_1g_2-g_1-g_2)^2} \tag{2.295}$$

$$= \left(\frac{\lambda}{\pi}\right)^2 \frac{L(R_1-L)(R_2-L)(R_1+R_2-L)}{(R_1+R_2-2L)^2}. \tag{2.296}$$

All these quantities for the two-mirror resonator are shown in Figure 2.79.

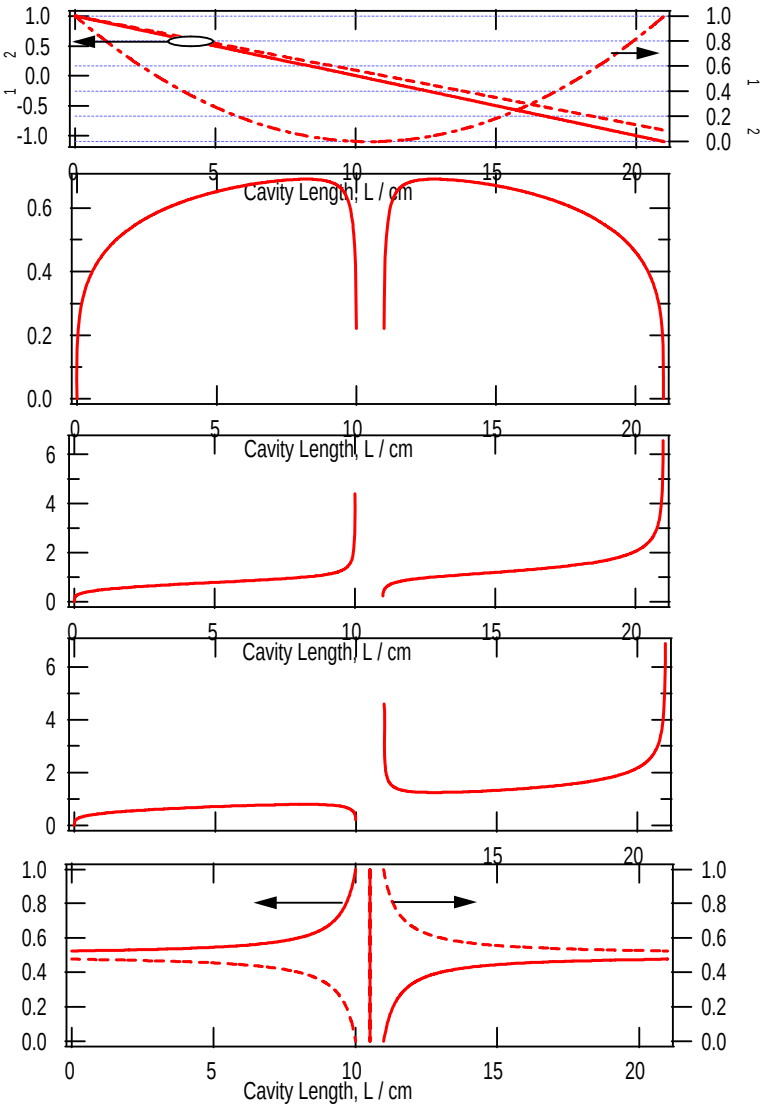

Figure 2.79: From top to bottom: Cavity parameters, g_1, g_2, S, w_0, w_1, w_2, z_1 and z_2 for the two-mirror resonator with $R_1 = 10$ cm and $R_2 = 11$ cm.

Hermite-Gaussian-Beams ($\mathbf{TEM}_{pq}$-Beams)

It turns out that the Gaussian Beams are not the only solution to the paraxial wave equation (2.219). The stable modes of the resonator reproduce themselves after one round-trip,

$$\begin{aligned}\widetilde{E}_{l,m}(x,y,z) &= A_{l,m}\left[\frac{w_0}{w(z)}\right] G_l\left[\frac{\sqrt{2x}}{w(z)}\right] G_m\left[\frac{\sqrt{2y}}{w(z)}\right] \cdot \\ &\quad \exp\left[-jk_0\left(\frac{x^2+y^2}{2R(z)}\right) + j(l+m+1)\zeta(z)\right]\end{aligned} \tag{2.297}$$

where

$$G_l[u] = H_l[u]\exp\left[-\frac{u^2}{2}\right], \text{ for } l = 0,1,2,... \tag{2.298}$$

are the Hermite-Gaussians with the Hermite-Polynomials

$$\begin{aligned}H_0[u] &= 1, \\ H_1[u] &= 2u, \\ H_2[u] &= 4u^2 - 1, \\ H_3[u] &= 8u^3 - 12u,\end{aligned} \tag{2.299}$$

and $\zeta(z)$ is the Guoy-Phase-Shift according to Eq.(2.241). The lower order Hermite Gaussians are depicted in Figure 2.80

Figure 2.80: Hermite-Gauissians $G_l(u)$ for $l = 0, 1, 2$ and 3.

and the intensity profile of the first higher order resonator modes are shown in Figure 2.81.

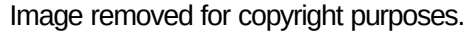

Figure 2.81: Intensity profile of TEM_{lm}-beams, [6], p. 103.

Besides the different mode profiles, the higher order modes experience greater phase advances during propogation, because they are made up of k-vectors with larger transverse components.

Axial Mode Structure

As we have seen for the Fabry-Perot resonator, the longitudinal modes are characterized by a roundtrip phase that is a multiple of 2π. Back then, we did not consider transverse modes. Thus in a resonator with finite transverse beam size, we obtain an extended family of resonances, with distinguishable field patterns. The resonance frequencies ω_{pmn} are determined by the roundtrip phase condition

$$\phi_{pmn} = 2p\pi, \text{ for } p = 0, \pm 1, \pm 2, ... \tag{2.300}$$

For the linear resonator according to Figure 2.74, the roundtrip phase of a Hermite-Gaussian T_{pmn}-beam is

$$\phi_{pmn} = 2kL - 2(m+n+1)\left(\zeta(z_2) - \zeta(z_1)\right), \tag{2.301}$$

where $\zeta(z_2) - \zeta(z_1)$ is the additional Guoy-Phase-Shift, when the beam goes through the focus once on its way from mirror 1 to mirror 2. Then the resonance frequences are

$$\omega_{pmn} = \frac{c}{L}\left[\pi p + (m+n+1)\left(\zeta(z_2) - \zeta(z_1)\right)\right]. \tag{2.302}$$

If the Guoy-Phase-Shift is not a rational number times π, then all resonance frequencies are non degenerate. However, for the special case where the two mirrors have identical radius of curvature R and are spaced a distance $L = R$ apart, which is called a confocal resonator, the Guoy-Phase-shift is $\zeta(z_2) - \zeta(z_1) = \pi/2$, with resonance frequencies

$$\omega_{pmn} = \frac{c}{L}\left[\pi p + (m+n+1)\frac{\pi}{2}\right]. \tag{2.303}$$

In that case all even, i.e. $m+n$, transverse modes are degenerate to the longitudinal or fundamental modes, see Figure 2.82.

Image removed for copyright purposes.

Figure 2.82: Resonance frequencies of the confocal Fabry-Perot resonator, [6], p. 128.

The odd modes are half way inbetween the longitudinal modes. Note, in contrast to the plan parallel Fabry Perot all mode frequencies are shifted by $\pi/2$ due to the Guoy-Phase-Shift.

2.7 Waveguides and Integrated Optics

As with electronics, miniaturization and integration of optics is desired to reduce cost while increasing functionality and reliability. One essential element is the guiding of the optical radiation in waveguides for integrated optical devices and optical fibers for long distance transmission. Waveguides can be as short as a few millimeters. Guiding of light with exceptionally low loss in fiber (0.1dB/km) can be achieved by using total internal reflection. Figure 2.83 shows different optical waveguides with a high index core material and low index cladding. The light will be guided in the high index core. Similar to the Gaussian beam the guided mode is made up of mostly paraxial plane waves that hit the high/low-index interface at grazing incidence and therefore undergo total internal reflections. The concomittant lensing effect overcomes the diffraction of the beam that would happen in free space and leads to stationary mode profiles fof the radiation.

Depending on the index profile and geometry one distinguishes between different waveguide types. Figure 2.83 (a) is a planar slab waveguide, which guides light only in one direction. This case is analyzed in more detail, as it has simple analytical solutions that show all phenomena associated with waveguiding such as cutoff, dispersion, single and multimode operation, coupling of modes and more, which are used later in devices and to achieve certain device properties. The other two cases show complete waveguiding in the transverse direction; (b) planar strip waveguide and (c) optical fiber.

Figure 2.83: Dark shaded area constitute the high index regions. (a) planar slab waveguide; (b) strip waveguide; (c) optical fiber [6], p. 239.

In integrated optics many components are fabricated on a single sub-

strate, see Figure 2.84 with fabrication processes similar to those in microelectronics.

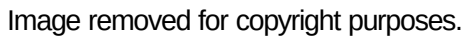

Figure 2.84: Integrated optical device resembling an optical transmitter/receiver, [6], p. 2.83.

As this example shows, the most important passive component to understand in an integrated optical circuit are waveguides and couplers.

2.7.1 Planar Waveguides

To understand the basic physics and phenomena in waveguides, we look at a few examples of guiding in one transverse dimension. These simple cases can be treated analytically.

Planar-Mirror Waveguides

The planar mirror waveguide is composed of two ideal metal mirrors a distance d apart, see Figure 2.85

Figure 2.85: Planar mirror waveguide, [6], p. 240.

We consider a TE-wave, whose electric field is polarized in the $y-$direction and that propagates in the $z-$direction. The reflections of the light at the ideal lossless mirrors will guide or confine the light in the $x-$direction. The field will be homogenous in the $y-$direction, i.e. will not depend on y. Therefore, we make the following trial solution for the electric field of a monochromatic complex TE-wave

$$\underline{\vec{E}}(x,z,t) = \underline{E}_y(x,z)\ e^{j\omega t}\ \vec{e}_y. \tag{2.304}$$

Note, this trial solution also satisfies the condition $\nabla \cdot \vec{E} = 0$, see (2.12)

Modes of the planar waveguide Furthermore, we are looking for solutions that do not change their field distribution transverse to the direction of propagation and experience only a phase shift during propagation. We call such solutions modes of the waveguide, because they don't change its transverse field profile. The modes of the above planar waveguide can be expressed as

$$\underline{\vec{E}}_y(x,z) = u(x)\ e^{-j\beta z}\ \vec{e}_y, \tag{2.305}$$

where β is the propagation constant of the mode. This solution has to obey the Helmholtz Eq.(2.18) in the free space section between the mirrors

$$\frac{d^2}{dx^2}u_y(x) = \left(\beta^2 - k^2\right) u_y(x) \text{ with } k^2 = \frac{\omega^2}{c^2}. \tag{2.306}$$

The presence of the metal mirrors requires that the electric fields vanish at the metal mirrors, otherwise infinitely strong currents would start to flow to shorten the electric field.

$$u_y(x = \pm d/2) = 0 \tag{2.307}$$

.Note, that Eq.(2.306) is an eigenvalue problem to the differential operator $\frac{d^2}{dx^2}$

$$\frac{d^2}{dx^2}u(x) = \lambda u(x) \text{ with } u(x = \pm d/2) = 0. \tag{2.308}$$

in a space of functions u, that satisfies the boundary conditions (2.307). The eigenvalues λ are for the moment arbitrary but constant numbers. Depending on the sign of the eigenvalues the solutions can be sine or cosine functions ($\lambda < 0$) or exponentials with real exponents for ($\lambda > 0$). In the latter case, it is impossible to satiesfy the boundary conditions. Therefore, the eigensolutions are

$$u_m(x) = \begin{cases} \sqrt{\frac{2}{d}}\cos(k_{x,m}x) \text{ with }, k_{x,m} = \frac{\pi}{d}m, \ m = 1,3,5,..., \text{ even modes} \\ \sqrt{\frac{2}{d}}\sin(k_{x,m}x) \text{ with }, k_{x,m} = \frac{\pi}{d}m, \ m = 2,4,6,..., \text{ odd modes} \end{cases} \tag{2.309}$$

Propagation Constants The propagation constants for these modes follow from comparing (2.306) with (2.308) to be

$$\beta^2 = k^2 - k_{x,m}^2 \tag{2.310}$$

or

$$\beta = \pm\sqrt{\frac{\omega^2}{c^2} - \left(\frac{\pi}{d}m\right)^2} = \pm\sqrt{\left(\frac{2\pi}{\lambda}\right)^2 - \left(\frac{\pi}{d}m\right)^2} \tag{2.311}$$

where $\lambda = \lambda_0/n(\lambda_0)$ is the wavelength in the medium between the mirrors. This relationship is shown in Figure 2.86. The lowest order mode with index $m = 1$ has the smallest k-vector component in x-direction and therefore the largest k-vector component into z-direction. The sum of the squares of both components has to be identical to the magnitude sqaure of the k-vector in the medium k. Higher order modes have increasingly more nodes in the x-direction, i.e. largest k_x-components and the wave vector component in z-direction decreases, until there is no real solution anymore to Eq.(**??**) and the corresponding propagation constants β_m become imaginary. That is, the corresponding waves become evanescent waves, i..e they can not propagate in a waveguide with the given dimensions.

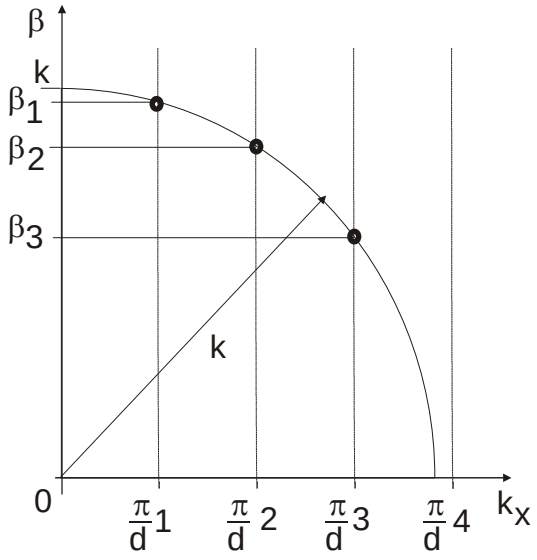

Figure 2.86: Determination of propagation constants for modes

Field Distribution The transverse electric field distributions for the various TE-modes is shown in Figure 2.87

Image removed for copyright purposes.

Figure 2.87: Field distributions of the TE-modes of the planar mirror waveguide [6], p. 244.

Cutoff Wavelength/Frequency For a given planar waveguide with separation d, there is a lowest frequency, i.e. longest wavelength, beyond which no propagating mode exists. This wavelenth/frequency is refered to as cutoff

wavelength/frequency which is

$$\lambda_{cutoff} = 2d \tag{2.312}$$

$$f_{cutoff} = \frac{c}{2d}. \tag{2.313}$$

The physical origin for the existence of a cutoff wavelength or frequency is that the guided modes in the mirror waveguide are a superposition of two plane waves, that propagate under a certain angle towards the z-axis, see Figure 2.88

Figure 2.88: (a) Condition for self-consistency: as a wave reflects twice it needs to be in phase with the previous wave. (b) The angles for which self-consistency is achieved determine the x-component of the $\vec{k}$-vectors involved. The corresponding two plane waves setup an interference pattern with an extended node at the position of the metal mirrors satisfying the boundary conditions, [6], p. 241.

In order that the sum of the electric field of the two plane waves fulfills the boundary conditions, the phase of one of the plane waves after reflection on both mirrors needs to be inphase with the other plane wave, i.e. the x-component of the $\vec{k}$-vectors involved, k_x, must be a multiple of 2π

$$2k_x d = \pm 2\pi m.$$

If we superimpose two plane waves with $k_{x,m} = \pm\pi m/d$, we obtain an interference pattern which has nodes along the location of the metal mirrors, which obviously fulfills the boundary conditions. It is clear that the minimum distance between these lines of nodes for waves of a given wavelength λ is $\lambda/2$, hence the separation d must be greater than $\lambda/2$ otherwise no solution is possible.

Single-Mode Operation For a given separation d, there is a wavelength range over which only a single mode can propagate, we call this wavelength range single-mode operation. From Figure 2.86 it follows for the planar mirror waveguide

$$\frac{\pi}{d} < k < \frac{\pi}{d}2 \tag{2.314}$$

or

$$d < \lambda < 2d \tag{2.315}$$

Waveguide Dispersion Due to the waveguiding, the relationship between frequency and propagation constant is no longer linear. This does not imply that the waveguide core, i.e. here the medium between the plan parallel mirrors, has dispersion. For example, even for $n = 1$, we find for phase and group velocity of the m-th mode

$$\frac{1}{v_p} = \frac{\beta(\omega)}{\omega} = \frac{1}{c}\sqrt{1 - \left(\frac{c\pi}{d\omega}m\right)^2} \tag{2.316}$$

$$= \frac{1}{c}\sqrt{1 - \left(\frac{\lambda}{2d}m\right)^2} \tag{2.317}$$

and

$$\frac{1}{v_g} = \frac{d\beta(\omega)}{d\omega} = \frac{1}{2\sqrt{\frac{\omega^2}{c^2} - \left(\frac{\pi}{d}m\right)^2}}2\frac{\omega}{c^2} \tag{2.318}$$

or

$$v_g \cdot v_p = c^2. \tag{2.319}$$

Thus different modes have different group and phase velocities. Figure 2.89 shows group and phase velocity for the different modes as a function of the normalized wave number kd/π.

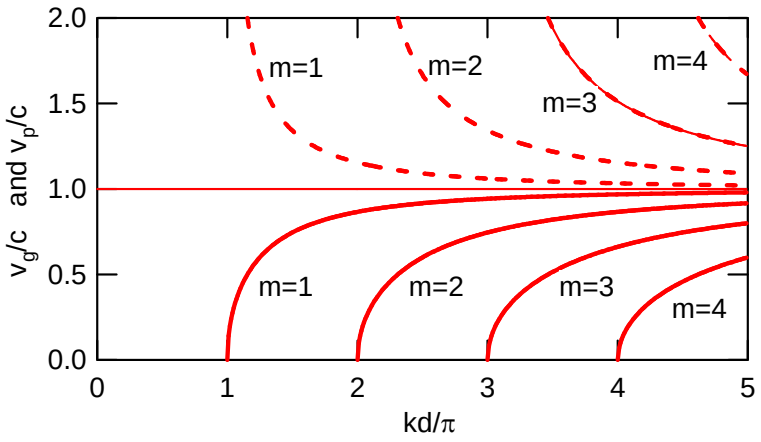

Figure 2.89: Group and phase velocity of propagating modes with index m as a function of normailzed wave number.

TM-Modes The planar mirror waveguide does not only allow for TE-waves to propagate. There are also TM-waves, which have only a magnetic field component transverse to the propagation direction and parallel to the mirrors, i.e. in y-direction

$$\vec{\underline{H}}(x,z,t) = \underline{H}_y(x,z)\; e^{j\omega t}\; \vec{e}_y, \tag{2.320}$$

and now $\underline{H}(x,z)$ has to obey the Helmholtz equation for the magnetic field. The corresponding electric field can be derived from Ampere's law

$$\vec{\underline{E}}(x,z) = \frac{-1}{j\omega\varepsilon}\nabla \times \left(\underline{H}_y(x,z)\; \vec{e}_y\right) \tag{2.321}$$

$$= \frac{1}{j\omega\varepsilon}\frac{\partial \underline{H}_y(x,z)}{\partial z}\vec{e}_x + \frac{-1}{j\omega\varepsilon}\frac{\partial \underline{H}_y(x,z)}{\partial x}\vec{e}_z. \tag{2.322}$$

The electric field tangential to the metal mirrors has to vanish again, which leads to the boundary condition

$$\frac{\partial \underline{H}_y(x,z)}{\partial x}(x = \pm d/2) = 0. \tag{2.323}$$

After an analysis very similar to the discussion of the TE-waves we find for the TM-modes with

$$\underline{H}_y(x,z) = u(x)\ e^{-j\beta z}\ \vec{e}_y, \tag{2.324}$$

the transverse mode shapes

$$u_m(x) = \begin{cases} \sqrt{\frac{2}{d}}\cos\left(k_{x,m}x\right) \text{ with }, k_{x,m} = \frac{\pi}{d}m,\ m = 2,4,6,..., \text{ even modes} \\ \sqrt{\frac{2}{d}}\sin\left(k_{x,m}x\right) \text{ with }, k_{x,m} = \frac{\pi}{d}m,\ m = 1,3,5,..., \text{ odd modes} \end{cases} \tag{2.325}$$

Note, that in contrast to the electric field of the TE-waves being zero at the metal surface, the transverse magnetic field of theTM-waves is at a maximum at the metal surface. We will not consider this case further, because the discussion of cutoff frequencies and dispersion can be worked out very analogous to the case for TE-modes.

Multimode Propagation Depending on the boundary conditions at the input of the waveguide at $z = 0$ many modes may be excited. Eventually there are even excitations with such high transverse wavevectors k_x present, that are below cutoff. Depending on the excitation amplitudes of each mode, the total field in the waveguide will be the superposition of all modes. Lets assume that there are only TE-modes excited, then the total field is

$$\underline{\vec{E}}(x,z,t) = \sum_{m=1}^{\infty}\left(\underline{a}_m\ e^{-j\beta_m z} + \underline{b}_m\ e^{j\beta_m z}\right)\ u_m(x)\ e^{j\omega t}\ \vec{e}_y, \tag{2.326}$$

where the amplitudes $\underline{a}_m$ and $\underline{b}_m$ are the excitations of the m-th mode in forward and backward direction, respectively. It is easy to show that these excitation amplitudes are determined by the transverse electric and magnetic fields at $z = 0$ and $t = 0$. In many cases, the excitation of the waveguide will be such that only the forward propagating modes are excited.

$$\underline{\vec{E}}(x,z,t) = \sum_{m=1}^{\infty}\underline{a}_m\ u_m(x)\ e^{-j\beta_m z}\ e^{j\omega t}\ \vec{e}_y, \tag{2.327}$$

When many modes are excited, the transverse field distribution will change during propagation, see Figure 2.90

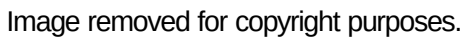

Figure 2.90: Variation of the intensity distribution in the transverse direction x at different distances z. Intensity profile of (a) the fundamental mode $m = 1$, (b) the second mode with $m = 2$ and (c) a linear combination of the fundamental and second mode, [6], p. 247.

Modes which are excited below cutoff will decay rapidly as evanescent waves. The other modes will propagate, but due to the different propagation constants these modes superimpose differently at different propagation distances along the waveguide. This dynamic can be used to build many kinds of important integrated optical devices, such as multimode interference couplers (see problem set 5). Depending on the application, undesired multimode excitation may be very disturbing due to the large group delay difference between the different modes. This effect is called modal dispersion.

Mode Orthogonality

It turns out that the transverse modes determined by the functions $u_m(x)$ build an orthogonal set of basis functions into which any function in a certain function space can be decomposed. This is obvious for the case of the planar-mirror waveguide, where the $u_m(x)$ are a subset of the basis functions for a Fourier series expansion of an arbitrary function $f(x)$ in the interval $[-d/2, 3d/2]$ which is antisymmetric with respect to $x = d/2$ and fullfills the boundary condition $f(x = \pm d/2) = 0$. It is

$$\int_{-d/2}^{d/2} u_m(x)\ u_n(x)\ dx = \delta_{mn}, \tag{2.328}$$

$$f(x) = \sum_m a_m\ \ u_m(x) \tag{2.329}$$

$$\text{with } a_m = \int_{-d/2}^{d/2} u_m(x)\ f(x)\ dx \tag{2.330}$$

From our familiarity with Fourier series expansions of periodic functions, we can accept these relations here without proof. We will return to these equations later in Quantum Mechanics and discuss in which mathematical sense Eqs.(2.328) to (2.329) really hold.

Besides illustrating many important concepts, the planar mirror waveguide is not of much practical use. More in use are dielectric waveguides.

Planar Dielectric Slab Waveguide

In the planar dielectric slab waveguide, waveguiding is not achieved by real reflection on a mirror but rather by total internal reflection at interfaces between two dielectric materials with refractive indices $n_1 > n_2$, see Figure 2.91

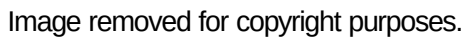

Figure 2.91: Symmetric planar dielectric slab waveguide with $n_1 > n_2$. The light is guided by total internal reflection. The field is evanescent in the cladding material and oscillatory in the core, [6], p. 249.

Waveguide Modes As in the case of the planar mirror waveguide, there are TE and TM-modes and we could find them as a superposition of correspondingly polarized TEM waves propagating with a certain transverse k-vector such that total internal reflection occurs. We do not want to follow this procedure here, but rather use immediately the Helmholtz Equation. We again write the electric field

$$\underline{\vec{E}}_y(x,z) = u(x)\ e^{-j\beta z}\ \vec{e}_y. \tag{2.331}$$

The field has to obey the Helmholtz Eq.(2.18) both in the core and in the cladding

$$\text{core} \quad : \quad \frac{d^2}{dx^2}u(x) = \left(\beta^2 - k_1^2\right) u(x) \text{ with } k_1^2 = \frac{\omega^2}{c_0^2}n_1^2, \tag{2.332}$$

$$\text{cladding} \quad : \quad \frac{d^2}{dx^2}u(x) = \left(\beta^2 - k_2^2\right) u(x) \text{ with } k_2^2 = \frac{\omega^2}{c_0^2}n_2^2 \tag{2.333}$$

The boundary conditions are given by the continuity of electric and magnetic field components tangential to the core/cladding interfaces as in section 2.2.

Since the guided fields must be evanescent in the cladding and oscillatory in the core, we rewrite the Helmholtz Equation as

$$\text{core} \quad : \quad \frac{d^2}{dx^2}u(x) = -k_x^2 u(x) \text{ with } k_x^2 = \left(k_1^2 - \beta^2\right), \tag{2.334}$$

$$\text{cladding} \quad : \quad \frac{d^2}{dx^2}u(x) = \kappa_x^2 u(x) \text{ with } \kappa_x^2 = \left(\beta^2 - k_2^2\right) \tag{2.335}$$

where κ_x is the decay constant of the evanescent waves in the cladding. It is obvious that for obtaining guided modes, the propagation constant of the mode must be between the two propagation constants for core and cladding

$$k_2^2 < \beta^2 < k_1^2. \tag{2.336}$$

Or by defining an effective index for the mode

$$\beta = k_0 n_{eff}, \text{ with } k_0 = \frac{\omega}{c_0} \tag{2.337}$$

we find

$$n_1 > n_{eff} > n_2, \tag{2.338}$$

and Eqs.(2.334), (2.335) can be rewritten as

$$\text{core} \quad : \quad -\frac{d^2}{dx^2}u(x) - k_0^2\left(n_1^2 - n_{eff}^2\right)u(x) = 0 \tag{2.339}$$

$$\text{cladding} \quad : \quad -\frac{d^2}{dx^2}u(x) + \kappa_0^2\left(n_{eff}^2 - n_2^2\right)u(x) = 0 \tag{2.340}$$

For reasons, which will become more obvious later, we draw in Figure 2.92 the negative refractive index profile of the waveguide.

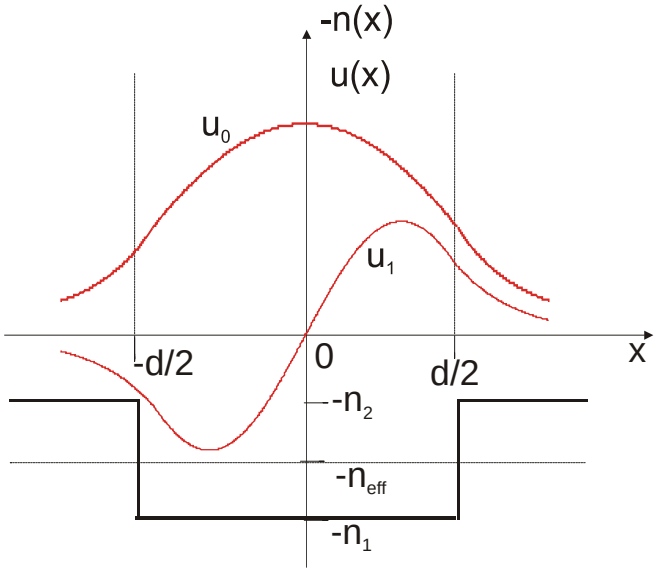

Figure 2.92: Negative refractive index profile and shape of electric field for the fundamental and first higher order transverse TE-mode

From Eq.(2.339) we find that the solution has the general form

$$u(x) = \begin{cases} A\exp(-\kappa_x x) + B\exp(\kappa_x x), & \text{for } x < -d/2 \\ C\cos(k_x x) + D\sin(k_x x), & \text{for } |x| < d/2 \\ E\exp(-\kappa_x x) + F\exp(\kappa_x x), & \text{for } |x| > d/2 \end{cases} \tag{2.341}$$

For a guided wave, i.e. $u_m(x \to \pm\infty) = 0$ the coefficients A and F must be zero. It can be also shown from the symmetry of the problem, that the solutons are either even or odd (proof later)

$$u^{(e)}(x) = \begin{cases} B\exp(\kappa_x x), & \text{for } x < -d/2 \\ C\cos(k_x x), & \text{for } |x| < d/2 \\ E\exp(-\kappa_x x), & \text{for } |x| > d/2 \end{cases}, \tag{2.342}$$

$$u^{(o)}(x) = \begin{cases} B\exp(\kappa_x x), & \text{for } x < -d/2 \\ D\sin(k_x x), & \text{for } |x| < d/2 \\ E\exp(-\kappa_x x), & \text{for } |x| > d/2 \end{cases}. \tag{2.343}$$

The coefficients B and E in each case have to be determined from the boundary conditions. From the continuity of the tangential electric field $\underline{E}_y$, and

the tangential magnetic field $\underline{H}_z$, which follows from Faraday's Law to be

$$\underline{H}_z(x) = \frac{1}{-j\omega\mu_0}\frac{\partial \underline{E}_y}{\partial x} \sim \frac{du}{dx} \tag{2.344}$$

we obtain the boundary conditions for $u(x)$

$$u(x = \pm d/2 + \epsilon) = u(x = \pm d/2 - \epsilon), \tag{2.345}$$

$$\frac{du}{dx}(x = \pm d/2 + \epsilon) = \frac{du}{dx}(x = \pm d/2 - \epsilon). \tag{2.346}$$

Note, these are four conditions determining the coefficients B, D, E and the propagation constant β or refractive index n_{eff}. These conditions solve for the parameters of even and odd modes separately. For the case of the even modes, where $B = E$, we obtain

$$B\exp\left(-\kappa_x\frac{d}{2}\right) = C\cos\left(k_x\frac{d}{2}\right) \tag{2.347}$$

$$B\ \kappa_x\exp\left(-\kappa_x\frac{d}{2}\right) = Ck_x\sin\left(k_x\frac{d}{2}\right) \tag{2.348}$$

or by division of the both equations

$$\kappa_x = k_x\tan\left(k_x\frac{d}{2}\right). \tag{2.349}$$

Eqs.(2.334) and (2.335) can be rewritten as one equation

$$k_x^2 + \kappa_x^2 = \left(k_1^2 - k_2^2\right) = k_0^2\left(n_1^2 - n_2^2\right) \tag{2.350}$$

Eq.(2.349) together with Eq.(2.350) determine the propagation constant β via the two relations.

$$\kappa_x\frac{d}{2} = k_x\frac{d}{2}\tan\left(k_x\frac{d}{2}\right), \text{ and} \tag{2.351}$$

$$\left(k_x\frac{d}{2}\right)^2 + \left(\kappa_x\frac{d}{2}\right)^2 = \left(k_0\frac{d}{2}NA\right)^2 \tag{2.352}$$

where

$$NA = \sqrt{(n_1^2 - n_2^2)} \tag{2.353}$$

is called the numerical apperture of the waveguide. We will discuss the physical significance of the numerical apperture shortly. A graphical solution of these two equations can be found by showing both relations in one plot, see Figure 2.93.

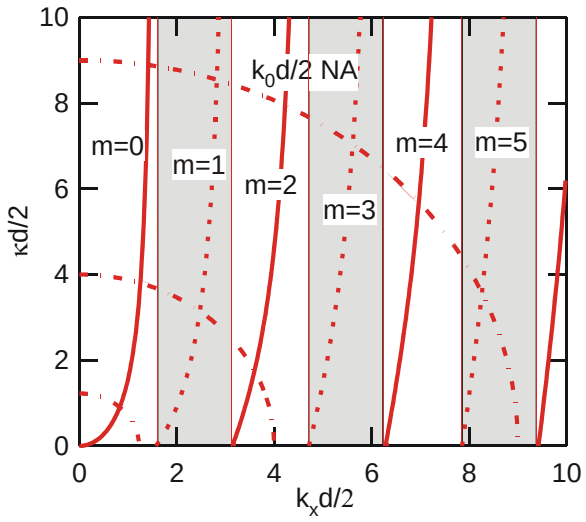

Figure 2.93: Graphical solution of Eqs.(2.351) and (2.352), solid line for even modes and Eq.(2.354) for the odd modes. The dash dotted line shows (2.352) for different values of the product $\left(k_0 \frac{d}{2}\right) NA$

Each crossing in Figure 2.93 of a solid line (2.351) with a circle (2.352) with radius $k_0 \frac{d}{2} NA$ represents an even guided mode. Similarly one finds for the odd modes from the boundary conditions the relation

$$\kappa_x \frac{d}{2} = -k_x \frac{d}{2} \cot\left(k_x \frac{d}{2}\right), \tag{2.354}$$

which is shown in Figure 2.93 as dotted line. The corresponding crossings with the circle indicate the existence of an odd mode.

There are also TM-modes, which we don't want to discuss for the sake of brevity.

Numerical Aperture Figure 2.93 shows that the number of modes guided is determined by he product $k_0 \frac{d}{2} NA$, where NA is the numerical apperture

defined in Eq.(2.353)

$$M = Int\left[k_0\frac{d}{2}NA/(\pi/2)\right]+1, \tag{2.355}$$

$$= Int\left[2\frac{d}{\lambda_0}NA\right]+1, \tag{2.356}$$

where the function $Int[x]$means the largest integer not greater than x. Note, that there is always at least one guided mode no matter how small the sized and the refractive index contrast between core and cladding of the waveguide is. However, for small size and index contrast the mode may extend very far into the cladding and the confinement in the core is low.

The numberical apperture also has an additional physical meaning that becomes obvious from Figure 2.94.

Figure 2.94: Maximum angle of incoming wave guided by a waveguide with numerical apperture NA, [6], p. 262.

The maximum angle of an incoming ray that can still be guided in the waveguide is given by the numerical apperture, because according to Snell's Law

$$n_0\sin(\theta_a) = n_1\sin(\theta), \tag{2.357}$$

where n_0 is the refractive index of the medium outside the waveguide. The maximum internal angle θ where light is still guided in the waveguide by total internal reflection is determined by the critical angle for total internal reflection (2.126) , i.e. $\theta_{\max} = \pi/2 - \theta_{tot}$ with

$$\sin(\theta_{tot}) = \frac{n_2}{n_1}. \tag{2.358}$$

Thus for the maximum angle of an incoming ray that can still be guided we find

$$n_0 \sin(\theta_{a,\max}) = n_1 \sin(\theta_{\max}) = n_1 \sqrt{1 - \left(\frac{n_2}{n_1}\right)^2} = NA. \tag{2.359}$$

Most often the external medium is air with $n_0 \approx 1$ and the refractive index contrast is week, so that $\theta_{a,\max} \ll 1$ and we can replace the sinusoid with its argument, which leads to

$$\theta_{a,\max} = NA. \tag{2.360}$$

Field Distributions Figure 2.95 shows the field distribution for the TE guided modes in a dielectric waveguide. Note, these are solutions of the second order differential equations (2.339) and (2.340) for an effective index n_{eff}, that is between the core and cladding index. These guided modes have a oscillatory behavior in those regions in space where the negative effective index is larger than the negative local refractive index, see Figure 2.92 and exponentially decaying solutions where the negative effective index is smaller than than the negative local refractive index.

Figure 2.95: Field distributions for TE guided modes in a dielectric waveguide. These results should be compared with those shown in Figure 2.87 for the planar-mirror waveguide [6], p. 254.

Figure 2.96 shows a comparison of the guided modes in a waveguide with a Gaussian beam. In contrast to a the Gaussian beam which diffracts,

in a waveguide diffraction is balanced by the guiding action of the index discontinuity, i.e. total internal reflection. Most importantly the cross section of a waveguide mode stays constant and therefore a waveguide mode can efficiently interact with the medium constituting the core or a medium that is incorporated in the core.

Figure 2.96: Comparison of Gaussian beam in free space and a waveguide mode, [6], p. 255.

Besides integration, this prolong interaction disctance is one of the major reasons for using waveguides. The interaction lenght can be arbitrarily long, only limited by the waveguide loss, in contrast to a Gaussian beam, which stays focused only over the confocal distance or Rayleigh range.

As in the case of a planar-mirror waveguide, one can show that the transverse mode functions are orthogonal to each other. At first, a striking difference here is that we have only a finite number of guided modes and one might worry about the completeness of the transverse mode functions. The answer is that in addition to the guided modes, there are unguided modes or leaky modes, which together with the guided modes from a complete set. Each initial field can be decomposed into these modes. The leaky modes rapidly loose energy because of radiation and after a relatively short propagation distance only the field of guided modes remains in the waveguide. We will not pursue this further in this introductory class. The interested reader should consult with [11].

Confinement Factor

A very important quantity for a waveguide mode is its confinement in the core, which is called the confinement factor

$$\Gamma_m = \frac{\int_0^{d/2} u_m^2(x)\ dx}{\int_0^{\infty} u_m^2(x)\ dx}. \tag{2.361}$$

The confinement factor quantifies the fraction of the mode energy propagating in the core of the waveguide. This is very important for the interaction of the mode with the medium of the core, which may be used to amplify the mode or which may contain nonlinear media for frequency conversion.

Waveguide Dispersion

For the guided modes the effective refractive indices of the modes and therefore the dispersion relations must be between the indices or dispersion relations of core and cladding, see Figure 2.97

Figure 2.97: Dispersion relations for the different guided TE-Modes in the dielectric slab waveguide.

The different slopes $d\omega/d\beta$ for each mode indicate the difference in group velocity between the modes. Note, that there is at least always one guided mode.

2.7.2 Two-Dimensional Waveguides

Both the planar-mirror waveguide and the planar dielectric slab waveguide confine light only in one direction. It is straight forward to analyze the modes of the two-dimensional planar-mirror waveguide, which you have already done in 6.013. Figure 2.98 shows various waveguides that are used in praxis for various devices. Here, we do not want to analyze them any further, because this is only possible by numerical techniques.

Figure 2.98: Various types of waveguide geometries: (a) strip: (b) embedded strip: (c) rib ro ridge: (d) strip loaded. The darker the shading, the higher the refractive index [6], p. 261.

2.7.3 Waveguide Coupling

The core size of a waveguide can range from a fraction of the free space wavelength to many wavelength for a multimode fiber. For example a typical high-index contrast waveguide with a silicon core and a silica cladding for 1550 nm has a cross section of $0.2\mu m \times 0.4\mu m$, single-mode fiber, which we will discuss in the next section with an index contrast of 0.5-1% between core and cladding has a typical mode-field radius of $6\mu m$.

If the mode cross section is not prohibitively small the simplest approach to couple light into a waveguide is by using a proper lens, see Figure 2.99 (a) or direct butt coupling of the source to the waveguide if the source is a waveguide based device itself.

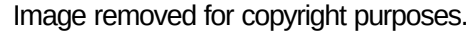

Figure 2.99: Coupling to a waveguide by (a) a lens; (b) direct butt coupling of an LED or laser diode, [6], p. 262

The lens and the beam size in free space must be chosen such that the spot size matches the size of the waveguide mode while the focusing angle in free space is less than the numerical aperture of the waveguide, (see problem set). Other alternatives are coupling to the evanscent field by using a prism coupler, see Figure 2.100

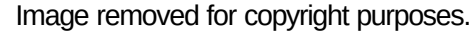

Figure 2.100: Prism coupler, [6], p. 263.

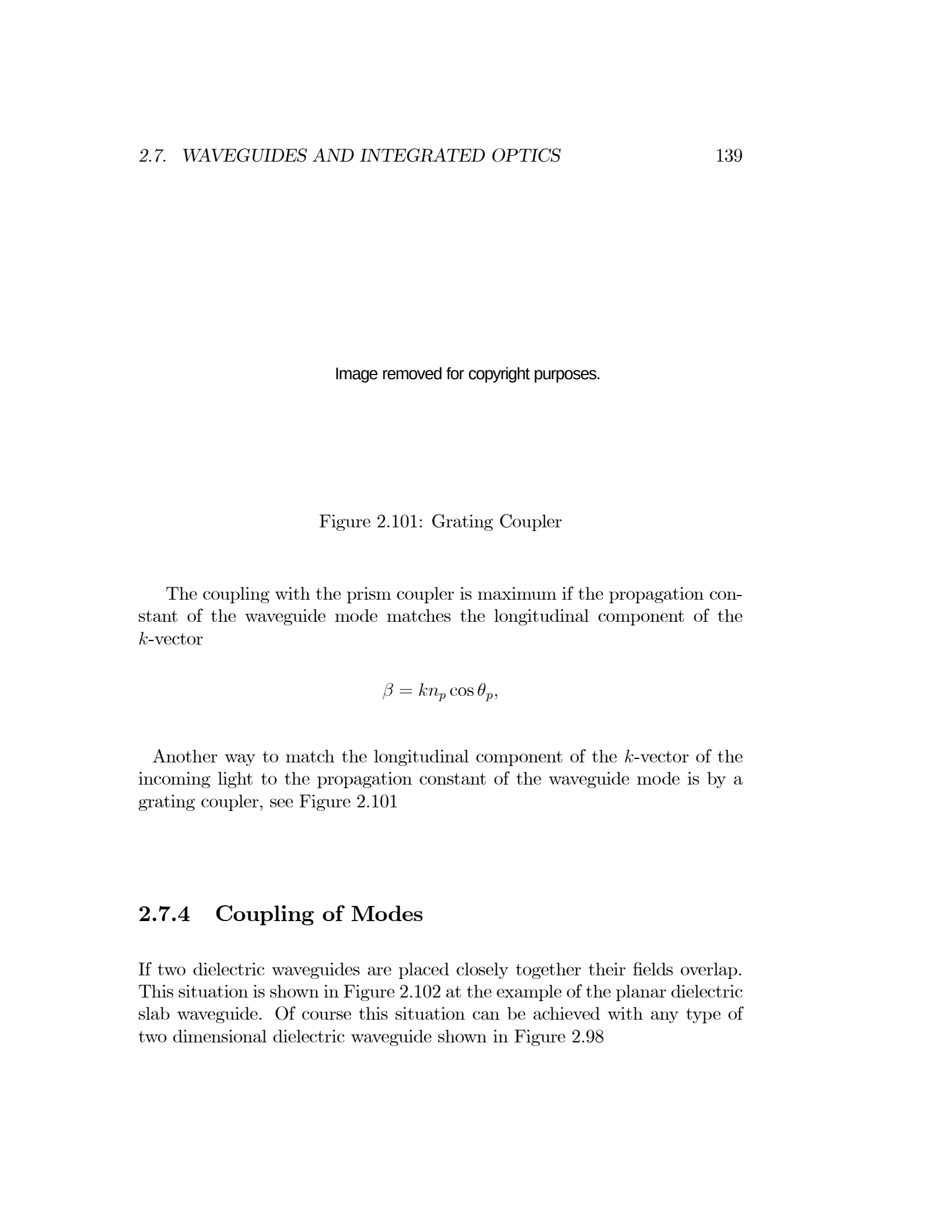

Figure 2.101: Grating Coupler

The coupling with the prism coupler is maximum if the propagation constant of the waveguide mode matches the longitudinal component of the k-vector

$$\beta = kn_p \cos\theta_p,$$

Another way to match the longitudinal component of the k-vector of the incoming light to the propagation constant of the waveguide mode is by a grating coupler, see Figure 2.101

2.7.4 Coupling of Modes

If two dielectric waveguides are placed closely together their fields overlap. This situation is shown in Figure 2.102 at the example of the planar dielectric slab waveguide. Of course this situation can be achieved with any type of two dimensional dielectric waveguide shown in Figure 2.98

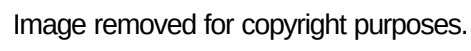

Figure 2.102: Coupling between the two modes of the dielectric slab waveguide, [6], p. 264.

Once the fields significantly overlap the two modes interact. The shape of each mode does not change very much by the interaction. Therefore, we can analyze this situation using perturbation theory. We assume that in zero-th order the mode in each waveguide is independent from the presence of the other waveguide. We consider only the fundamental TE-modes in each of the waveguide which have excitation amplitudes $\underline{a}_1(z)$ and $\underline{a}_2(z)$, respectively. The dynamics of each mode can be understood in terms of this wave amplitude. In the absence of the second waveguide, each waveguide amplitude undergoes only a phase shift during propagation according to its dispersion relations

$$\frac{d\underline{a}_1(z)}{dz} = -j\beta_1\underline{a}_1(z), \tag{2.362}$$

$$\frac{d\underline{a}_2(z)}{dz} = -j\beta_2\underline{a}_2(z). \tag{2.363}$$

The polarization generated by the field of mode 2 in waveguide 1 acts as a source for the field in waveguide 1 and the other way arround. Therefore, the coupling of the modes can be described by adding a source term in each equation proportional to the free propagation of the corresponding wave in

the other guide

$$\frac{d\underline{a}_1(z)}{dz} = -j\beta_1\underline{a}_1(z) - j\kappa_{12}\underline{a}_2(z), \tag{2.364}$$

$$\frac{d\underline{a}_2(z)}{dz} = -j\kappa_{21}\underline{a}_1(z) - j\beta_2\underline{a}_2(z). \tag{2.365}$$

κ_{12} and κ_{21} are the coupling constants of the modes. An expression in terms of waveguide properties is derived in the appendix. These coupled mode equations describe a wealth of phenomena and are of fundamental importance in many areas.

As we will see, there is only a significant interaction of the two modes if the two propagation constants are not much different from each other (phase matching). Therefore, we write the propagation constants in terms of the average β_0 and the phase mismatch $\Delta\beta$

$$\beta_{1/2} = \beta_0 \pm \Delta\beta \text{ with} \tag{2.366}$$

$$\beta_0 = \frac{\beta_1 + \beta_2}{2} \text{ and } \Delta\beta = \frac{\beta_1 - \beta_2}{2}. \tag{2.367}$$

and we take the overall trivial phase shift of both modes out by introducing the slowly varying relative field amplitudes

$$\tilde{\underline{a}}_1(z) = \underline{a}_1(z)e^{j\beta_0 z} \text{ and } \tilde{\underline{a}}_2(z) = \underline{a}_2(z)e^{j\beta_0 z} \tag{2.368}$$

which obey the equation

$$\frac{d}{dz}\tilde{\underline{a}}_1(z) = -j\Delta\beta\tilde{\underline{a}}_1(z) - j\kappa_{12}\tilde{\underline{a}}_2(z), \tag{2.369}$$

$$\frac{d}{dz}\tilde{\underline{a}}_2(z) = -j\kappa_{21}\tilde{\underline{a}}_1(z) + j\Delta\beta\tilde{\underline{a}}_2(z). \tag{2.370}$$

Power conservation during propagation demands

$$\frac{d}{dz}\left(|\tilde{\underline{a}}_1(z)|^2 + |\tilde{\underline{a}}_2(z)|^2\right) = 0 \tag{2.371}$$

which requests that $\kappa_{21} = \kappa_{12}^2$, i.e. the two coupling coefficients are not independent from each other (see problem set).

Note, Eqs.(2.369) and (2.370) are a system of two linear ordinary differential equations with constant coefficients, which is straight forward to solve.

Given the excitation amplitudes $\tilde{\underline{a}}_1(0)$ and $\tilde{\underline{a}}_2(0) = 0$ at the input of the waveguides, i.e. no input in waveguide 2 the solution is

$$\tilde{\underline{a}}_1(z) = \tilde{\underline{a}}_1(0)\left(\cos\gamma z - j\frac{\Delta\beta}{\gamma}\sin\gamma z\right), \tag{2.372}$$

$$\tilde{\underline{a}}_2(z) = -j\tilde{\underline{a}}_1(0)\frac{\kappa_{21}}{\gamma}\sin\gamma z, \tag{2.373}$$

with

$$\gamma = \sqrt{\Delta\beta^2 + |\kappa_{12}|^2}. \tag{2.374}$$

The optical powers after a propagation distance z in both waveguides are then

$$P_1(z) = |\tilde{\underline{a}}_1(z)|^2 = P_1(0)\left(\cos^2\gamma z + \left(\frac{\Delta\beta}{\gamma}\right)^2\sin^2\gamma z\right), \tag{2.375}$$

$$P_2(z) = P_1(0)\left(\frac{|\kappa_{21}|^2}{\gamma}\right)^2\sin^2\gamma z. \tag{2.376}$$

This solution shows, that depending on the difference in phase velocity between the two-waveguides more or less power is coupled back and fourth between the two waveguides, see Figure 2.103.

The period at which the power exchange occurs is

$$L = \frac{2\pi}{\gamma}. \tag{2.377}$$

If both waveguides are identical, i.e. $\Delta\beta = 0$ and $\gamma = |\kappa_{12}|$, the waves are phase matched, Eqs.(2.375) and (2.376) simplify to

$$P_1(z) = P_1(0)\cos^2\gamma z \tag{2.378}$$

$$P_2(z) = P_1(0)\sin^2\gamma z. \tag{2.379}$$

Complete transfer of power occurs between the two waveguides after a distance

$$L_0 = \frac{\pi}{2\gamma}, \tag{2.380}$$

see Figure 2.104

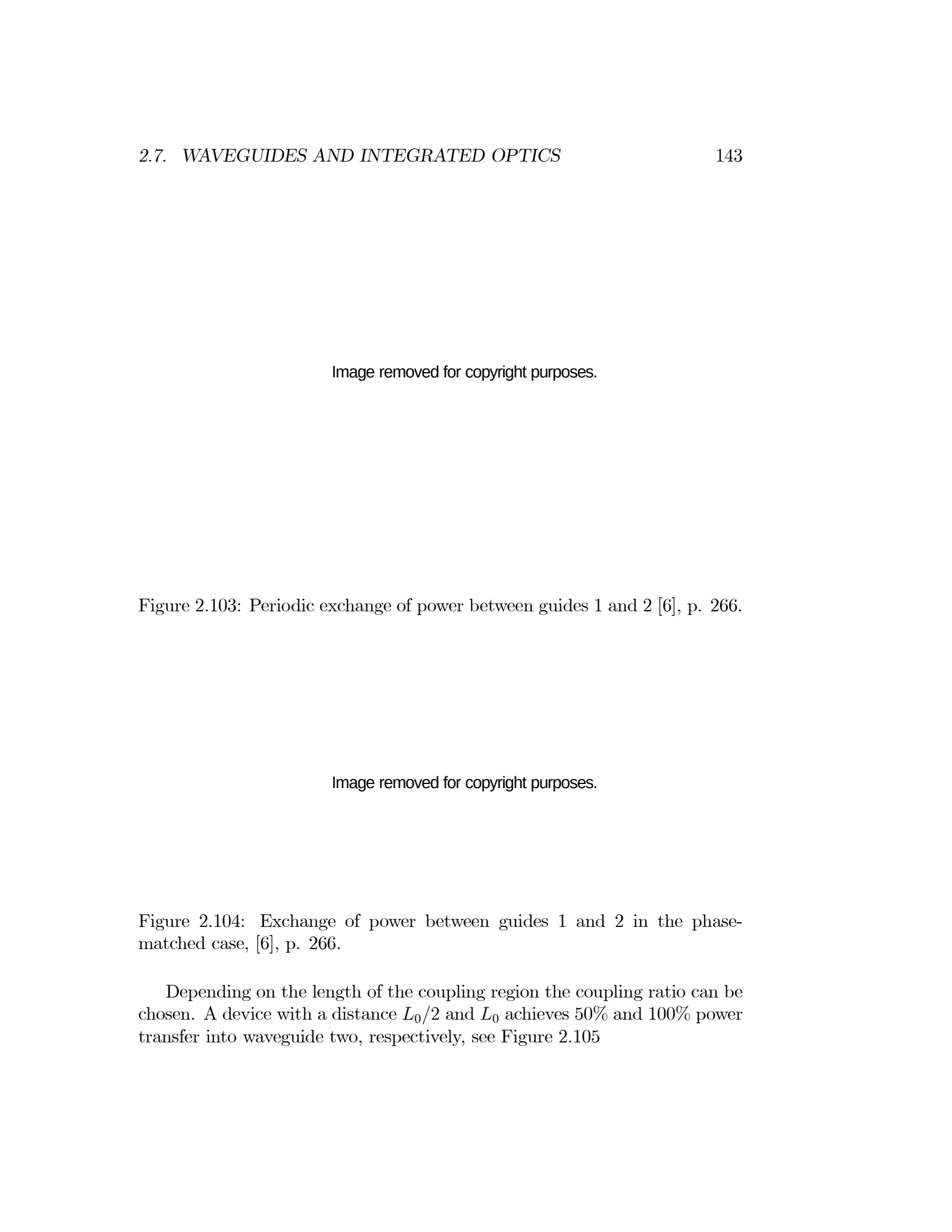

Figure 2.103: Periodic exchange of power between guides 1 and 2 [6], p. 266.

Figure 2.104: Exchange of power between guides 1 and 2 in the phase-matched case, [6], p. 266.

Depending on the length of the coupling region the coupling ratio can be chosen. A device with a distance $L_0/2$ and L_0 achieves 50% and 100% power transfer into waveguide two, respectively, see Figure 2.105

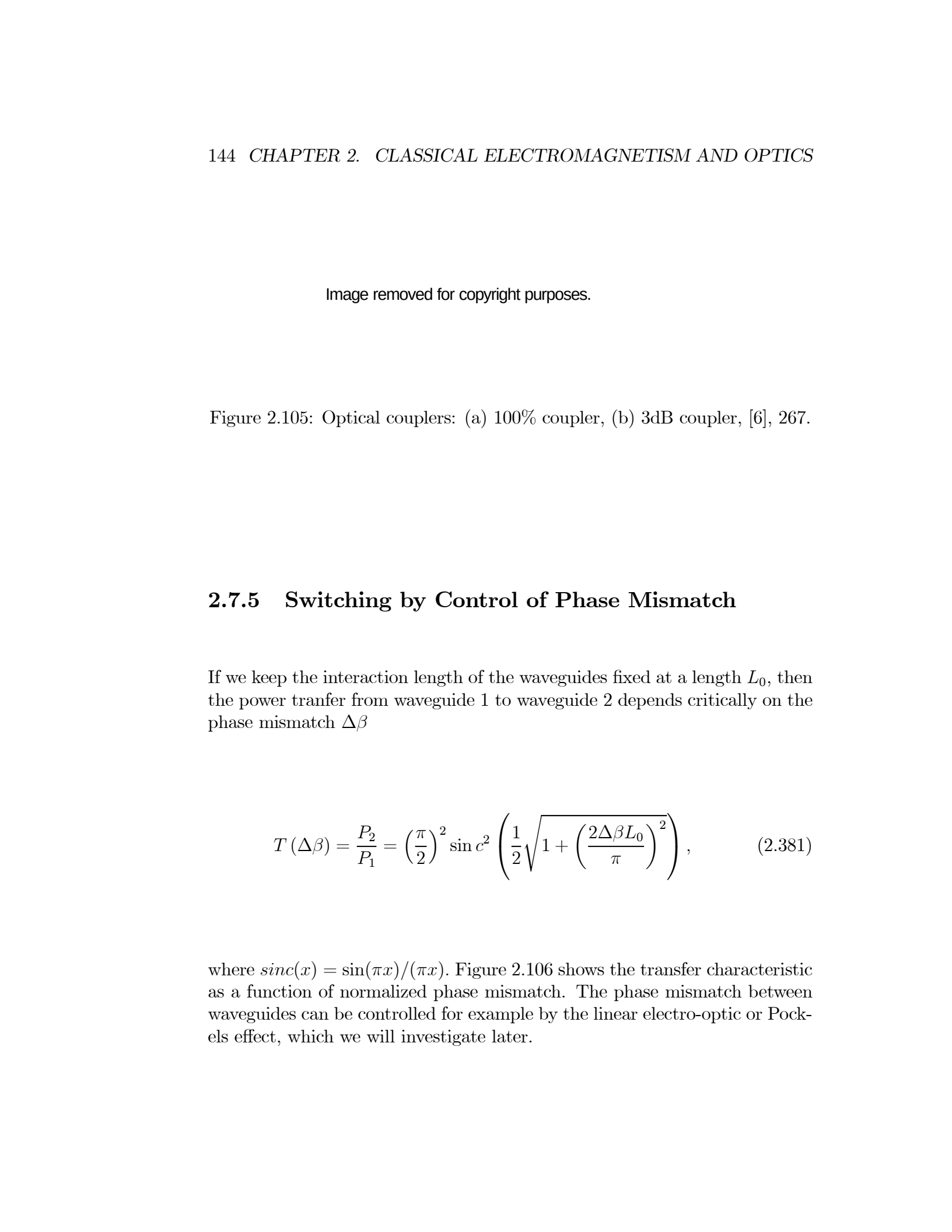

Figure 2.105: Optical couplers: (a) 100% coupler, (b) 3dB coupler, [6], 267.

2.7.5 Switching by Control of Phase Mismatch

If we keep the interaction length of the waveguides fixed at a length L_0, then the power tranfer from waveguide 1 to waveguide 2 depends critically on the phase mismatch $\Delta\beta$

$$T\left(\Delta\beta\right) = \frac{P_2}{P_1} = \left(\frac{\pi}{2}\right)^2 \sin c^2 \left(\frac{1}{2}\sqrt{1 + \left(\frac{2\Delta\beta L_0}{\pi}\right)^2}\right), \tag{2.381}$$

where $sinc(x) = \sin(\pi x)/(\pi x)$. Figure 2.106 shows the transfer characteristic as a function of normalized phase mismatch. The phase mismatch between waveguides can be controlled for example by the linear electro-optic or Pockels effect, which we will investigate later.

Figure 2.106: Dependence of power transfer from waveguide 1 to waveguide 2 as a function of phase mismatch, [6], p. 267.

The implementation of such a waveguide coupler switch is shown in Figure 2.107.

Figure 2.107: Integrated waveguide coupler switch, [6], p. 708

2.7.6 Optical Fibers

Optical fibers are cylindrical waveguides, see Figure 2.108, made of low-loss materials such as silica glass.

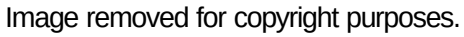

Figure 2.108: Optical fibers are cylindrical dielectric waveguides, [6], p. 273.

Similar to the waveguides studied in the last section the most basic fibers consist of a high index core and a lower index cladding. Today fiber technology is a highly developed art which has pushed many of the physical parameters of a waveguide to values which have been thought to be impossible a few decades ago:

- Fiber with less than 0.16dB/km loss
- Photonic crystal fiber (Nanostructured fiber)
- Hollow core fiber
- Highly nonlinear fiber
- Er-doped fiber for amplifiers
- Yb-doped fiber for efficient lasers and amplifiers
- Raman gain fiber
- Large area single mode fibers for high power (kW) lasers.

Figure 2.109 shows the ranges of attenuation coefficients of silica glass single-mode and multimode fiber.

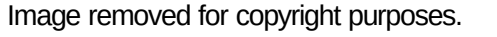

Figure 2.109: Ranges of attenuation coefficients of silica glass single-mode and multimode fiber, [10], p. 298.

For the purpose of this introductory class we only give an overview about the mode structure of the most basic fiber, the step index fiber, see Figure 2.110 (b)

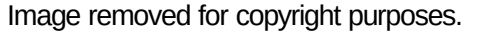

Figure 2.110: Geometry, refractive index profile, and typical rays in: (a) a multimode step-index fiber, (b) a single-mode step-index fiber, (c) a multimode graded-index fiber [6], p. 274

Step-index fiber is a cylindrical dielectric waveguide specified by its core and cladding refractive indices, n_1 and n_2 and the core radius a, see Figure 2.108. Typically the cladding is assumed to be so thick that the finite cladding radius does not need to be taken into account. The guided modes need to be sufficiently decaded before reaching the cladding boundary, which is usually strongly scattering or absorbing. In standard fiber, the cladding indices differ only slightly, so that the relative refractive-index difference

$$\Delta = \frac{n_1 - n_2}{n_1} \tag{2.382}$$

is small, typically $10^{-3} < \Delta < 2 \cdot 10^{-2}$. Most fibers currently used in medium to long optical communication systems are made of fused silica glass (SiO_2) of high chemical purity. The increase in refractive index of the core is achieved by doping with titanium, germanium or boron, among others. The refractive index n_1 ranges from 1.44 to 1.46 depending on the wavelength utilized in the fiber. The acceptance angle of the rays coupling from free space into guided modes of the waveguide is determined by the numerical apperture as already discussed for the dielectric slab waveguide, see Figure 2.111

$$\theta_a \sim \sin(\theta_a) = NA = \sqrt{n_1^2 - n_2^2} \approx n_1\sqrt{2\Delta}. \tag{2.383}$$

Figure 2.111: The acceptance angle of a fiber and numerical aperture NA [6], p. 276.

Guided Waves

Again the guided waves can be found by looking at solutions of the Helmholtz equations in the core and cladding where the index is homogenous and by additionally requesting the continuity of the tangential electric and magnetic fields at the core-cladding boundary. In general the fiber modes are not anylonger pure TE or TM modes but rather are hybrid modes, i.e. the modes have both transverse and longitudinal electric and magnetic field components. Only the radial symmetric modes are still TE or TM modes. To determine the exact mode solutions of the fiber is beyond the scope of this class and the interested reader may consult reference [2]. However, for weakly guiding fibers, i.e. $\Delta \ll 1$, the modes are actually very much TEM like, i.e. the longitudinal field components are much smaller than the radial field components. The linear in x and y directions polarized modes form orthogonal polarization states. The linearly polarized (l, m) mode is usually denoted as the LP_{lm}-mode.The two polarizations of the mode with indices (l, m) travel with the same propagation constant and have identical intensity distributions.

The generic solutions to the Helmhotz equation in cylindrical coordinates are the ordinary, $J_m(kr)$, and modified, $K_m(kr)$, Bessel functions (analogous to the $\cos(x)/\sin(x)$ and exponential functions $e^{\pm\kappa x}$, that are solutions to the Helmholtz equation in cartesian coordinates). Thus, a generic mode function for a cylinder symmetric fiber has the form

$$u_{l,m}(r,\varphi) = \begin{cases} J_l(k_{l,m}r) \begin{cases} \cos(l\varphi) \\ \sin(l\varphi) \end{cases}, \text{ for } r < a, \text{ core} \\ K_l(k_{l,m}r) \begin{cases} \cos(l\varphi) \\ \sin(l\varphi) \end{cases}, \text{ for } r > a, \text{ cladding} \end{cases} \tag{2.384}$$

For large r, the modified Bessel function approaches an exponential, $K_l(k_{l,m}r) \sim e^{-\kappa_{\ln m} r} \begin{cases} \cos(l\varphi) \\ \sin(l\varphi) \end{cases}$. The propagation constants for this two dimensional waveguide have to fullfil the additional constraints

$$k_{l,m}^2 = \left(n_1^2 k_0^2 - \beta^2\right), \tag{2.385}$$

$$\kappa_{l,m}^2 = \left(\beta^2 - n_2^2 k_0^2\right), \tag{2.386}$$

$$k_{l,m}^2 + \kappa_{l,m}^2 = k_0^2 N A^2. \tag{2.387}$$

Figure 2.112 shows the radial dependence of the mode functions

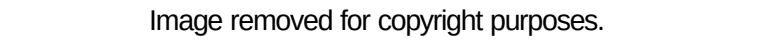

Figure 2.112: Radial dependence of mode functions $u(r)$,[6], p.279.

The transverse intensity distribution of the linearly polarized $LP_{0,1}$ and $LP_{3,4}$ modes are shown in Figure 2.113.

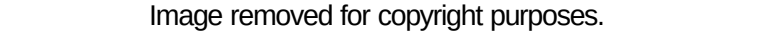

Figure 2.113: Intensity distribtuion of the (a) LP_{01} and (b) $\mathrm{LP}_{3,4}$ modes in the transverse plane. The LP_{01} has a intensity distribution similar to the Gaussian beam, [6], p. 283.

Number of Modes

It turns out, that as in the case of the dielectric slab waveguide the number of guided modes critically depends on the numerical aperture or more precisely

on the V-parameter, see Eq.(2.355)

$$V = k_0 \frac{d}{2} NA. \tag{2.388}$$

Without proof the number of modes is

$$M \approx \frac{4}{\pi^2} V^2, \text{ for } V \gg 1. \tag{2.389}$$

which is similar to Eq.(2.355) for the one-dimensional dielectric slab waveguide, but the number of modes here is now related to the square of the V-parameter, because of the two-dimensional transverse confinement of the modes in the fiber. As in the case of the dielectric waveguide, there is always at least one guided mode (two polarizations). However, the smaller the V-parameter the more the mode extends into the cladding and the guiding properties become weak, i.e. small bending of the fiber may already lead to high loss.

2.8 Wave Propagation in Anisotropic Media

So far we have always assumed that the medium in which the electromagnetic wave propagates is isotropic. This causes the induced polarization to be parallel to the applied electric field. In crystaline materials or materials with microscopic fine structure in general, this is no longer the case. Instead of the simple relation

$$\underline{\vec{P}} = \epsilon_0 \underline{\chi} \cdot \underline{\vec{E}}, \tag{2.390}$$

where the susceptibility is a scalar, the induced polarization may have a general lineare dependence on $\vec{E}$ not necessarily parallel to the applied field

$$\underline{P}_x = \epsilon_0 \left(\underline{\chi}_{xx} \underline{E}_x + \underline{\chi}_{xy} \underline{E}_y + \underline{\chi}_{xz} \underline{E}_z \right), \tag{2.391}$$

$$\underline{P}_y = \epsilon_0 \left(\underline{\chi}_{yx} \underline{E}_x + \underline{\chi}_{yy} \underline{E}_y + \underline{\chi}_{yz} \underline{E}_z \right), \tag{2.392}$$

$$\underline{P}_z = \epsilon_0 \left(\underline{\chi}_{zx} \underline{E}_x + \underline{\chi}_{zy} \underline{E}_y + \underline{\chi}_{zz} \underline{E}_z \right). \tag{2.393}$$

The tensor $\underline{\chi}$ is called the electric susceptibility tensor. As shown in Table 2.7 the crytaline structure determines to a large extend the values of the susceptibility tensor elements or in other words the symmetry properties of

isotropic	$\begin{bmatrix} xx & 0 & 0 \\ 0 & xx & 0 \\ 0 & 0 & xx \end{bmatrix}$	cubic
uniaxial	$\begin{bmatrix} xx & 0 & 0 \\ 0 & xx & 0 \\ 0 & 0 & zz \end{bmatrix}$	Tetragonal Trigonal Hexagonal
biaxial	$\begin{bmatrix} xx & 0 & 0 \\ 0 & yy & 0 \\ 0 & 0 & zz \end{bmatrix}$	Orthorhombic
	$\begin{bmatrix} xx & 0 & xz \\ 0 & yy & 0 \\ xz & 0 & zz \end{bmatrix}$	Monoclinic
	$\begin{bmatrix} xx & xy & xz \\ xy & yy & yz \\ xz & yz & zz \end{bmatrix}$	Triclinic

Table 2.7: Form of the electric susceptibility tensor for various crystal systems.

the crystal reflect themselves in the symmetry properties of the susceptibility tensor.

Elementary algebra tells us that we can choose a new coordinate system with axis x', y', z', such that the susceptibility tensor has diagonal form

$$\underline{P}_{x'} = \epsilon_0 \underline{\chi}_{x'x'} \underline{E}_{x'}, \tag{2.394}$$

$$\underline{P}_{y'} = \epsilon_0 \underline{\chi}_{y'y'} \underline{E}_{y'}, \tag{2.395}$$

$$\underline{P}_{z'} = \epsilon_0 \underline{\chi}_{z'z'} \underline{E}_{z'}. \tag{2.396}$$

These directions are called the principle axes of the crystal. In the following, we consider that the crystal axes are aligned with the principle axes. If a TEM-wave is launched along the $z-$axis with the elecric field polarized along one of the prinicple axes, lets say x, the wave will experience a refractive index

$$n_x^2 = 1 + \underline{\chi}_{xx} \tag{2.397}$$

and the wave will have a phase velocity

$$c = c_0/n_x. \tag{2.398}$$

If on the other hand the wave is polarized along the y-axis it will have a different phase velocity corresponding to n_y. If the wave propagates along the $z-$axis with electric field components along both the x- and y-axis, the wave can be decomposed into the two polarization components. During propagation of the wave the will experience a differential phase shift with respect to each other and the state of polarization may change. Later, this phenomenon will be exploited for the construction of modulators and switches.

2.8.1 Birefringence and Index Ellipsoid

If we consider the propagation of a wave into an arbitrary direction of the crystal it is no longer obvious what the plane wave solution and its phase velocity is. We have

$$\vec{D} = \boldsymbol{\varepsilon}\vec{E} \tag{2.399}$$

with

$$\boldsymbol{\varepsilon} = \varepsilon_0 \begin{bmatrix} \boldsymbol{\varepsilon}_x & 0 & 0 \\ 0 & \boldsymbol{\varepsilon}_y & 0 \\ 0 & 0 & \boldsymbol{\varepsilon}_z \end{bmatrix}. \tag{2.400}$$

Let's assume there are plane wave solutions

$$\underline{\vec{E}} = \underline{\vec{E}}_0 \mathrm{e}^{-j\vec{k}\cdot\vec{r}}$$

then Ampere's and Faraday's law give

$$\vec{k} \times \underline{\vec{H}} = -\omega\boldsymbol{\varepsilon}\underline{\vec{E}}, \tag{2.401}$$

$$\vec{k} \times \underline{\vec{E}} = \omega\mu_0\underline{\vec{H}}, \tag{2.402}$$

resulting in the wave equation

$$\vec{k} \times \vec{k} \times \underline{\vec{E}} = -\omega^2\mu_0\boldsymbol{\varepsilon}\underline{\vec{E}}. \tag{2.403}$$

Note, that the wavevector $\vec{k}$ is orthogonal to the dielectric displacement $\vec{D}$ and the magnetic field $\vec{H}$, but not necessarily to the electric field $\vec{E}$. There is

$$\vec{k} \perp \left(\boldsymbol{\varepsilon}\vec{E} = \vec{D}\right) \perp \vec{B}. \tag{2.404}$$

This situation is reflected in Figure 2.114

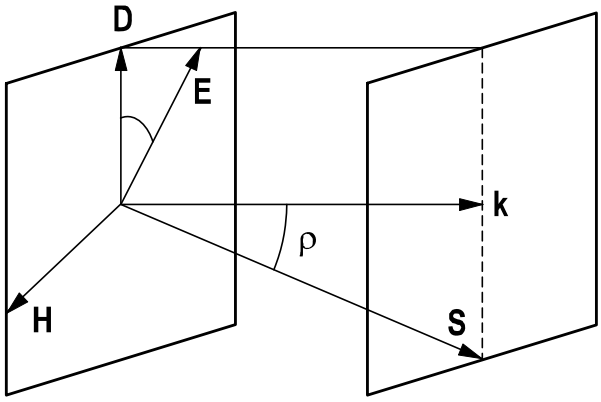

Figure 2.114: Wave propagation in anisotropic media. KDB-system.

One distinguishes between isotropic, uniaxial und biaxial media. We have extensively studied the isotropic case. The most general case is the biaxial case, where the dielectric constants along the three axes are all different. These dielectic constants, or corresponding indices, define an index ellipsoid

$$\frac{x^2}{n_x^2} + \frac{y^2}{n_y^2} + \frac{z^2}{n_z^2} = 1, \tag{2.405}$$

see Figure 2.115.

Here we want to consider the case of an uniaxial crystal, where

$$\boldsymbol{\varepsilon}_{xx} = \boldsymbol{\varepsilon}_{yy} = \boldsymbol{\varepsilon}_1 \neq \boldsymbol{\varepsilon}_{zz} = \boldsymbol{\varepsilon}_3. \tag{2.406}$$

The refractive indices corresponding to these susceptibilities are called ordinary and extraordinary indices

$$n_1 = n_o \neq n_3 = n_e. \tag{2.407}$$

Further, there is a distinction between positive, $n_e > n_o$, and negative, $n_e < n_o$, uniaxial crystals. The uniaxial case corresponds to an index ellipsoid that has rotational symmectry around the z-axis, see Figure 2.115.

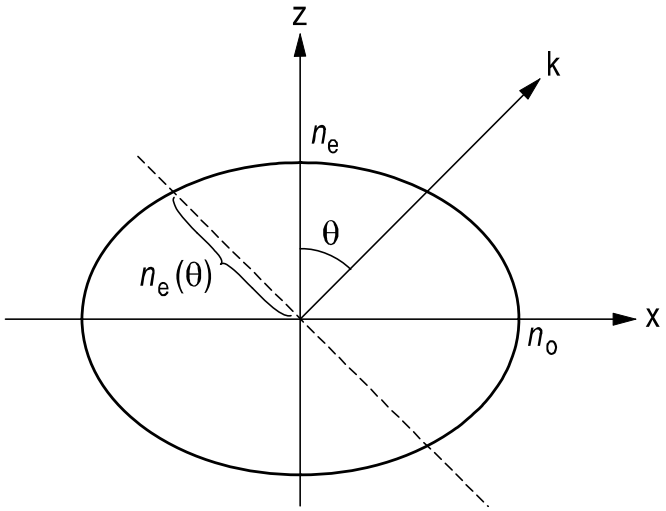

Figure 2.115: Index Ellipsoid

The general case is then a wave with wave vector $\vec{k}$ propagating under an angle θ with respect to the z-axis; the z-axis is also often called the fast axis or c-axis or optical axis. Without restrictions, we assume that the wave vector is in the $x-z-$plane. If the wave vector is aligned with the fast axis, there is no birefringence, because the index experienced by the wave is independent from its polarization. If there is a finite angle, $\theta \neq 0$, then there are two waves with different phase velocity and group velocity as we will show now, see 2.115, and birefringence occurs. With the identity $\vec{A} \times \left(\vec{B} \times \vec{C}\right) = \left(\vec{A} \cdot \vec{C}\right) \vec{B} - \left(\vec{A} \cdot \vec{B}\right) \vec{C}$, when applied to Eq.(2.403), follows

$$\left(\vec{k} \cdot \vec{E}\right) \vec{k} - k^2 \vec{E} + \omega^2 \mu_0 \boldsymbol{\varepsilon} \vec{E} = 0. \tag{2.408}$$

This equation determines the dispersion relation and polarization of the possible waves with wave vector $\vec{k}$. Since the wave vector is in the $x-z-$plane this equation reads

$$\begin{pmatrix} k_0^2 n_o^2 + k_x^2 - k^2 & & k_x k_z \\ & k_0^2 n_o^2 - k^2 & \\ k_z k_x & & k_0^2 n_e^2 + k_z^2 - k^2 \end{pmatrix} \vec{E} = 0 \tag{2.409}$$

This equation clearly shows that a wave polarized along the $y-$axis or in general orthogonal to the plane composed of the wave vector and the fast axis decouples from the other components.

2.8.2 Ordinary Wave

This wave is called the ordinary wave, because it has the dispersion relation

$$k^2 = k_0^2 n_o^2. \tag{2.410}$$

As with the TEM waves in an isotropic medium, the wave vector and the field components build an orthogonal trihedral, $\vec{k} \perp \vec{E} \perp \vec{H}$.

2.8.3 Extraordinary Wave

Eq.(2.409) allows for another wave with a polarization in the $x-z-$plane, and therefore this wave has a longitudinal electric field component. This wave is called extraordinary wave and its dispersion relation follows from

$$\det \begin{vmatrix} k_0^2 n_o^2 + k_x^2 - k^2 & k_x k_z \\ k_z k_x & k_0^2 n_e^2 + k_z^2 - k^2 \end{vmatrix} = \mathbf{0}. \tag{2.411}$$

Calculating the determinant and simplifying we find

$$\frac{k_z^2}{n_o^2} + \frac{k_x^2}{n_e^2} = k_0^2. \tag{2.412}$$

With $k_x = k \sin(\theta)$, $k_z = k \cos(\theta)$ and $k = n(\theta) k_0$ we obtain for the refractive index seen by the extraordinary wave

$$\frac{1}{n(\theta)^2} = \frac{\cos^2(\theta)}{n_o^2} + \frac{\sin^2(\theta)}{n_e^2}. \tag{2.413}$$

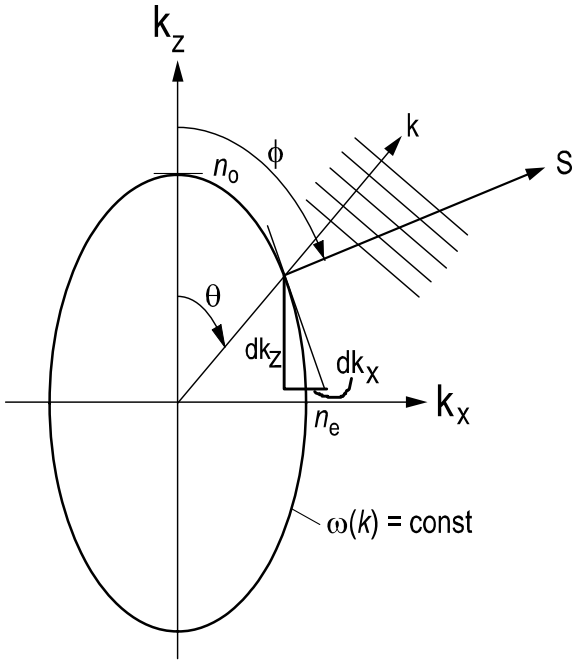

Figure 2.116: Cut through the surface with a constant free space wave number $k_o(k_x, k_y, k_z)$ or frequency, which is also an ellipsoid, but with exchanged principle axis when compared with Figure 2.114

Eqs.(2.412) and (2.413) also describe an ellipse. This ellipse is the location of a constant free space wave number or frequency, $\omega = k_0 c_0$, and therefore determines the refractive index, $n(\theta)$, of the extraordinary wave, see Figure 2.115. The group velocity is found to be parallel to the Poynting vector

$$\boldsymbol{v}_g = \nabla_k \omega(\mathbf{k}) \parallel \mathbf{S}, \tag{2.414}$$

and is orthogonal to the surface. For completeness, we give a derivation of the walk-off angle between the ordinary and extraordinary wave

$$\tan\theta = \frac{k_x}{k_z} \tag{2.415}$$

$$\tan\phi = -\frac{dk_z}{dk_x} \tag{2.416}$$

From Eq.(2.412) we obtain by differentiation along the surface of the ellipsoid

$$\frac{2k_z dk_z}{n_o^2} + \frac{2k_x dk_x}{n_e^2} = 0. \tag{2.417}$$

$$\tan\phi = \frac{n_o^2 k_x}{n_e^2 k_z} = \frac{n_o^2}{n_e^2}\tan\theta$$

Thus, we obtain for the walk-off-angle ϱ between Poynting vector and wave vector

$$\tan\varrho = \tan(\theta - \phi) = \frac{\tan\theta - \tan\phi}{1 + \tan\theta\tan\phi} \tag{2.418}$$

or

$$\tan\varrho = -\frac{\left(\frac{n_0^2}{n_e^2} - 1\right)\tan\theta}{1 + \frac{n_0^2}{n_e^2}\tan^2\theta}. \tag{2.419}$$

2.8.4 Example: Calcite

One example of a birefringent materialis calcite, which is also often used in optical devices, such as polarizers for example. Figure 2.117 and 2.118 show the arrangement of atoms in calcite.

Figure 2.117: Arrangement of atoms in calcite, [1], p. 231.

Figure 2.118: Atomic arrangement of calcite looking down the optical axis [1], p. 232.

Figure 2.119 shows a crystal cleaved along the crystal axis (cleavage form).

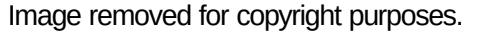

Figure 2.119: Calcite cleavage form [1], p. 232.

Figure 2.120 shows the light path of two orthogonally polarized light beams where one propagates as an ordinary and the other as an extraordinary wave through the crystal. This leads to a double image when an object is viewed through the crystal, see Figure 2.121.

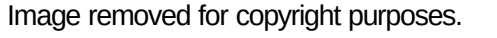

Figure 2.120: A light beam with two orthogonal field components traversing a calcite principal section [1], p. 234.

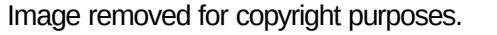

Figure 2.121: Double image formed by a calcite crystal (not cleavage form) [1], p. 233.

Table 2.8 gives the ordinary and extraordinary refractive indices of some

uniaxial crystals. Birefringent materials enable the construction of wave

Crystal	n_o	n_e
Tourmaline	1.669	1.638
Calcite	1.6584	1.4864
Quartz	1.5443	1.5534
Sodim Nitrate	1.5854	1.3369
Ice	1.309	1.313
Rutile (TiO_2)	2.616	1.903

Table 2.8: Refractive indices of some uniaxial birefringent crystals ($\lambda = 589.3$nm) [1], p.236

plates or retardation plates, which enable the manipulation of polarization in a very unique way.

2.9 Polarization and Crystal Optics

So far we have discussed linearly polarized electromagnetic waves, where the electric field of a TEM-wave propagating along the $z-$direction was either polarized along the $x-$ or $y-$axis. The most general TEM-wave has simultaneously electric fields in both polarizations and the direction of the electric field in space, i.e. its polarization, can change during propagation. A description of polarization and polarization evolution in optical systems can be based using Jones vectors and matrices.

2.9.1 Polarization

A general complex TEM-wave propagating along the $z-$direction is given by

$$\vec{\underline{E}}(z,t) = \begin{pmatrix} \underline{E}_{0x} \\ \underline{E}_{0y} \\ 0 \end{pmatrix} e^{\mathrm{j}(\omega t - kz)}, \tag{2.420}$$

where $\underline{E}_{0x} = E_{0x}e^{j\varphi_x}$ and $\underline{E}_{0y} = E_{0y}e^{j\varphi_y}$ are the complex field amplitudes of the $x-$ and $y-$ polarized components of the wave. The real electric field is

given by

$$\vec{E}(z,t) = \begin{pmatrix} E_{0x}\cos(\omega t - kz + \varphi_x) \\ E_{0y}\cos(\omega t - kz + \varphi_y) \\ 0 \end{pmatrix}, \tag{2.421}$$

Both components are periodic functions in $\omega t - kz = \omega(t - z/c)$.

Linear Polarization

If the phases of the complex field amplitudes along the $x-$ and $y-$axis are equal, i.e.

$$\underline{E}_{0x} = |\underline{E}_{0x}|\, e^{j\varphi} \text{ and } \underline{E}_{0y} = \left|\underline{E}_{0y}\right| e^{j\varphi}$$

then the real electric field

$$\vec{E}(z,t) = \begin{pmatrix} \underline{E}_{0x} \\ \underline{E}_{0y} \\ 0 \end{pmatrix} \cos(\omega t - kz + \varphi) \tag{2.422}$$

always oscillates along a fixed direction in the x-y-plane, see Figure 2.122

Image removed for copyright purposes.

Figure 2.122: Linearly polarized light. (a) Time course at a fixed position z. (b) A snapshot at a fixed time t, [6], p. 197.

The angle between the polarization direction and the x-axis, α, is given by $\alpha = \arctan(E_{0y}/E_{0x})$. If there is a phase difference of the complex field amplitudes along the $x-$ and $y-$axis, the direction and magnitude of the electric field amplitude changes periodically in time at a given position z.

Circular Polarization

Special cases occur when the magnitude of the fields in both linear polarizations are equal $E_{0x} = E_{0y} = E_0$, but there is a phase difference $\Delta\varphi = \pm\frac{\pi}{2}$ in both components. Then we obtain

$$\vec{E}(z,t) = E_0 \,\mathrm{Re}\left\{ \begin{pmatrix} e^{j\varphi} \\ e^{j(\varphi-\Delta\varphi)} \\ 0 \end{pmatrix} e^{\mathrm{j}(\omega t - kz)} \right\} \tag{2.423}$$

$$= E_0 \begin{pmatrix} \cos(\omega t - kz + \varphi) \\ \sin(\omega t - kz + \varphi) \\ 0 \end{pmatrix}. \tag{2.424}$$

For this case, the tip of the electric field vector describes a circle in the $x-y-$plane, as

$$|E_x(z,t)|^2 + |E_y(z,t)|^2 = E_0^2 \text{ for all } z,t, \tag{2.425}$$

see Figure 2.123.

Figure 2.123: Trajectories of the tip of the electric field vector of a right and left circularly polarized plane wave. (a) Time course at a fixed position z. (b) A snapshot at a fixed time t. Note, the sense of rotation in (a) is opposite to that in (b) [6], p. 197.

Right Circular Polarization If the tip of the electric field at a given time, t, rotates counter clockwise with respect to the phase fronts of the wave, here in the positive $z-$direction, then the wave is called right circularly polarized light, i.e.

$$\vec{E}_{rc}(z,t) = E_0 \,\mathrm{Re}\left\{ \begin{pmatrix} 1 \\ j \\ 0 \end{pmatrix} e^{\mathrm{j}(\omega t - kz + \varphi)} \right\} = E_0 \begin{pmatrix} \cos(\omega t - kz + \varphi) \\ -\sin(\omega t - kz + \varphi) \\ 0 \end{pmatrix}. \tag{2.426}$$

A snapshot of the lines traced by the end points of the electric-field vectors at different positions is a right-handed helix, like a right-handed screw pointing in the direction of the phase fronts of the wave, i.e. $k-$vector see Figure 2.123 (b).

Left Circular Polarization If the tip of the electric field at a given fixed time, t, rotates clockwise with respect to the phase fronts of the wave, here in the again in the positive $z-$direction, then the wave is called left circularly polarized light, i.e.

$$\vec{E}_{lc}(z,t) = E_0 \,\mathrm{Re}\left\{ \begin{pmatrix} 1 \\ -j \\ 0 \end{pmatrix} e^{\mathrm{j}(\omega t - kz + \varphi)} \right\} = E_0 \begin{pmatrix} \cos(\omega t - kz + \varphi) \\ \sin(\omega t - kz + \varphi) \\ 0 \end{pmatrix}. \tag{2.427}$$

Eliptical Polarization The general polarization case is called eliptical polarization, as for arbitrary $\underline{E}_{0x} = E_{0x} e^{j\varphi_x}$ and $\underline{E}_{0y} = E_{0y} e^{j\varphi_y}$, we obtain for the locus of the tip of the electric field vector from

$$\vec{E}(z,t) = \begin{pmatrix} E_{0\times} \cos(\omega t - kz + \varphi_x) \\ E_{0y} \cos\left(\omega t - kz + \varphi_y\right) \\ 0 \end{pmatrix}. \tag{2.428}$$

the relations

$$\frac{E_y}{E_{0y}} = \cos\left(\omega t - kz + \varphi_y\right) \tag{2.429}$$

$$= \cos(\omega t - kz + \varphi_x)\cos\left(\varphi_y - \varphi_x\right) - \sin(\omega t - kz + \varphi_x)\sin\left(\varphi_y - \varphi_x\right). \tag{2.430}$$

and

$$\frac{E_x}{E_{0x}} = \cos\left(\omega t - kz + \varphi_x\right). \tag{2.431}$$

These relations can be combined to

$$\frac{E_y}{E_{0y}} - \frac{E_x}{E_{0x}}\cos\left(\varphi_y - \varphi_x\right) = -\sin\left(\omega t - kz + \varphi_x\right)\sin\left(\varphi_y - \varphi_x\right) \tag{2.432}$$

$$\sin\left(\omega t - kz + \varphi_x\right) = \sqrt{1 - \left(\frac{E_x}{E_{0x}}\right)^2} \tag{2.433}$$

Substituting Eq.(2.433) in Eq.(2.432) and building the square results in

$$\left(\frac{E_y}{E_{0y}} - \frac{E_x}{E_{0x}}\cos\left(\varphi_y - \varphi_x\right)\right)^2 = \left(1 - \left(\frac{E_x}{E_{0x}}\right)^2\right)\sin^2\left(\varphi_y - \varphi_x\right). \tag{2.434}$$

After reordering of the terms we obtain

$$\left(\frac{E_x}{E_{0x}}\right)^2 + \left(\frac{E_y}{E_{0y}}\right)^2 - 2\frac{E_x}{E_{0x}}\frac{E_y}{E_{0y}}\cos\left(\varphi_y - \varphi_x\right) = \sin^2\left(\varphi_y - \varphi_x\right). \tag{2.435}$$

This is the equation of an ellipse making an angle α with respect to the x-axis given by

$$\tan 2\alpha = \frac{2E_{0x}E_{0y}\cos\left(\varphi_y - \varphi_x\right)}{E_{0x}^2 - E_{0y}^2}. \tag{2.436}$$

see Figure 2.124.

Image removed for copyright purposes.

Figure 2.124: (a) Rotation of the endpoint of the electric field vector in the x-y-plane at a fixed position z. (b) A snapshot at a fixed time t [6], p. 197.

Elliptically polarized light can also be understood as a superposition of a right and left cicular polarized light, see Figure 2.125.

Image removed for copyright purposes.

Figure 2.125: Elliptically polarized light as a superposition of right and left circularly polarized light [1], p. 223.

2.9.2 Jones Calculus

As seen in the last section, the information about polarization of a TEM-wave can be tracked by a vector that is proportional to the complex electric-field vector. This vector is called the Jones vector

$$\begin{pmatrix} \underline{E}_{0x} \\ \underline{E}_{0y} \end{pmatrix} \sim \vec{\underline{V}} = \begin{pmatrix} \underline{V}_x \\ \underline{V}_y \end{pmatrix} : \text{Jones Vector} \tag{2.437}$$

Jones Matrix

Figure 2.126 shows a light beam that is normally incident on a retardation plate along the $z-$axis with a polarization state described by a Jones vector

Figure 2.126: A retardation plate rotated at an angle ψ about the z-axis. f("fast") and s("slow") are the two principal dielectric axes of the crystal for light propagating along the $z-$axis [2], p. 17.

The principle axis ($s-$ for slow and $f-$ for fast axis) of the retardation plate are rotated by an angle ψ with respect to the $x-$ and $y-$axis. Let n_s and n_f be the refractive index of the slow and fast principle axis, respectively. The polarization state of the emerging beam in the crystal coordinate system is thus given by

$$\begin{pmatrix} V_s' \\ V_f' \end{pmatrix} = \begin{pmatrix} e^{-jk_o n_s L} & 0 \\ 0 & e^{-jk_o n_f L} \end{pmatrix} \begin{pmatrix} V_s \\ V_f \end{pmatrix}, \tag{2.438}$$

The phase retardation is defined as the phase difference between the two components

$$\Gamma = (n_s - n_f)\, k_o L. \tag{2.439}$$

In birefringent crystals the difference in refractive index is much smaller than the index itself, $|n_s - n_f| \ll n_s, n_f$, therefore parallel to the evolving differential phase a large absolute phase shift occurs. Taking the mean phase shift

$$\phi = \frac{1}{2}(n_s + n_f)\, k_o L, \tag{2.440}$$

out, we can rewrite (2.438) as

$$\begin{pmatrix} V_s' \\ V_f' \end{pmatrix} = e^{-j\phi} \begin{pmatrix} e^{-j\Gamma/2} & 0 \\ 0 & e^{j\Gamma/2} \end{pmatrix} \begin{pmatrix} V_s \\ V_f \end{pmatrix}. \tag{2.441}$$

The matrix connecting the Jones vector at the input of an optical component with the Jones vector at the output is called a Jones matrix.

If no coherent additon with another field is planned at the output of the system, the average phase ϕ can be dropped. With the rotation matrix, R, connecting the (x, y) coordinate system with the (s, f) coordinate system

$$R(\psi) = \begin{pmatrix} \cos\psi & \sin\psi \\ -\sin\psi & \cos\psi \end{pmatrix}, \tag{2.442}$$

we find the Jones matrix W describing the propagation of the field components through the retardation plate as

$$\begin{pmatrix} V_x' \\ V_y' \end{pmatrix} = W \begin{pmatrix} V_x \\ V_y \end{pmatrix}. \tag{2.443}$$

with

$$W = R(-\psi) W_0 R(\psi). \tag{2.444}$$

and

$$W_0 = \begin{pmatrix} e^{-j\Gamma/2} & 0 \\ 0 & e^{j\Gamma/2} \end{pmatrix}. \tag{2.445}$$

Carrying out the matix multiplications leads to

$$W = \begin{pmatrix} e^{-j\Gamma/2}\cos^2(\psi) + e^{j\Gamma/2}\sin^2(\psi) & -j\sin\frac{\Gamma}{2}\sin(2\psi) \\ -j\sin\frac{\Gamma}{2}\sin(2\psi) & e^{-j\Gamma/2}\sin^2(\psi) + e^{j\Gamma/2}\cos^2(\psi) \end{pmatrix}. \tag{2.446}$$

Note that the Jones matrix of a wave plate is a unitary matrix, that is

$$W^\dagger W = 1.$$

Unitary matrices have the property that they transform orthogonal vectors into another pair of orthogonal vectors. Thus two orthogonal polarization states remain orthogonal when propagating through wave plates.

Polarizer

A polarizer is a device that absorbs one component of the polarization vector. The Jones matrix of polarizer along the x-axis or y-axis is

$$P_x = \begin{pmatrix} 1 & 0 \\ 0 & 0 \end{pmatrix}, \text{ and } P_y = \begin{pmatrix} 0 & 0 \\ 0 & 1 \end{pmatrix}. \tag{2.447}$$

Half-Wave Plate

A half-wave plate has a phase retardation of $\Gamma = \pi$, i.e. its thickness is $t = \lambda/2(n_e - n_o)$. The corresponding Jones matrix follows from Eq.(2.446)

$$W = -j \begin{pmatrix} \cos(2\psi) & \sin(2\psi) \\ \sin(2\psi) & -\cos(2\psi) \end{pmatrix}. \tag{2.448}$$

For the special case of $\psi = 45^o$, see Figure 2.127, the half-wave plate rotates a linearly polarized beam exactly by 90^0, i.e. it exchanges the polarization axis. It can be shown, that for a general azimuth angle ψ, the half-wave plate will rotate the polarization by an angle 2ψ, see problem set. When the incident light is circularly polarized a half-wave plate will convert right-hand circularly polarized light into left-hand circularly polarized light and vice versa, regardless of the azimuth angle ψ.

Figure 2.127: The effect of a half-wave plate on the polarziation state of a beam, [2], p.21.

Quarter-Wave Plate

A quarter-wave plate has a phase retardation of $\Gamma = \pi/2$, i.e. its thickness is $t = \lambda/4(n_e - n_o)$. The corresponding Jones matrix follows again from Eq.(2.446)

$$W = \begin{pmatrix} \frac{1}{\sqrt{2}}\left[1 - j\cos(2\psi)\right] & -j\frac{1}{\sqrt{2}}\sin(2\psi) \\ -j\frac{1}{\sqrt{2}}\sin(2\psi) & \frac{1}{\sqrt{2}}\left[1 + j\cos(2\psi)\right] \end{pmatrix}. \tag{2.449}$$

and for the special case of $\psi = 45^o$, see Figure 2.127 we obtain

$$W = \frac{1}{\sqrt{2}} \begin{pmatrix} 1 & -j \\ -j & 1 \end{pmatrix}, \tag{2.450}$$

see Figure 2.128.

Figure 2.128: The effect of a quarter wave plate on the polarization state of a linearly polarized input wave [2], p.22.

If the incident beam is vertically polarized, i.e.

$$\begin{pmatrix} V_x \\ V_y \end{pmatrix} = \begin{pmatrix} 0 \\ 1 \end{pmatrix}, \tag{2.451}$$

the effect of a 45^o -oriented quarter-wave plate is to convert vertically polarized light into left-handed circularly polarized light. If the incident beam is horizontally polarized the outgoing beam is a right-handed circularly polarized, see Figure 2.128.

$$\begin{pmatrix} V'_x \\ V'_y \end{pmatrix} = \frac{-j}{\sqrt{2}} \begin{pmatrix} 1 \\ j \end{pmatrix}. \tag{2.452}$$

Bibliography

[1] Hecht and Zajac, "Optics," Addison and Wesley, Publishing Co., 1979.

[2] B.E.A. Saleh and M.C. Teich, "Fundamentals of Photonics," John Wiley and Sons, Inc., 1991.

[3] Bergmann and Schaefer, "Lehrbuch der Experimentalphysik: Opitk," 1993.

[4] H. Kogelnik and T. Li, "Laser Beams and Resonators," Appl. Opt. **5**, pp. 1550 – 1566 (1966).

[5] H. Kogelnik, E. P. Ippen, A. Dienes and C. V. Shank, "Astigmatically Compensated Cavities for CW Dye Lasers," IEEE J. Quantum Electron. **QE-8**, pp. 373 – 379 (1972).

[6] H. A. Haus, "Fields and Waves in Optoelectronics", Prentice Hall 1984.

[7] F. K. Kneubühl and M. W. Sigrist, "Laser," 3rd Edition, Teubner Verlag, Stuttgart (1991).

[8] A. E. Siegman, "Lasers," University Science Books, Mill Valley, California (1986).

[9] Optical Electronics, A. Yariv, Holt, Rinehart & Winston, New York, 1991.

[10] Photonic Devices, Jia, Ming-Liu , Cambridge University Press, 2005.

[11] T. Tamir, "Guided-Wave Optoelectronics," Springer, 1990.